NEURAL RESPONSES TO INJURY: PREVENTION, PROTECTION, AND REPAIR
Annual Technical Report
1996-1997

Submitted by

Nicolas G. Bazan, M.D., Ph.D.
Project Director

Period Covered: 20 September, 1996 through 19 September, 1997

Cooperative Agreement DAMD17-93-V-3013

between

United States Army Medical Research and Development Command
(Walter Reed Army Institute of Research)

and

Louisiana State University Medical Center
Neuroscience Center of Excellence

Volume 2 of 9

Repair and Regeneration of Peripheral Nerve Damage

Project Directors:
Roger Beuerman, Ph.D.
David Kline, M.D.
Austin Sumner, M.D.

Volume 2 Repair and Regeneration of Peripheral Nerve Damage

Project Directors: Roger Beuerman, Ph.D.
David Kline, M.D.
Austin Sumner, M.D.

Participating Scientists: John England, M.D.
Harry J. Gould, III, M.D., Ph.D.
Daniel Kim, M.D.
Cheryl Weill, Ph.D.

England JD, Happel LT, Kline DG, Gamboni F, Thouron CL, Liu ZP, Levinson SR: Sodium channel accumulation in human painful neuromas. Neurology 47:272-276, 1996.

England JD, Levinson SR, Shrager P: Immunocytochemical investigations of sodium channels along nodal and internodal portions of demyelinated axons. Microsc Res Tech 33:445-451, 1996.

Lu G, Beuerman RW, Zhao S, Sun G, Nguyen DH, Ma S, Kline DG: Tumor necrosis factor alpha and interleukin-1 induce activation of MAP kinase and SAP kinase in human neuroma fibroblasts. Neurochem Int 30:401-410, 1997.

Zhao S, Beuerman RW, Kline DG: Neurotization of motor nerves innervating lower extremity by utilizing lower intercostal nerves. J Reconstr Microsurg 13:39-45, 1997.

Gould HJ, Gould TN, Reeb SC, Paul D: The effect of gabapentin on inflammatory pain in rats. Analgesia, in press.

ABSTRACTS

Beuerman R, Zhao S, Tran H, Ma S, Kim D, Kline D: Epidermal growth factor and fibroblast growth factor in human neuroma tissue. Soc Neurosci ABS Vol. 20, 1994.

Ma Q, Beuerman RW, Zhao S, Pedroza L, Tran H, Nguyen D, Kline DG: Immunolocalization and quantitation of fibroblast growth factor receptor-1 in the human peripheral neuroma. Soc Neurosci ABS Vol. 21, 1995.

Lu G, Beuerman RW, Zhao S, Sun G, Nguyen DH, Ma S, Kline DG: TNF-α and IL-1 activate MAP and SAP kinase in human neuroma fibroblasts. Soc Neurosci ABS Vol. 22, 1996.

Zeiller S, Awasthi D, Carey ME, Beuerman RW, Nguyen D, Soblosky JS, Colgin L: Effects of cortical impact injury plus hypotension on gene expression. Soc Neurosci ABS Vol. 23, 1997.

Zhao S, Beuerman RW, Lu G, Varnell R, Kline DD: CSF changes following brachial plexus avulsion and spinal cord injury. Soc Neurosci ABS Vol. 23, 1997.

Beuerman RW, Ma Q, England J, Levinson R: Immunohistochemical studies of the distribution of sodium and potassium channels in rat corneal nerves. Invest Ophthalmol Vis Sci ABS 38(4), 1997.

Tiel R, Jacques L, Kline D: Differential susceptibility of peroneal division of sciatic to injury regeneration. The Sunderland Society ABS 1997.

Beuerman RW, Lu G, Zhao S, Ma Z, Ma Q, Kline DG: Intracellular pathways and growth factors in transected and optimally repaired rat sciatic nerve. The Sunderland Society ABS 1997.

Happel LT, England JD, Kline DG: Potassium channel distributions in normal human nerve and in neuromas. The Sunderland Society ABS 1997.

Gould TN, Paul DJ, Gould HJ: Analgesic effects of gabapentin on inflammatory pain in rat. J Invest Med ABS 45:6a, 1997.

Gould HJ, England JD, Liu AP, Levinson: Sodium channel augmentation in response to pain induced by chronic inflammation. American Pain Society ABS, October, 1997, in press.

I. GOALS

The overall focus of this project has been to understand the cellular and molecular biology of neuroma formation as a complication of damage to peripheral nerves. Several objectives have been clarified: 1) to establish in vitro models of cell lines of fibroblasts from normal peripheral nerves and neuromas that can be used to uncover the molecular mechanisms of the peripheral nerve fibroblast response to damage; 2) to understand the interactions of fibroblasts of peripheral nerve origin with cell signaling molecules in the neural environment after an injury and during the repair process; and 3) to understand the origin of pain that accompanies neuroma formation.

It is not known how the cellular physiology of the entrapped nerve endings is affected by the dense collagenous mass of tissue that makes up the neuroma. However, it is clear that abnormalities develop in gated ion channels in the entrapped nerve endings and that the neuroma is formed by an exaggerated fibroblast response to nerve damage. Studies using fibroblasts cultured from peripheral human nerves have shown that these cells express basic fibroblast growth factor and its receptor. Immunohistochemical studies and quantitative Western blots have shown that basic fibroblast growth factor and its receptor are found in all tissue samples taken directly from human neuromas. The goal of these ongoing studies is to elucidate the mechanisms that regulate the activities of these cells in injury and repair and ultimately to determine potential approaches to modification of these mechanisms that may prevent the development of neuromas and their associated morbidities in traumatized tissues.

II. INTRODUCTION

Peripheral nerve injuries are among the most common injuries. There is a substantial

incidence of this type of injury in the armed forces, where they have a debilitating effect on personnel; these injuries are also common in the general population as a result of motor vehicle accidents and violence. The outcome of repair of these injuries may be unsatisfactory in as many as 30-40% of cases; the result is a loss of motor function and reduced sensory capability. These complications can develop as part of the healing response after trauma and sometimes as a side effect of surgical repair; they are caused by the accumulation of cells and extracellular matrix at the site of injury, forming what is usually called a neuroma. In this study, it is hypothesized that the exaggerated healing response of the neural fibroblasts is driven by the cellular response to extracellular signals. The situation is further complicated by the local cellular environment, which may compartmentalize cell signaling molecules and cell interactions that are unique to the peripheral nerve, in which case growth factors and cytokines may be of primary importance. It is also hypothesized that cellular involvement could be altered in order to provide more normal healing with better functional recovery. Understanding the intracellular signaling pathway in these cells after trauma may provide a window for determining cellular actions that ultimately result in a neuroma.

To accomplish these objectives, we have worked simultaneously at several different levels. The first has been to understand the cellular mechanisms that may be operating in the mature human peripheral nerve neuroma. As reported in previous years, the only growth factor family commonly found in human neuroma tissue is that of basic fibroblast growth factor (bFGF or FGFII) and its receptor (FGF-R). Although an extensive search for a number of other growth factors, including acidic fibroblast growth factor (aFGF or FGFI), platelet-derived growth factor (PDGF), transforming growth factor beta 1 (TNFß-1), as well as important cytokines such as interleukin-1 (IL-1) and tumor necrosis factor α (TNF-α), was carried out using Western blots, only barely detectable amounts of

some and none at all of others were found. The absence of both IL-1 and TNF-α in the human neuroma suggests that the mature peripheral neuroma (six months or more post injury) is not characterized by an ongoing inflammatory process. However, the neuroma may be characterized as a poorly vascularized, encapsulated fibrous matrix and this matrix may be slightly acidic and hypoxic due to the lack of vascularity. In support of this characterization is the finding that the neuroma, which develops uniquely in the proximal part of the nerve stump, is a complex interaction of several cell types including growing neurites.

In the first year of this project, fibroblast cell lines were established from tissue specimens of human neuromas and leftover normal nerve used in surgical repair. These cell lines were grown to passage 5-6; at these passage numbers, cell morphology in culture remained stable. Several of these cell lines have been maintained for the entire period of this project and will remain a resource. Fibroblasts from the internal part of the nerve are thought to be the most important for neuroma formation; therefore, particular care was taken to ensure that the cells cultured were from the internal or endoneuria portion of the normal nerve or neuroma. It was found that the fibroblast cell lines from neuromas did not grow with the vitality of some other fibroblast cell lines. For this reason, one study included in this year's report, which involved an inhibitor of mitogen-activated protein kinase (MAPK), was performed using a fibroblast cell line from the human cornea. It was found that the acidic S-100 protein was not reliable to differentiate fibroblasts from Schwann cells, as fibroblasts from several human tissues stain for this protein. However, the low affinity nerve growth factor receptor (NGFR) antibody was able to consistently differentiate these cells types. Schwann cells from both normal human nerve and neuromas were found to stain with the NGFR antibody.

As mentioned above, the other focus of the first year was the collection of human neuroma

tissue for analysis of growth factors and cytokines. This project was carried over into year two. The method of choice for this analysis was Western blot. Initially, mRNA was collected from the small pieces of tissue that were provided for this purpose. Tissue taken from the operating room was used partially for histopathology and also for the ion channel analysis studies. However, transmission electron microscopy of neuroma samples showed that the cellularity of neuromas is very variable. For this reason, the amount of RNA obtained was often too small for probing, considering the number of growth factors and cytokines that needed to be tested for. This problem made it unlikely that consistent results could be obtained. Because Western blots could be reprobed at least 2-3 times, this approach was adopted. The results of these studies were presented at the Sunderland Society meeting, an organization dedicated to the understanding of the complications of peripheral nerve injury and surgery.

In year two, the analysis of tissue samples continued. The origin of bFGF (or FGFII) was further investigated using double labeling of passage 1-2 mixed cultures and immunotransmission electron microscopy. Fibroblasts and Schwann cells were found to be positive for the growth factor; however, only the fibroblasts were found to be positive for the receptor. Schwann cells were found to make up no more than 20% of these cultures. Acidic FGF (or FGFI) was not found. Immunoelectron microscopy was carried out using two sizes of gold particles, one for the receptor and another for the growth factor. Micrographs of neuroma fibroblasts were obtained depicting the localization of growth factor and receptor arrayed along the cell membrane. This suggested that interactions between Schwann cells and fibroblasts are probably important during neuroma formation.

In year three of this project, experiments continued on the intracellular signaling pathways.

The focus of this work was to determine the effects of an inhibitor of the pathway that leads to cell proliferation, the MAPK pathway. In addition, experiments on stretch injury to the brachial plexus were begun. Brachial plexus injuries are complicated due to the possibility of avulsion injury, as well as neuroma formation. Avulsion injuries occur at the interface of the peripheral and central nervous system and often lead to permanent disability.

In the fourth (current) year of this project, work in three areas is submitted. The first is the analysis of PD98059 on the components of the MAPK pathway and the expression of the *fos* gene and Fos protein expression. An important aspect of this study is that it clearly links growth factor stimulation with activation of the MAPK pathway, *fos* gene expression, and cell proliferation. Moreover, the study shows that blocking a single phosphorylation step immediately upstream from MAPK blocks all of the downstream effects. The results suggest that this low molecular weight compound is very effective at reducing the effect of growth factors without being toxic. This study has been submitted for publication.

Following the *in vivo* application of this compound in an experimental neuroma model in the rat, it will be tested in the primate model of the human neuroma that was developed in year two. The rat is not a good model of a neuroma as rat nerves regenerate with tremendous vigor; however, the rat model will be used to check for nerve toxicity.

The second area of emphasis has been to continue the studies of stretch injury to the brachial plexus. The effects of two types of nerve injuries -- a distal transection and a stretch injury -- on cells of the spinal cord were compared using immunohistochemistry to detect the presence of the Fos protein. The number of cells positive for Fos expression was significantly increased after a stretch injury in all lamina of the cord. However, after distal transection, the increase in the numbers of Fos-

positive cells was found primarily in the dorsal horn of the cord. In these types of injuries, the therapeutic window may be related to the duration of immediate gene expression and Fos is an important transcription factor for later events such as cell death. The results of this study are being submitted for publication.

Almost all stretch injury models, including the one used in our studies over the past year, are non-quantitative and/or require a surgical approach. A quantitative model that does not require surgical intervention is in the early stages of testing, with promising results thus far. In this model, an anesthetized rat is placed in a novel device that provides a controlled acceleration to one forelimb. The parameters can be varied to apply a light stretch or a stretch sufficient to provide avulsion. This work is continuing, with studies on apoptosis and Fos expression planned. In addition, using an bioengineering approach, plans are underway to study nerve stress, as well as other parameters, during the application of the injury procedure. This model is valuable as it also allows measurements of behavioral outcomes and the effects of various types of therapeutic interventions to be correlated with detailed studies of the molecular response of the cells of the spinal cord to stretch injuries of variable intensity.

III. MITOGEN-ACTIVATED PROTEIN KINASE IN GROWTH FACTOR STIMULATION OF HUMAN CORNEAL FIBROBLAST PROLIFERATION AND THE EFFECT OF AN INHIBITOR

INTRODUCTION

Corneal cells express the message for several growth factors and their receptors, including bFGF, EGF, and PDGF (1,2). Injury to the cornea may change the regulation of these messages as part of the wound response; however, the protein found at the injury site can result from local release from cells, release from inflammatory cells, or from the tears (3-5). The therapeutic use of the growth factors has been evaluated *in vivo* by direct application of the growth factor to the cornea or by application to corneal cells in culture. The results of such studies have shown that these growth factors may accelerate epithelial and stromal healing, improve wound strength, and modulate the wound healing response after a variety of corneal injuries (6-12). Receptors for some growth factors have been detected in all layers of the cornea, and expression of their mRNA was detected in the tissue and in cultured cells (1,3).

Stromal cells after injury are activated and transformed into fibroblasts which may proliferate and secrete extracellular matrix and collagen, both of which are believed to be important steps in the repair process (13-15). However, for growth factors to be effective, they must bind to the appropriate membrane receptor, which triggers a cascade of protein phosphorylation directed to the nucleus where the final products mediate the regulation of gene expression. Previous studies have demonstrated that growth factors can promote proliferation of human diploid FS-4 skin fibroblasts, NIH 3T3 cells, and other cell types through binding of membrane tyrosine kinase receptors and subsequent activation of components of the MAP kinase cascade (16-19). The mitogenic-activated

protein kinases (MAPK), also called extracellular signal regulated kinases (ERKs), are found as two isoforms (ERK_1, 44 kDa; ERK_2, 42 kDa). Activation occurs as a result of phosphorylation of threonine and tyrosine residues.

Mutations in the regulatory domain of MEK (the upstream kinase from MAPK) and MAP kinase have been used to demonstrate direct linkage of these enzymes to proliferation. Over-expression of non-activated forms of MEK-1 in 3T3 cells significantly reduced their proliferation rate, which was correlated to a similar reduction in MAP kinase activity (19,20). On the other hand, increasing basal levels of MAP kinase activity can accelerate proliferation. Activated MAP kinase translocates into the nucleus and increases DNA synthesis by participating in the production of *c-fos* protein, a product of the immediate early gene. Fos protein is critical for reentry of quiescent fibroblasts into the cell cycle, and activation of MAP kinase is closely related with the G0/G1 transition of the cell cycle in fibroblasts (21-25). In the present study, we show that the growth factors bFGF, EGF, and PDGF-bb can initiate human corneal fibroblast proliferation by activation of the MAP kinase cascade and upregulate *c-fos* gene expression. However, an inhibitor of MEK prevents these actions. These results may be involved in the intracellular mechanisms that regulate the responses of these cells after injury to the cornea.

MATERIALS AND METHODS

Cell Culture and Stimulation

Human corneas were obtained from the eye bank (NDRI). The epithelium was removed and the corneas were cut into 2 x 2 x 2 mm^3 pieces and cultured in DMEM medium (Gibco BRL, Grand Island, NY) containing 20% fetal bovine serum (FBS), 100 units/ml/penicillin, 100 µg/ml

streptomycin, and maintained at 37°C in a humidified atmosphere with 5% CO_2. The cells (about $1x10^6$ cells at passage 5 to 10) were seeded in 100 mm polystyrene tissue culture dishes and allowed to grow to confluence. The medium was changed to essential medium containing 0.3% FBS for 24 hr and then changed to serum-free medium for another 24 hr. The quiescent cells were treated by adding 10 ng/ml bFGF (UBI, Lake Placid, NY), 20 ng/ml EGF, 20 ng/ml PDGF-bb, and 300 ng/ml PMA (Sigma Chemical, St. Louis, MO) at 37°C for 15 min. These were added alone or in combination with inhibitor PD 98059 (New England Biolabs, Beverly, MA) (26,27), at 10 μM for 30 min pretreatment. The inhibitor was solubilized in DMSO. To equalize any potential effect of DMSO in the experiments in our study, the same amount of DMSO was added to the normal control cells and to the growth factor-treated cells. The cells were washed three times with ice-cold PBS and scraped into 300 μl lysis buffer containing 25 mM HEPES at pH 7.7, 0.3 M NaCl, 1.5 mM $MgCl_2$, 0.2 mM EDTA, 0.1% Triton X-100, 0.5 mM DTT, 20 mM b-glycerophosphate, 0.1 mM Na_3VO, 2 μg/ml of leupeptin, and 100 μg/ml of PMSF. The lysis was centrifuged at 12,000 rpm at 4°C for 10 min. The supernatant was collected and stored at -70° C.

Protein Kinase Assay

The protein kinase activity in the cells was determined using myelin basic protein (MBP) as the substrate. The procedure used was similar to that previously used: 15 μl of cell extract, 10μl (2 μg/μl) MBP (Sigma Chemical, St. Louis, MO) ,15 μl reaction buffer mixture containing 70 mM b-glycerophosphate, 10 mM NaF, 0.6 mM EDTA, 15 mM $MgCl_2$, 2 mM DTT, 2 μCi of [r-^{32}P] ATP (ICN, Irvine, CA), and 10 μM ATP (28). Tubes were vortexed gently and incubated at 30°C for 10 min. The reaction was stopped by putting 20 μl of the kinase assay mixture onto p81, 2 x 2 cm^2

phospho-cellulose papers. The papers were washed in 0.75% phosphoric acid for 15 min with three changes of the buffer. After rinsing the papers in acetone for 5 min, each paper was transferred into a scintillation vial, and radiolabel incorporation was determined by liquid scintillation counting.

In Gel Protein Kinase Assay

The procedure used was similar to that previously published (29). In brief, 20 μl of cell extract and 10 μl of kinase loading buffer were mixed, boiled for 3 min, and subjected to 10% polyacrylamide gel electrophoresis containing MBP at a concentration of 0.1 mg/ml. After electrophoresis, the gel was treated in a buffer containing 20% isopropanol, 5 mM β-mercaptoethanol and 50 mM Tris-HCl, pH 8.0, for 60 min, with one change of the buffer. The protein in the gels was denatured at room temperature in a buffer containing 6 M quinidine-HCl, 5mM β-mercaptoethanol, 50 mM Tris-HC1, pH 8.0, for one hr, with one change of the buffer. The protein was then renatured at 4°C in a buffer containing 0.04% Tween-40, 5 mM β- mercaptoethanol and 50 mM Tris-HCL, pH 8.0, for 16 hr, with several changes of the buffer. For the protein kinase assay, the gel was preincubated with kinase assay buffer: 10mM $MgC1_2$, 15 mM glycerophosphate, 0.3 mM Na_3VO, 0.1 mM EGTA, 2 mM DTT, and 20 mM Tris, pH 7.2. The reaction was initiated by changing the preincubation buffer to a fresh kinase buffer containing 50 μM ATP and 10 μCi/ml [r-^{32}P] ATP. After reacting at 37°C for 30 min, the gel was washed extensively with 5% trichloroacetic acid and 1% sodium pyrophosphate, and then dried for autoradiography.

Immunoprecipitation MAP Kinase Assay

A polyclonal antibody to activated MAP kinase (Promega, Madison, WI) was incubated with

protein A-agarose (Sigma, St. Louis, MO) in binding buffer for 30 min, then an equal volume of the immunocomplex of antibody-protein A-agarose was added into each sample, the volume of which was diluted to 700 μl and incubated at 4°C for 4 hr, pelleted, and washed three times with binding buffer. The precipitated MAP kinase was reacted with MBP in 50 μl kinase buffer containing 5 μCi of [r-^{32}P] ATP, 10 μM ATP at 30°C for 10 min. The reaction was stopped by adding 30 μl of 2x kinase sample buffer. After boiling for three min, 20 μl of each sample was subjected to 10% SDS-PAGE. The gel was then dried and exposed to film.

Immunoblotting

Equal volumes of cell lysate were loaded onto each lane of a 12% polyacrylamide gel. Following electrophoresis, protein in the gel was transferred onto a nitrocellulose membrane and blocked with 5% non-fat milk in a buffer containing 0.05% Tween-20, 150 mM NaC1, 10 mM Tris, pH 7.4, and probed with a primary antibody to MAP kinase in the same fresh buffer at 4°C overnight. The membrane was washed in the buffer several times and incubated in the buffer containing secondary antibody labeled with horse radish peroxidase for 2 hr at room temperature. After washing, the immunocomplexes on the membrane were detected with an ECL kit (Amersham Life Sci., Buckinghamshire, England).

RT-PCR Measurement of *c-fos* Gene Expression

The human corneal fibroblasts were treated as above for growth factor stimulation. For detection of *c-fos* mRNA expression, the experiment of nested RT-PCR was designed as previously described (30,31). Total RNA was extracted by using TRI regent (Molecular Research Center, INC,

Cincinnati, OH). After determination of the RNA concentration, the sample was adjusted to obtain 0.25 μg/μl RNA, then 3μg of total RNA was denatured at 70°C for 10 min and subjected to reverse transcription for synthesis of cDNA by using Superscript TM II (GiBco BRL). Then, 2μg cDNA was subjected to PCR, which was amplified in 100 μl of reaction buffer containing 10 mM Tris HC1, pH 8.3, 1.5 mM $MgC1_2$, 50 mM KCL, 1.25 mM of each dNTP, 2.5 units of Taq DNA polymerase, (Qiagen, Chatsworth, CA), and 15 pmol of 'outer' primers (sense 5-AAGGTGGAACAGGTGAGGAAC-3', antisense 5'-TTGAGGAGAGGCAGGGTGAAG-3') and human glyceraldehyde-3-phosphate dehydrogenase (GAPDH) primer (sense 5'-GTCATCATCTCAGCCCCCTCCTC-3', antisense 5'-CCTAAGCCCCTCCCCTCCTCCAG-3') at 94°C for 1 min, 62°C for 1 min, 72°C for 2 mins with 30 cycles. The first round PCR products were diluted to 1:100. The nested PCR was carried out by using 2 μl of diluted PCR products as inner primer with target sequences: sense 5-CAACCGGAGGAGGGAGCTGAC -3', antisense 5'-GATCAAGGGAAGCCACAGACA-3' under the same condition with 30 cycles, human (GAPDH) primers at 94°C for 1 min, 62°C for 1 min, 72°C for 2 mins with 30 cycles. Finally, both nested PCR and control products were separated by electrophoresis on a 1.0% agarose gel and visualized by ethidium bromide staining. Using these primers, the predicted size of the *c-fos* amplicon DNA is 317 bp in human tissue and the size of GAPDH is 419 bp.

Radioimmunoprecipitation Assay of Fos Protein Synthesis

Human corneal fibroblasts were grown to confluence and continued for another 16 hr in serum-free, D-MEM medium without methionine and supplemented with 2 mM glutamine (32). The cells were treated with a growth factor or a growth factor in combination with inhibitor (as detailed

above) for 15 min, then 100 μCi/ml of ^{35}S-methionine (Dupont NEN, Boston, MA) was added for another 15 min. The medium was removed and cells were washed three times with ice-cold Trisaline, pH 7.4, and immediately lysed in a buffer containing 20 mM Tris, 150 mM NaCl, 1 mM EDTA, 0.5% deoxycholate, 1% Triton X-100, and 0.1% SDS. The lysate was centrifuged at 4°C for 15 min at 10000 rpm and the supernatant collected. An equal amount of radioactivity (4 x 10^6 cpm) was used for radioimmunoprecipitation. A polyclonal antibody (rabbit IgG) to *c-fos* protein (Santa Cruz Biotechnology, Santa Cruz, CA) was bound to protein A agarose complex. The supernatant was incubated with this complex at 4°C for 4 hr and pelleted with three washings to remove non-specific binding. The *c-fos* proteins labeled with ^{35}S-methionine were subjected to 10% SDS-PAGE. The gel was dried and exposed to film.

Cell Proliferation

Cells were seeded in 12-well plates, grown to confluence, changed to 0.5 ml/well of an essential medium containing 0.3% FBS, and continually incubated at 37°C for 24 hr. Cells were used for the following experimental groups: 1) growth factor stimulation; 2) growth factor stimulation and MEK inhibitor; and 3) normal control cells that did not receive either manipulation. Growth factor treatment to stimulate cellular proliferation was for 20 hr. For the final 4 hr, 0.5 μCi of ^{3}H-thymidine (ICN Irvine, CA) or ^{3}H-thymidine with the inhibitor was added. The medium was removed, and the cells were washed twice with PBS, fixed with 5% TCA, resolved in 2% SDS, then transferred into scintillation counting vials. Radioactive incorporation was determined by scintillation counting.

RESULTS

Growth Factors Activate MAP Kinase in Human Corneal Fibroblasts

MAP kinase activation induced by bFGF, EGF, or PDGF-bb was evaluated by measuring phosphorylation of MBP, a relatively specific substrate for MAP kinase *in vitro*. Activation following growth factor exposure was compared with PMA, a potent activator of MAP kinase (33). After stimulation for 15 min, the activity of the kinase was increased, in contrast to cells treated with inhibitor, where the kinase activity remained at essentially the same levels as in the untreated controls (Fig. 1).

We measured MAP kinase activation in a gel containing a substrate, MBP, which allows the determination of the phosphorylation of MBP by the kinase *in situ*. The results showed two bands migrating at 42 kDa and 44 kDa, which correspond to two isoforms of MAP kinase (Fig. 2). Several bands at higher molecular weight may be protein kinases which can also phosphorylate MBP. However, in order to specifically determine if this protein kinase is MAP kinase, immunoblotting and the immunoprecipitation kinase assay were used to demonstrate that the activated protein kinase is MAP kinase. The differences in the production of the activated form of the kinase in the presence of growth factors with and without inhibitor are shown in Figures 3 and 4.

The results of this experiment showed that the molecular species of MAPK activated by growth factors was the same as that induced following treatment with PMA.

Activation of the MAP Kinase Pathway Induces *c-fos*

Fos proteins play a critical role in fibroblast proliferation and have been thought of as key components of the transcription factor complex, AP-1. Moreover, activation of MAP kinase has been

shown to be correlated to the initiation of cell cycle transition and proliferation. These experiments were designed to investigate the relationship between MAP kinase activity, *c-fos* gene expression and Fos protein production. To rule out any artificial events in RT-PCR experiments, a "housekeeping" gene, GAPDH, was used as a control under the same condition in all reaction steps. The data indicated that the RT-PCR results were of high quality and reliable. An increase in *c-fos* mRNA expression was found following growth factor stimulation, but in the cells exposed to the MEK inhibitor, the amount of c-fos mRNA expression remained at the control level (Fig. 5). Downstream of *c-fos* mRNA expression, Fos protein production was determined by ^{35}S-methionine uptake. The results showed a significant increase in the production of Fos protein in cells treated with growth factors. In contrast, in the cells that were treated with growth factors but had the activation of the MAP kinase pathway blocked with the MEK inhibitor, protein production was much lower, compared with the cells that did not undergo the inhibition treatment (Fig. 6). In this procedure, radioimmunoprecipitation was used to detect the amount of ^{35}S-methionine uptake in the cells. Fos protein measured here was newly synthesis in the cells. The results of RT-PCR and ^{35}S-methionine uptake indicated that activated MAP kinase can upregulate *c-fos* gene expression and protein production in human corneal fibroblasts, but inhibition of MAP kinase phosphorylation can abolish both *c-fos* gene expression and protein production, even in the presence of growth factors.

Activation of the MAP Kinase Pathway and Cell Proliferation

We have demonstrated that growth factors can induce an increase in the phosphorylation of p42 and p44 MAPK, and that PD98059 can inhibit MAP kinase activation and abolish Fos protein production in human corneal fibroblasts. However, the increase in *c-fos* protein accumulation

following growth factor stimulation must be shown to be related to cell proliferation since Fos protein production has been shown to be associated with cell differentiation as well as apoptotic cell death. We next used ^{3}H-thymidine uptake to determine if the increase in *c-fos* protein accumulation after activation of MAP kinase is associated with cell proliferation. The results of this experiment showed that growth factors enhance ^{3}H-thymidine uptake dramatically; however,^{3} H-thymidine incorporation induced by growth factor stimulation was abolished by inhibiting MAP kinase activation with PD98059, as was Fos protein production by pretreatment with the inhibitor of the enzyme activating MAPK (Fig. 7). This result suggested that activation of the MAP kinase pathway is required for the mitogenic effect of the growth factors on human corneal fibroblasts.

DISCUSSION

The results of the present study have confirmed that bFGF, EGF, and PDGF-bb induce a rapid activation of MAP kinase in human corneal fibroblasts. The criteria for this have included increased phosphorylation of MBP *in vitro* by treated crude cell extracts and by the proteins immunoprecipitated from the extracts with a specific antibody to MAP kinase. The substrate for MAP kinase was also phosphorylated at 44 kDa and 42 ka in SDS gels. Two high-density bands were detected in the cells treated with growth factors using a specific antibody to activated MAP kinase. On the other hand, in the cells treated with growth factors and the inhibitor, there was little change in the kinase activity when compared to non-stimulated cells. These results strongly suggest that the activated kinase detected is MAP kinase.

The growth factors treated in this study activate different membrane-associated receptors (35-38). bFGF binds preferentially to FGFR-1 and FGFR-2, which have been found to be expressed in

human corneal fibroblasts. The receptor for EGF is a 170 kDa transmembrane tyrosine kinase receptor which was detected in full-thickness cornea tissues by immunofluorescence staining and expressed in corneal fibroblasts. PDGF-bb is an isoform that is a potent mitogen and can bind to both a and b receptor subtypes. However, only PDGFR-b has been shown to be expressed in human corneal fibroblasts (3). The receptors of these growth factors are characteristic for tyrosine kinase activity, and there is a great degree of commonality in the types of receptors for intracellular signaling pathways initiated by the proteins. Binding of these growth factors to the extracellular domain of the receptor activates the tyrosine kinase in the cytoplasmic domain, leading to downstream activation of a number of signaling molecules including Ras, Raf, MEK, and MAP kinase (34-39). In the MAP kinase pathway, there are three protein kinase cascades consisting of a serine/threonine protein kinase; MAPKKK, which activates a dual-specific protein kinase; and MAPKK (or MEK), which in turn phosphorylates MAP kinase. Introduction of an anti-Ras antibody or deletion of the Ras gene can block this signal transduction pathway and eliminate the effects of these growth factors (38,39). This indicates that bFGF, EGF, and PDGF-bb activate common upstream component or components, and commonality in the downstream MEK1 component is shown in the present study by the fact that the inhibitor blocked the stimulatory effects on all of the anticipated outcomes of MAP kinase activation.

Previous studies indicate that activated MAP kinase can translocate into the nucleus, where it regulates *c-fos* gene expression and *c-fos* protein production (23,40). The Fos protein and pre-existing Jun protein form a hetero-dimer, which forms the AP-1 transcription factor, resulting in high levels of AP-1 DNA binding activity (23,24,41). The *c-fos* protein has been implicated as a key molecule in cell proliferation, differentiation, and transformation, but Fos protein has also been

associated with apoptotic cell death in response to cellular injury (42,43). That study suggested that Fos protein plays a causal role in the activation of apoptosis in a p53-dependent manner, but the Fos protein functioning as a transcriptional repressor is not newly synthesized (42).

Our study demonstrated that growth factors activate MAP kinase; subsequently, activated MAP kinase can enhance Fos protein accumulation, which was confirmed to be a newly synthesized protein by radioimmunoprecipitation assay with ^{35}S-methionine uptake. This suggestion is reinforced by the parallel experiment, which showed that the inhibitor blocks activation of MAP kinase and abolishes Fos protein and *c-fos* message production, as well as DNA synthesis. We observed that growth factors activate MAP kinase, which is associated with an increase in protein production and DNA synthesis in human corneal fibroblasts. This result is in agreement with previous observations that cell cycle transition into proliferation is related to activation of MAP kinase. MAP kinase also enhances the activity of transcriptional factor AP-1 by upregulation of *c-fos* protein production (23). The phenomena of a parallel relationship between MAP kinase activity and the mitogenic effect suggested that activation of MAP kinase is required for growth factor stimulation to drive human corneal fibroblast proliferation. This signal transduction pathway serves to link the signals from the cellular surface into cytoplasmic and nuclear events. Experiments that have injected oncogenic Ras or Raf into quiescent fibroblasts have shown stimulation of DNA synthesis in the absence of the growth factors, bFGF, EGF, or PDGFbb (44-48). This suggests commonality of upstream components from MAPK and the activation of nuclear events; however, intracytoplasmic activation remains to be completely elucidated.

Investigations *in vivo* and *in vitro* have demonstrated that growth factors accelerate corneal wound healing in a variety of ways including an increasing activity and growth of cells in all corneal

layers and by enhancement of corneal tensile strength (4,11,49). Growth factors can promote stromal fibroblasts to migrate to the site of injury, proliferate, and then synthesize extracellular matrix molecules, such as collagen (7). On the other hand, growth factors also stimulate the synthesis of fibronectin, hyaluronic acid, and collagenase, and cell adhesion and migration also require activation of MAP kinase (50). The results of this study and previous investigations suggest a mechanism of how growth factors act to regulate these important cellular functions. Initially, growth factors bind to tyrosine receptors on the cell membrane triggering autophosphorylation of the cytoplasmic domain of the receptor and downstream activation of the MAP kinase cascade. Serial phosphorylation of intracellular protein cascades with nuclear translocation results in the upregulation of *c-fos* gene transcription and the Fos protein product with increased AP-1 activity. The subsequent activation of a large number of genes required for DNA synthesis moves the cell into a round of cell division, increasing the activity of the wound response. However, it should be borne in mind that *in vivo* responses to injury are complex biological processes and more sophisticated mechanisms will probably be discovered in future studies.

REFERENCES

1. McAvoy JW, Chamberlain CG. Growth factors in the eye. Prog Growth Factor Res 1990;2:29-43.

2. Lopez JG, Chew SJ, Thompson HW, et al. EGF cell surface receptor quantitation on ocular cells by an immunocytochemical flow cytometry technique. Invest Ophthalmol Vis Sci 1992;33:2053-2062.

3. Li DQ, Tseng SCG. Three patterns of cytokine expression potentially involved in epithelial-fibroblast interactions of human ocular surface. J Cell Physiol 1995;163:61-79.

4. Schulz G, Khaw PT, Oxford K, et al. Growth factors and ocular wound healing. Eye 1994;8:184-187.

5. Ohashi Y, Motokura M, Kinoshita Y, et al. Presence of epidermal growth factor in human tears. Invest Ophthalmol Vis Sci 1989;30:11879-11882.

6. David T, Rieck P, Renard G, et al. Corneal wound healing modulation using basic fibroblast growth factor after excimer laser photorefractive keratectomy. Cornea 1995;14:227-234.

7. Stern ME, Waltz KM, Beuerman RW, et al. Effect of platelet-derived growth factor on rabbit corneal wound healing. Wound Rep Reg 3:59-65, 1995.

8. Assouline M, Chew SJ, Thompson HW, et al. Effect of growth factors on collagen lattice contraction by human keratocytes. Invest Ophthalmol Vis Sci 1992;33:1742-1755.

9. Brazzell RK, Stern ME, Aquavella JV, et al. Human recombinant epidermal growth factor in experimental corneal wound healing. Invest Ophthalmol Vis Sci 1991;32:336-390.

10. Tripathi RC, Kolli SP, Tripathi BJ. Fibroblast growth factor in the eye and prospects for its therapeutic use. Drug Dev Res 1990;19:225-237.

11. Beaubien J, Biosjoly HM, Gagnon P, et al. Mechanical properties of the rabbit cornea during wound healing after treatment with epidermal growth factor. Can J Ophthalmol 1994;29:61-65.

12. Beuerman RW, Thompson HW. Molecular and cellular responses of the corneal epithelium to wound healing. Acta Ophthalmol 1992;70(Suppl):7-12.

13. Jester JV, Petroll WM, Barry PA, et al. Temporal, 3-dimensional, cellular anatomy of

corneal wound tissue. J Anat 1995;186:301-311.

14. Garana RMR, Petrol WM, Chen WT, et al. Radial keratotomy. II. Role of the myofibroblast in corneal wound contraction. Invest Ophthalmol Vis Sci 1992;33:3271-3282.

15. Murali S, Hardten DR, DeMartelaere S, et al. Effect of topically administered platelet-derived growth factor on corneal wound healing strength. Curr Eye Res 1994;13:857-862.

16. Lubinus M, Meier KE, Smith EA, et al. Independent effects of platelet-derived growth factor isoform on mitogen-activated protein kinase activation and mitogenesis in human dermal fibroblasts. J Biol Chem 1994;269:9822-9825.

17. Cano E, Mahadevan LC. Parallel signal processing among mammalian MAPKs. Trends Biochem Sci 1995;20:117-122.

18. Seger R, Krebs EG. The MAPK signaling cascade. FASEB J 1995;9:726-735.

19. Seger R, Seger D, Reszka D, et al. Overexpression of mitogen-activated protein kinase (MAPKK) and its mutants in NIH - 3T3 cells: evidence that MAPKK involvement in cellular proliferation is regulated by phosphorylation of serine residues in its kinase subdomains VII and VIII. J Biol Chem 1994;269:25699-25709.

20. Pages G, Lenorman P, L Allemain G, et al. Mitogen-activated protein kinases p42mapk and p44mapk are required for fibroblast proliferation. Proc Natl Acad Sci USA 1993;90:8319-8323.

21. Janknecht R, Ernst WH, Pingoud V, et al. Activation of ternary complex factor Elk-1 by MAP kinases. EMBO J 1993;12:5097-5104.

22. Gille H, Kortenjiann M, Strahl T, et al. Phosphorylation-dependent formation of a quaternary complex at the *c-fos* SRE. 1996;16:1094-1102.

23. Karin M. The regulation of AP-1 activity by mitogen-activated protein kinases. J Biol Chem 1995;270:16483-16486.

24. Angel P, Karin M. The role of Jun, Fos and the AP-1 complex in cell-proliferation and transformation. Biochim Biophys Acta 1991;1072:129-157.

25. Meloche S. Cell cycle reentry of mammalian fibroblasts is accompanied by the sustained activation of P44Mapk and P42mapk isoform in the G1 phase and their inactivation at the G1/S transmission. J Cell Physiol 1995;163:577-588.

26. Dudley DT, Pang L, Decker SJ, et al. A synthetic inhibitor of the mitogen-activated protein kinase cascade. Proc Natl Acad Sci USA 1995;92:7686-7689.

27. Pang L, Sawanda T, Decker SJ, et al. Inhibition of MAP kinase blocks the differentiation of PC-12 cells induced by nerve growth factor. J Biol Chem 1995;270:13585-13588.

28. Lu G, Beuerman RW, Zhao SR, et al. Tumor necrosis factor alpha and interleukin-1 induced activation of MAP kinase and SAP kinase in human neuroma fibroblasts. Neurochem Int 1997;30:401-410.

29. Chen CT, Pan BT. Oncogenic Ras stimulates a 96-kDa histone H2b kinase activity in activated *Xenopus* egg extracts. J Biol Chem 1994;269:28024-28043.

30. Platt JE, He X, Tang D, Slater J, et al. *C-fos* expression in vivo in human lymphocytes in response to stress. Prog Neuropsychopharmacol Biol Psychiatry 1995;19:65-74.

31. Schafer H, Zheng J, Gundlach F, et al. PACAP stimulates transcription of *c-fos* and c-jun and activates the AP-1 transcription factor in rate pancreatic carcinoma cells. Biochem Biophys Commun 1996;221:111-116.

32. Brach MA, Gruss HJ, Sott C, et al. The mitogen response to tumor necrosis factor alpha requires c-Jun/AP-1. Mol Cell Biol 1993;13:4284-4290.

33. Adams PD, Parker PJ. TPA-induced activation of MAP kinase. FEBS Lett 1991;290:77-82.

34. Givol D, Yaon A. Complexity of FGF receptors: genetic basis of structural diversity and functional specificity. FASEB J 1992; 6:3362-3369.

35. Klagsburn M. The fibroblast growth factor family: structural and biological properties. Prog Growth Factor Res 1989;1:207-235.

36. Westermark B, Claesson-Welsh L, Heldin CH. Structural and functional aspects of the receptors for platelet-derived growth factor. Prog Growth Factor Res 1989;1:253-266.

37. Hsuan JJ, Panayotou G, Waterfield MD. Structural basis for epidermal growth factor receptor function. Prog Growth Factor Res 1989;1:253-266.

38. Marshall CJ. Specificity of receptor tyrosine kinase signaling: transient versus sustained extracellular signal-regulated kinase activation. Cell 1995;80:179-185.

39. Lange-Carter CA, Johnson GO. Ras-dependent growth factor regulation of ME kinase in PC-12 cells. Science 1994;265:1458-1461.

40. Lenormand P, Sardet C, Pages G, et al. Growth factor induces nuclear translocation of MAP kinases (p42mapk and p44mapk) but not of their activator MAP kinase (p45mapk) in fibroblasts. J Cell Biol 1993;122:1079-1088.

41. Whitmarsh AJ, Davis RJ: Transcription factor AP-1 regulation by mitogen-activated protein kinase signal transduction pathways. J Mol Med 1996;74; 589-607.

42. Preston GA, Lyon TT, Yin YX, et al. Induction of apoptosis by *c-fos* protein. Mol Cell Biol 1996;16:211-218.

43. Verrier B, Muller D, Bravo R, et al. Wounding a fibroblast monolayer results in the rapid induction of the *c-fos* proto-oncogene. EMBO J 1986;5:913-917.

44. Moodie SA, Willusen BM, Weber MJ, et al. Complexes of Ras - GTP with Raf-1 and mitogen-activated protein kinase. Science 1993;260:1658-1661.

45. Treisman R. Ternary complex factors: Growth factor regulated transcriptional activators. Curr Opin Genet Dev 1994;4:96-101.

46. Thomas SM, DeMarco M, D'Arcangelo G, et al. Ras is essential for nerve growth factor- and phobol ester-induced tyrosine phosphorylation of MAP kinases. Cell 1992;68:1031-1040.

47. Troppmair J, Bruder JT, App H, et al. Ras controls coupling of growth factor receptors and protein kinase C in the membrane to Raf-1 and B-raf protein serine kinases in the cytosol. Oncogene 1992;7:1867-1873.

48. Miltenberger RJ, Cortner J, Farnham PJ. An inhibitory Raf-1 mutuant suppresses expression of a subset of v-raf-activated genes. J Biol Chem 1993;268:15674-15680.

49. Crosson CE, Klyce SD, Beuerman RW: Epithelial wound closure in the rabbit cornea. Invest Ophthalmol Vis Sci 27: 464-473, 1986.

50. Klemke RL, Cai S, Giannini AL, et al. Regulation of cell motility by mitogen-activated protein kinase. J Cell Biol. 137:481-492, 1997.

FIGURE LEGENDS

Fig. 1. Growth factors induce and MEK1 inhibitor prevents phosphorylation of myelin basic protein (MBP). Human corneal fibroblasts were treated with 10 ng/ml bFGF, 20 ng/ml EGF, 20 ng/ml PDGF-bb, and 300 ng/ml PMA alone for 15 min or in combination with inhibitor (I). Gross cell lysates were incubated in kinase assay buffer containing [r-^{32}P] ATP and MBP. Phosphorylation of MBP was determined by the protein kinase assay. Statistical analysis (Student's *t*-test) showed that growth factor-treated cells demonstrated greater amounts of MAPK activity, compared to control cells ($p=0.05$ or better for all cases). Inhibition of MAPK activity was significant in all situations (βFGF, $p=0.04$; EGF, $p=0.01$; PDGF, $p=0.04$; PMA, $p=0.01$).

Fig. 2. The inhibitor blocks growth factor activation of 44 kDa and 42 kDa protein kinases. In these experiments, 20 μl of cell extract were subjected to 10% polyacrylamide gel containing 0.1 mg/ml of MBP. After electrophoresis, the gel was treated as indicated in Materials and Methods and the protein kinase was detected. Right side of panel indicates molecular weight.

Fig. 3. The inhibitor PD98059 abolished growth factor increases of the active form of MAP kinase. Equal volumes of cell lysates, treated or untreated, were separated by 12% SDS-PAGE. The protein in the gel was transferred onto a membrane and blocked with a primary antibody specific to the active form of MAP kinase, p44MAPK and p42MAPK. The immunocomplex on the membrane was detected with a secondary antibody labeled with horseradish peroxidase.

Fig. 4. PD98059 inhibition of growth factor-induced activation of MAP kinase. Anti-MAP kinase antibody was bound to protein A-agarose beads, and this complex was incubated with diluted cell lysate at 4° C for 4 hours. The precipitated MAP kinase protein was assayed by the phosphorylation of MBP by the presence of [r-^{32}P] ATP. The phosphorylated MBP was resolved in SDS-PAGE and dried for autoradiography.

Fig. 5. Regulation of *c-fos* gene expression in human corneal fibroblasts. The cells were treated as described in Materials and Methods and total RNA was extracted from the cells. Nested RT-PCR was carried out with GAPDH as an internal control. PCR products were resolved in a 1% agarose gel and visualized by ethidium bromide staining. The predicted size of the *c-fos* amplicon DNA is 317 bp and GAPDH is 419 bp. DNA base pair ladder markers are provided to the left of the panel.

Fig. 6. Inhibition of MAP kinase activation and elimination of *c-fos* protein synthesis. Confluent cells were starved in serum- and methionine-free medium for 16 hours, and treated with growth factors or growth factors plus inhibitor for 15 min. Then ^{35}S-methionine was added for another 15 min and lysated. Equal amounts of radioactivity were used for immunoprecipitation with antibody to Fos protein. The immune-complexes were subjected to SDS-PAGE and exposed to film.

Fig. 7. Human corneal fibroblast proliferation requires activation of MAP kinase. The cells grown to confluence were cultured in medium containing growth factors for 20 hours. For the final 4 hours, ^{3}H-thymidine or ^{3}H-thymidine with inhibitor (I) was added, the cells were washed, fixed with 5% TCA, resolved in 2% SDS, and transferred into scintillation counting. The means and standard errors

for three independent experiments are shown. Statistical analysis showed that cell proliferation was significantly increased by the presence of the growth factor or PMA ($p=0.03$ or greater).

Figure 1.

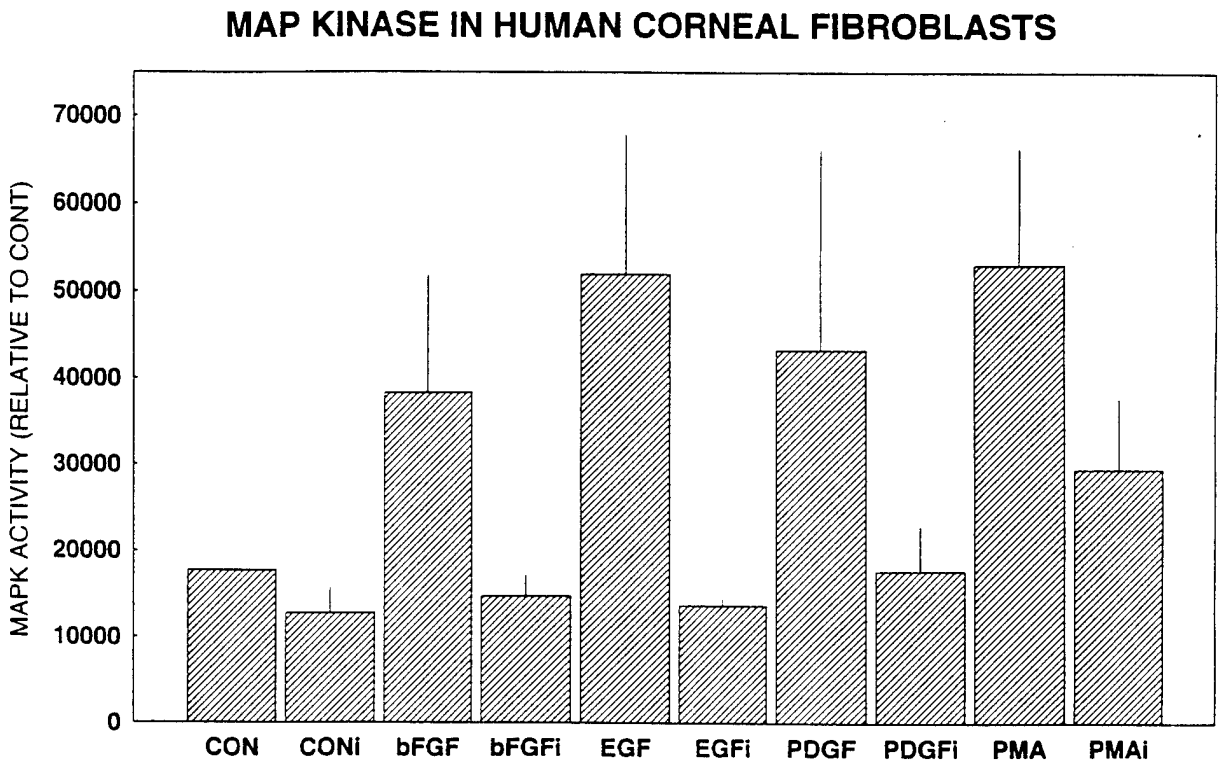
MAP KINASE IN HUMAN CORNEAL FIBROBLASTS
MAPK ACTIVITY (RELATIVE TO CONT)
70000
60000
50000
40000
30000
20000
10000
0
CON
CONi
bFGF
bFGFi
EGF
EGFi
PDGF
PDGFi
PMA
PMAi

Figure 2.


PMAi
PMA
PDGFi
PDGF
EGFi
EGF
bFGFi
bFGF
CON
220kD-
97kD-
66kD-
46kD-
30kD-

Figure 3.

Figure 4.

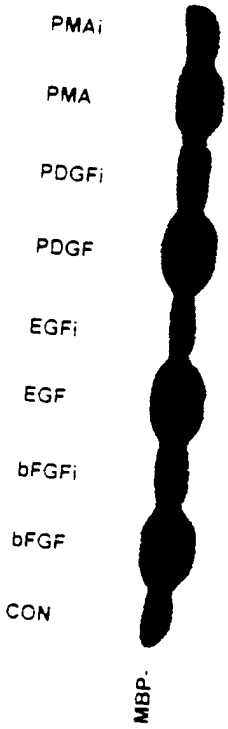

Figure 5.

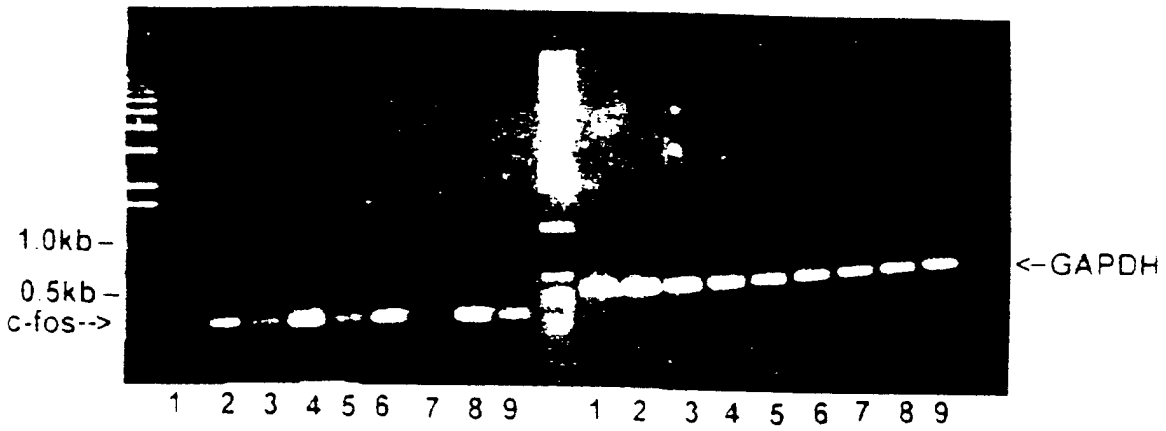

Figure 6.

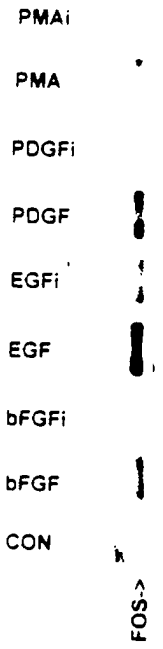

Figure 7.

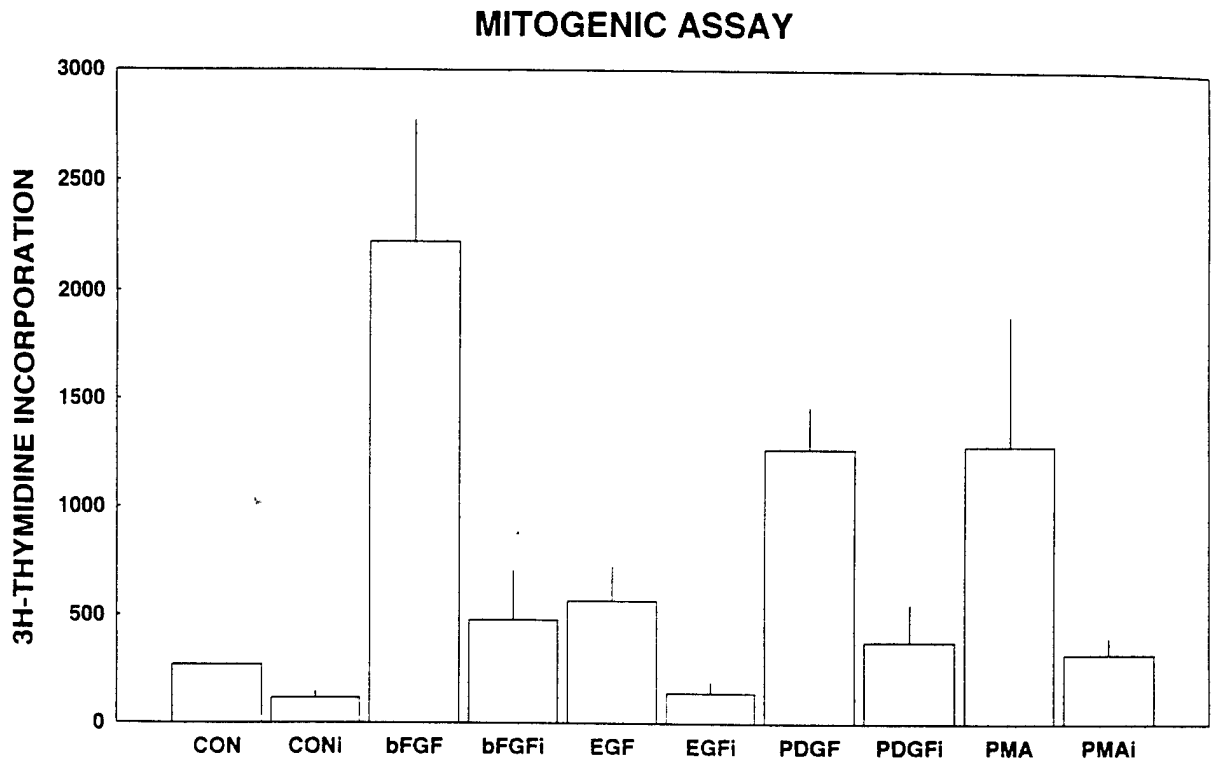
MITOGENIC ASSAY
3H-THYMIDINE INCORPORATION
3000
2500
2000
1500
1000
500
0
CON
CONi
bFGF
bFGFi
EGF
EGFi
PDGF
PDGFi
PMA
PMAi

IV. Expression of *c-fos* Protein in the Spinal Cord After Brachial Plexus Injury: A Comparison of Root Avulsion with Distal Nerve Transection

SUMMARY

To simulate an injury of the brachial plexus, adult male rats underwent an experimental injury while under transient anesthesia produced by halothane inhalation. The brachial plexus was lesioned by either root avulsion close to the spinal cord in one group, or distal nerve transection in the second group. The rats quickly revived, remained awake until sacrifice at 30, 60 and 120 min post-operatively. In rats with avulsive injury, traumatic sites on the dorsal horn and the ventral horn of the spinal cord were microscopically detected. Expression of c-*fos* protooncogene in the spinal cord was detected by immuno-cytochemistry for the Fos product. The two experimental groups were compared with each other and with the sham control animals at the same survival times. An increase in Fos-like immunoreactivity (FLI) in cells of the spinal cord at levels C4 to T1 was detected at 30 min after nerve transection or root avulsion. The number of FLI-positive cells continued to rise at 60 and 120 min post-nerve injury ($p=0.001$). FLI-positive cells compared at level C7 in laminae 1-2, 3-4, and 5-10 after the two treatments were found to be significantly more abundant after avulsion injury ($p=0.0001$); also, the number of positive cells continued to increase over time after injury ($p=0.001$). At all levels, both experimental groups demonstrated significantly greater numbers of positive cells than the controls; the group with nerve root avulsion showed significantly ($p = 0.0001$) greater incrases in positive cells compared with the group with distal nerve transection. These results suggest that nerve root avulsion of the spinal cord leads to heightened and prolonged expression of c-*fos* and potentially, transcription of new messages for cell recovery, cell survival, or cell death.

INTRODUCTION

Peripheral nerve damage is often part of the scenario resulting from extremity injury. Moreover, avulsion of one or more roots of the spinal cord happens in approximately 70% of severe brachial plexus stretch avulsion injuries (1). Nerve section at a distance from the dorsal root ganglion and spinal cord has classically been found to result in chromatolysis of sensory and motor neurons. Molecular responses in the cell body result in the increased transcription of novel messenger RNAs, which are involved in the production of structural and membrane proteins and which regulate the consequences and recovery from injury (2,3). In contrast, severe injury proximal to the brachial plexus or the lumbo-sacral plexus may have more deleterious long range consequences, accompanied by increased neuronal death. Permanent but variable losses in motor and/or sensory functions are common findings in such patients. The retrograde damage to the neuron resulting from injury close to the plexus can often be serious enough to be incompatible with neuronal survival (4).

Traumatic or ischemic injuries to the central nervous system initiate reactive molecular and biochemical changes, some of which are autodestructive and others neuroprotective (5). After peripheral nerve injury or various types of stimulation, an immediate-early gene (IEG), c-*fos*, has been shown to appear rapidly within cells of the spinal cord (6-15). This gene codes for the Fos protein products, which forms the Fos/Jun dimer, and binds to the consensus AP-1 binding site, regulating the expression of other genes (16). Avulsive injury of the brachial plexus close to the spinal cord is suggested to lead to severe degeneration of the neurons in the spinal cord when compared with distal peripheral nerve injury. Previous studies have shown that transection or crush of the rat sciatic nerve will induce expression of c-*fos* in the dorsal root ganglia, spinal cord, and higher centers (7,17-19). However, the expression of c-*fos* has not been investigated after an injury

close to the spinal cord, such as brachial plexus avulsive injury, which results in a more serious and complex neurosurgical problem and poorer outcome (20).

In the present study, the brachial plexus nerves were injured in rats by either avulsive injury of the brachial plexus close to the spinal cord, or by distal transection of the branches of the brachial plexus. The expression of Fos-protein in the rat spinal cord was investigated by using an immunocytochemical method and the number of neurons revealing FLI were quantified to compare the difference in neuronal responses in the spinal cord after these two types of injury. A variable time course of the appearance of c-*fos* protein increases in the CNS under different pathological conditions has been described (21). The largest change in positive Fos-like immunoreactivity was found to be within 2 hours after peripheral nerve injury or noxious stimulation (19,22). In the present study, FLI was found to increase over control after 30 minutes, but the avulsive injury resulted in significantly more positive cells than the distal nerve transection at 30, 60, and 120 minutes post-injury.

METHODS AND MATERIALS

Animal Model and Surgical Procedure

Male Sprague-Dawley rats (270-350 gram) were anesthetized by halothane inhalation. The brachial plexus (C4 to T1) was exposed from the outlet of the vertebrae down to the axilla by a ventral, midline incision extending to the axilla on both sides. After the skin and subcutaneous tissues were cut, sternohyoideus muscles were separated from the midline. The muscles were retracted laterally so that cervical vertebraes could be exposed. The cervical nerves 4 to 8 and thoracic nerve 1 were carefully separated from paraspinal muscles. All of the branches, except for

small dorsal branches, which were cut as far distally as possible, were separated and prepared to be used for one of the injury procedures. The following procedures were applied to rats randomly assigned to one of three groups: 1) In the first group, nerve roots of C4 to T1 were rapidly stretched out from the spinal cord with a small hemostat; the dorsal root ganglia were mobilized in the process. 2) In the next treatment group, the same nerves were cut from 1.5 to 2.5 cm from the spinal cord. 3) In the third group (sham controls), incisions were made without nerve injury. The time for the operation was about 10 min. The rats began to move their lower limbs and to awaken about 3 minutes after the halothane was eliminated.

Specimen Processing and Immunocytochemistry

The rats were anesthetized at 30 minutes, 60 minutes and 120 minutes with phenobarbital (IP), and prepared for perfusion through the heart with 250 ml saline followed by 250 ml of 4% paraformaldehyde. The spinal cord at levels C4 to T1 was removed and post-fixed in 4% paraformaldehyde for 4 hours and immersed for 24 hrs in 30% sucrose in PBS. Frozen sections of 40 μm were cut and processed for the avidin-biotin immunohistochemical procedure using the peroxidase Vectastain Elite ABC Kit (Vector Laboratories, Burlingame, CA) and the protocol suggested by the manufacturer. For detecting FLI, the sections were incubated in a 1:500 concentration of a polyclonal antibody for Fos protein (PC05, Oncogene Science, Uniondale, NY). Control sections were incubated in the presence of Fos peptides (PC09, PC10, Oncogene Science, Uniondale, NY) to which the antibodies were raised. After the DAB reaction was completed, sections were air dried, mounted, and cover slipped.

Quantification of Neurons with FLI

The sections were studied with darkfield and brightfield microscopy, and projection drawings were made using a camera lucida attachment (13,23). To map the pattern of cells that expressed Fos immunoreactivity, outlines of the C4 to T1 segments were drawn and the distribution of FLI neurons plotted onto the drawing under darkfield illumination. FLI-positive cells of spinal cord segments of C4 to T1 were counted. Labeled cells from three random histological sections in each segment were counted and averaged. Individual counts of grouped laminae were made to discern potential differences between the sensory and motor systems. Thus, laminae were grouped as follows: 1 and 2, 3 and 4, and 5-10. The counts were made by an investigator (YP) who was blind to the particular treatment that the animals received. Statistical analysis of the data was obtained by the use of the Statistical Analysis System program on an IBM-compatible computer (SAS Institute Inc. SAS Language Reference. Version 6. Cary, NC: SAS Institute, 1990). An analysis of variance was carried out to compare the effects of the sham procedure with the two treatments, nerve section and nerve avulsion, with the segment level of the spinal cord and also the time after each injury. The level of significance reported as statistically significant was p less than or equal to 0.05. Protected t-tests on least square means derived from the ANOVA were used to compare the interactions between treatment, spinal cord level, and time as well as the differences between the lamina. The means and standard errors were processed with Excel (Microsoft Corp, Seattle, WA) to plot out the histograms.

RESULTS

Spinal Cord Injury

Examination of the spinal cord and dorsal root ganglia at the time of sacrifice indicated that

the sham and distal nerve transection procedures had no effect on the normal structural appearance as seen under an operating microscope. On the other hand, bleeding within the dural cavity was seen in each rat with avulsive injury. The spinal cord injuries in the rats with avulsive injury could be seen under the microscope. Both the dorsal horn and the ventral horn were traumatically injured (Fig. 1, C and D). Most lesions on the dorsal horn were found in the superficial laminae 1 and 2. There were many neurons located within 100 μm of the lesion sites. Lesion sites were also detected within the ventral horns. Many motor neurons were close to the lesion sites.

Fos Protein Expression

In normal rats (n=2) quickly killed by pentobarbital and without any operative procedures, almost no FLI cells were seen in the spinal cord segments C4 to T1. However, the baseline statistical comparisons were made with a group of sham control animals that underwent the same halothane anesthesia, skin incision, and revival for 30 minutes, 60 minutes, and 120 minutes.

The sham control rats had a slight but non-significant increase in the number of FLI neurons in the medial half of the superficial dorsal horn (Fig.1). These segments corresponded to the termination site of cutaneous nerve afferents from the incision area (18,24).

Both experimental groups demonstrated greater Fos-like immunoreactivity than the sham operated animals. FLI detection in the spinal cord showed increased number of cells exhibiting c-*fos* protein expression 30 min postoperatively and at all postoperative times thereafter ($p = 0.0001$). The levels continued to rise from 30 to 60 min and from 60 to 120 min post-nerve injury (Fig. 2). The increased number of cells expressing FLI appeared mainly in the spinal cord from laminae 1 to 7 and 10, with the greatest number in laminae 1 and 2 (Fig. 3). The distribution was similar from 30 min

to 120 min in both nerve root avulsion and nerve transection. However, FLI increased more rapidly after nerve avulsion than after distal section. Thirty minutes after the procedures, the number of positive neurons was significantly greater for animals with nerve avulsion than for those with nerve section. The differences continued to exist at 60 min and 120 min postoperatively (Figs. 2 and 3). There were more neurons positive for FLI from superficial to the deep laminae of spinal cord in the rats with nerve root avulsion than in those with distal transection, especially in laminae 1 and 2 (Fig. 4; $p=0.0001$).

In the rats with nerve root avulsion, there were many neurons expressing Fos-protein in laminae 1 and 2 close to the lesion site at spinal cord levels C-6 and 7 of the dorsal horn (Fig.1). Expression of c-*fos* in the motor neurons was less distinctly detected in rats with distal nerve transection, but quite a few motor neurons were found to express c-*fos* in the nerve root avulsion animals (Fig. 1).

Analysis of the positive cell counts for c-*fos* for treatments showed that overall the avulsion injury stimulated c-*fos* expression in significantly more cells at all times after surgery ($p=0.0001$) (means ± s.e. 29.4± 0.3 and 19.5 ± 0.3, avulsion and nerve section, respectively). Cells expressing FLI immunoreactivity were also significantly greater in number even when the effect of the two injuries was considered at the three times after injury ($p=0.0001$). The primary effect on evoking FLI immunoreactivity was seen at levels C6 and C7 (Fig. 1 and 2). Moreover, at 2 hrs FLI expression was significant ($p=0.0001$) for all of these comparisons except for the 0.5 hr cell count at level C7, which was significant at the $p=0.0023$ level.

The increased number of cells expressing FLI appeared mainly in the spinal cord from laminae 1 to 7 and 10, with the greatest number in laminae 1 and 2 (Figures 1 and 4). Analysis of

the laminae at spinal cord level C-7 showed the clear effect of mechanical disruption of the cells of the dorsal horn compared to the more ventral lying neurons. Comparisons of laminae 1-2, 3-4, and 5-10 at the three times showed that the laminae and experimental treatment were significant ($p = 0.01$) and that the increased expression from 30 minutes to 120 minutes was significant at the $p=0.0001$ level. However, detailed statistical analysis of the data showed that this was primarily from increased FLI in laminae 1-2 at 60 minutes and 120 minutes (both comparisons with 3-4 and 5-10 found these to be significant at the $p=0.001$ level). Analysis of laminae 5-10 at all times showed no difference between avulsion and nerve transection at any of these times. However, if the positive spinal motor neurons were counted separately, the avulsion procedure would show an increase in FLI expression in this group.

DISCUSSION

Brachial plexus injury is commonly found following trauma by acceleration of the head, neck, and upper limbs (1,20). This injury usually causes a serious functional problem in the injured upper extremity. Disability is attributed to the fact that many neurons undergoing axonectomy do not survive. The current study provides evidence that avulsion close to the spinal cord may cause bleeding into the intra-dural cavity and spinal injury. There is no doubt that all the injuries to the dorsal horn and ventral horn can cause serious functional problems because of cell loss. Fos-like immunoreactivity in the neurons of the spinal cord is a marker used to map changes in neuronal activity following noxious or non-noxious stimulation (7,14,16,17,22,25). An increase in c-*fos* expression has been demonstrated in rats with sciatic nerve transection or crush (18,19,26,27). In this study, we detected elevated levels of Fos-like protein in the spinal cord of rats with either nerve root

avulsion or distal transection.

It is suggested that c-*fos* may participate in the regulation of increased opioid gene expression in the spinal cord; incrases in the products of the opioid family, including preprodynorphin and preproenkephalin, were induced in the spinal cord by peripheral inflammation (8). Other authors found that electroacupuncture can suppress c-*fos* expression; this effect was through to be mediated either by opiate sensitive circuitry or by non-opiate neurotransmitters (15). Anesthetics and systemic morphine can suppress c-*fos* expression and local anesthetic blockade of these neurons significantly decreased the number of FLI neurons (18,19,22,28). In the current study, the animals underwent nerve injury then were rapidly awakened, which may decrease the effects of anesthesia on *c-fos* protein expression.

Local stimulation by electricity or N-methyl-D-aspartate can induce c-*fos* expression of spinal neurons (29). In the current study, only the primary sensory neurons and motor neurons were stimulated directly in the animals with distal transection of spinal nerves. However, in the animals with nerve root avulsion, postsynaptic neurons located in the dorsal horn might be directly stimulated due to the injury to the spinal cord. The *c-fos* expression in rats with nerve root avulsion was more intense than that following distal nerve transection.

After axonectomy, apoptosis may be initiated in the lesioned neurons (30-32). Apoptosis is considered as a highly regulated process that ultimately leads to neuronal cell death. Cells undergoing apoptosis can be identified by cell shrinkage, chromatin condensation, and cellular fragmentation (33). It is interesting that some proteins that function as modulators in cell proliferation and differentiation also regulate the apoptotic process (34,35). The Fos protein appeared rapidly within the spinal neurons following nerve injury (13,26). This protein has been shown to

function as an activator to control subsequent transcription of other genes, the products of which could be required for long-term changes in neuronal excitability and repair (28,36). More recently, Fos protein has been demonstrated to function as a primary modulator of apoptotic cell death or programmed death (35,37,38). It is also reported that transection of sciatic nerve induced increased expression of c-*fos* and apoptosis in the spinal neurons (39). Our study showed that in the early stage of peripheral nerve injury, avulsion close to the spinal cord could damage the spinal cord gray matter, suggesting more intense stimuli to the spinal neurons compared with distal nerve transection. This pronounced induced c-*fos* expression in the neurons of the spinal cord may play a role in the apoptotic process, which may result in greater neuronal cell death in nerve root avulsion than in distal nerve transection. Loss of cells in the gray matter of the spinal cord is responsible for the functional deficit.

The relationship between neuronal degeneration and the remaining dendrite length after dendrite transection was investigated in cell culture (40-42). Dendrites were amputated at lesion distances of either 50 microns or 100 microns from their perikarya. Operated neurons showed ultrastructural damage that spread from the transection site towards the perikaryon within 15 min. The probability of cell survival was closely related to the remaining dendrite length. The neurons with the longer dendrites had a higher survival rate. The current study showed that in nerve root avulsion, the spinal cord can be seriously damaged, and neurons in the dorsal horn and the ventral horn can be injured. Many neurons may be axonectomized within 100μm of their cell bodies and these neurons may not survive. Expression of c-*fos* in these cells may imply that the Fos protein plays a role in the neuronal degeneration seen with spinal cord injury. The significantly higher c-*fos* expression in avulsive injury compared with distal nerve transection indicates that avulsive injury

exertes direct effects on spinal neurons, which may precede cell recovery or possibly cell death.

REFERENCES

1. Zorub D, Nashold BS, Cook WA. Avulsion of the brachial plexus: A review with implications on the therapy of intractable pain. Surg Neurol 1974;2:347-353.

2. Edstrom JE. Ribonucleic acid changes in motoneurons of frog during axon regeneration. J Neurochem 1959;5:43-49.

3. Ducker TB, Kaufmann FC. Metabolic factors in the surgery of peripheral nerves. Clin Neurosurg 1977;24:406-424.

4. Grafstein B, McQuarrie I. Role of the nerve cell body in axonal regeneration In: Cotman CW, ed: Neural Plasticity. New York: Raven Press, 1978.

5. Yakolev AG, Faden AI. Molecular strategies in CNS injury. J Neurotrauma 1995;12:767-777.

6. Hunt SP, Pini A, Evan G. Induction of c-*fos*-like protein in spinal cord neurons following sensory stimulation. Nature 1987;328:632-634.

7. Bullitt E. Induction of c-*fos*-like protein within the lumbar spinal cord and thalamus of the rat following peripheral stimulation. Brain Res 1989;493:391-397.

8. Draisci G, Iadarola MJ. Temporal analysis of increases in c-fos preprodynorphin and preproenkephalin mRNAs in rat spinal cord. Mol Brain Res 1989;6:31-37.

9. Menetrey D, Gannon A, Levine JD, et al. Expression of c-*fos* protein in interneurons and projection neurons of the rat spinal cord in response to noxious somatic articular and visceral stimulation. J Comp Neurol 1989;285:177-195.

10. Sheng M, Greenberg ME. The regulation and function of c-*fos* and other immediate early genes in the nervous system. Neuron 1990;4:477-485.

11. Williams S, Evan GI, Hunt SP. Changing patterns of c-*fos* induction in spinal neurons following thermal cutaneous stimulation in the rat. Neuroscience 1990;36:73-81.

12. DeLeo JA, Coombs DW, McCarthy LE. Differential c-fos protein expression in mechanically versus chemically induced visceral nociception. Mol Brain Res 1991;11:167-170.

13. Abbadie C, Lombard MC, Morain F, et al. Fos-like immunoreactivity in the rat superficial dorsal horn induced by formalin injection in the forepaw: effects of dorsal

rhizotomies. Brain Res 1992;578:17-25.

14. Bullitt E, Lee CL, Light AR, et al. The effect of stimulus duration on noxious-stimulus induced c-fos expression in the rodent spinal cord. Brain Res 1992;580:172-179.

15. Lee JH, Beitz AJ. Electroacupuncture modifies the expression of *c-fos* in the spinal cord induced by noxious stimulation. Brain Res 1992;577:80-91.

16. Morgan JI, Curran T. Stimulus-transcription coupling in the nervous system: involvement of the inducible proto-oncogenes *fos* and *jun*. Annu Rev Neurosci 1991;14:421-451.

17. Dragunow M. Presence and induction of Fos B-like immunoreactivity in neural but not non-neural cells in adult rat brain. Brain Res 1990;533:324-328.

18. Chi S, Levine JD, Basbaum AI. Effects of injury discharge on the persistent expression of spinal cord fos-like immunoreactivity produced by sciatic nerve transection in the rat. Brain Res 1993;617:220-224.

19. Chi S, Levine JD, Basbaum AI. Peripheral and central contributions to the persistent expression of spinal cord fos-like immunoreactivity produced by sciatic nerve transection in the rat. Brain Res 1993;617:225-237.

20. Kline DG, Hudson AR. Nerve Injuries: Operative Results for Injuries Entrapments and Tumors. Philadelphia: WB Saunders Company, 1995.

21. Phillips LL, Belardo ET. Expression of *c-fos* in the hippocampus following mild and moderate fluid percussion brain injury. J Neurotrauma 1992;9:323-332.

22. Presley RW, Menetrey D, Levine JD, et al. Systemic morphine suppresses noxious stimulus-evoked Fos protein-like immunoreactivity in the rat spinal cord. J Neurol Sci 1990;10:323-335.

23. Pang Y, Kiba H, Jayaraman A. Acute nicotine injections induce c-*fos* mostly in non-dopaminergic neurons of the midbrain of the rat. Mol Brain Res 1993;20:162-170.

24. Szentagothai J, Kiss T. Projection of dermatomes on the substantia gelatinosa. Arch Neurol Psychiatry 1949;62:734-744.

25. Morgan JI, Cohen DR, Hemstead JL, et al. Mapping patterns of *c-fos* expression in the central nervous system after seizure. Science 1987;237:192-197.

26. Jonse KJ, Evinger C. Differential neuronal expression of *c-fos* proto-oncogene following peripheral nerve injury or chemically-induced seizure. J Neurosci Res 1991;28:291-298.

27. Plantinga LC, Verhaagen J, Wong SL, et al. The neurotrophic peptide Org 2766 does not influence the expression of the immediate early gene *c-fos* following sciatic nerve crush in the rat. Int J Dev Neurosci 1994;12:117-125.

28. Munglani R, Hunt SP. Molecular biology of pain. Br J Anaesth 1995;75:186-192.

29. Sandkuhler J, Treier A-C, Liu X-G, et al. The massive expression of c-*fos* protein in spinal dorsal horn neurons is not followed by long-term changes in spinal nociception. Neuroscience 1996;73:657-666.

30. Berkelaar M, Clarke DB, Wang YC, et al. Axotomy results in delayed death and apoptosis of retinal ganglion cells in adult rats. J Neurosci 1994;14:4368-4374.

31. Gehrmann J, Banati RB. Microglial turnover in the injured CNS: Activated microglia undergo delayed DNA fragmentation following peripheral nerve injury. J Neuropathol Exp Neurol 1995;54:680-688.

32. Lo AC, Li L, Oppenheim RW, et al. Ciliary neurotrophic factor promotes the survival of spinal sensory neurons following axotomy but not during the period of programmed cell death. Exp Neurol 1995;134:49-55.

33. Searle J, Kerr JFR, Bishop CJ. Necrosis and apoptosis: distinct modes of cell death with fundamentally different significance. Pathol Annu 1982;17:229-259.

34. Evan GI, Wyllie AH, Gilbert CS, et al. Induction of apoptosis in fibroblasts by c-myc protein. Cell 1992;69:119-128.

35. Preston GA, Lyon TT, Yin Y, et al. Induction of apoptosis by c-Fos protein. Mol Cell Biol 1996;16:211-218.

36. Smith MA, Banerjee S, Gold PW, et al. Induction of c-*fos* mRNA in rat brain by conditioned and unconditioned stressors. Brain Res 1992;578:135-141.

37. Colotta F, Polentarutti N, Sironi M, et al. Expression and involvement of c-fos and c-jun proto-oncogenes in programmed cell death induced by growth factor deprivation in lymphoid cell lines. J Biol Chem 1992;267:18278-18283.

38. Smeyne RJ, Vendrell M, Hayward M, et al. Continuous c-*fos* expression precedes programmed cell death *in vivo.* Nature 1993;363:166-169.

39. Gu ZZ, Pan Y-C, Cui JK, et al. Gene expression and apoptosis in the spinal cord neurons after sciatic nerve injury Neurochem Int 1997;30:417-426.

40. Emery DG, Lucas JH, Gross GW. The sequence of ultrastructural changes in cultured neurons after dendrite transection. Exp Brain Res 1987;67:41-51.

41. Lucas JH, Emery DG, Higgins ML, et al. Neuronal survival and dynamics of ultrastructural damage after dendrotomy in low calcium. J Neurotrauma 1990;7:169-192.

42. Lucas JH. In vitro models of mechanical injury. J Neurotrauma 1992;9:117-120.

Figure Legends

Fig. 1. Photomicrographs from C7 segment illustrate examples of FLI neurons from rats two hours postoperatively. **A)** Dorsal horn of a rat with sham operation. FLI neurons appear in the medial half of the superficial spinal cord. The arrowheads show FLI neurons. **B)** Dorsal horn of a rat distal transection. FLI positive neurons mainly appear in the superficial laminae. The arrowheads show FLI neurons. **C)** Dorsal horn of a rat with nerve root avulsion. There are many FLI neurons in the superficial laminae near the lesion sites. Solid arrowheads: FLI neurons; open arrowhead: lesion sites. **D)** Ventral horn of the rat with root avulsion depicting many positive motor neurons near the lesion sites. Solid arrow heads: FLI neurons; open arrowhead: lesion sites. Scale bar = 32 μm.

Fig. 2. Histograms of the mean numbers of Fos-like immunoreactive cells in response to sham operation, distal transection, and nerve root avulsion. Solid bars: sham operation (n=4). Open bars: distal transection (n=8); Vertically striped bars: nerve root avulsion (n=8); Top: 30 min after operation. Middle: 60 min after operation. Bottom: 120 min after operation. Means and standard errors are shown. CONT: sham control; TRANS: distal transection; AVULS: nerve root avulsion.

Fig. 3. Camera lucida drawing showing the FLI in the spinal cord of C5 to C8. The filled circles represent FLI cells. The left side of the drawing represents avulsive injury and the right side represents distal nerve transection. Note that there are more labeled cells in the superficial dorsal horn than in the deeper layers of the spinal gray matter. Moreover, there are more labeled cells in the animals with avulsive injury (left side) than in those with distal nerve transection (right side).

Fig. 4. Histograms of the number of Fos-like immunoreactive cells in different laminae of spinal cord. Top: number of FLI neurons (mean ± S.E.) in the superficial laminae 1 and 2 at different time intervals. Middle: number of FLI neurons (mean ± S.E.) in laminae 3 and 4 at different time intervals. Bottom: number of FLI neurons (mean ± S.E.) in laminae 5-10 at different time intervals. CONT: sham control; TRANS: distal transaction; AVULS: nerve root avulsion.

Figure 1.

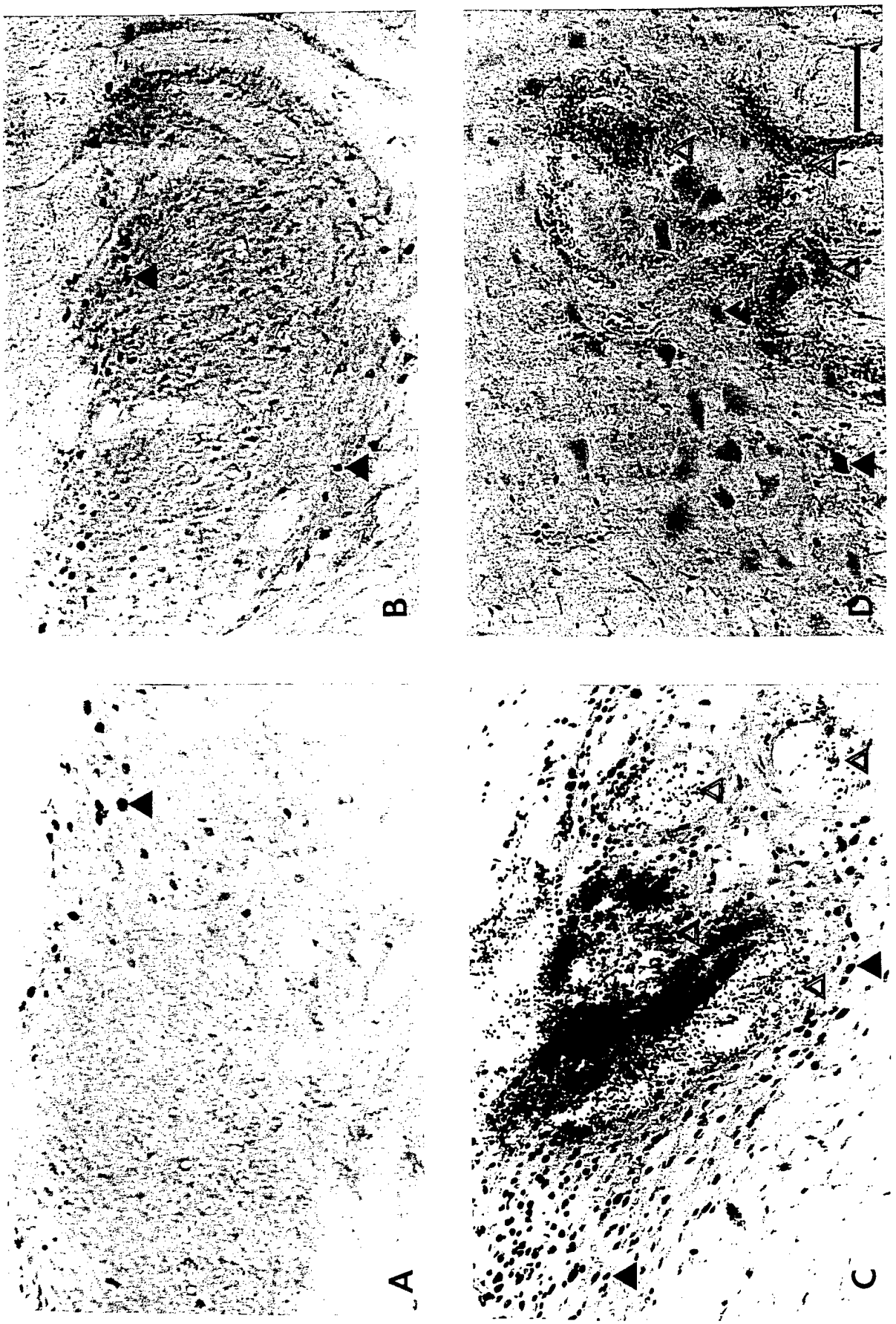

Figure 2.

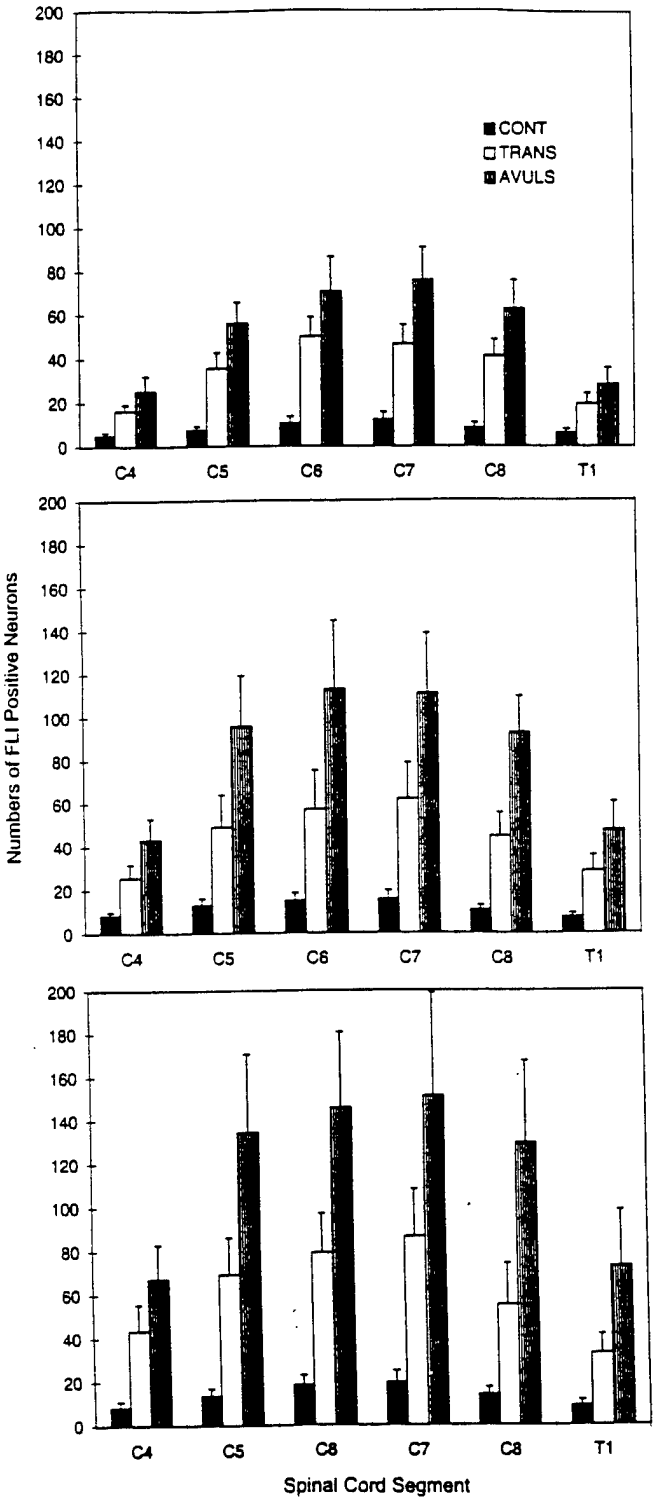
CONT
TRANS
AVULS
Numbers of FLI Positive Neurons
Spinal Cord Segment
C4
C5
C6
C7
C8
T1
0
20
40
60
80
100
120
140
160
180
200

Figure 3.

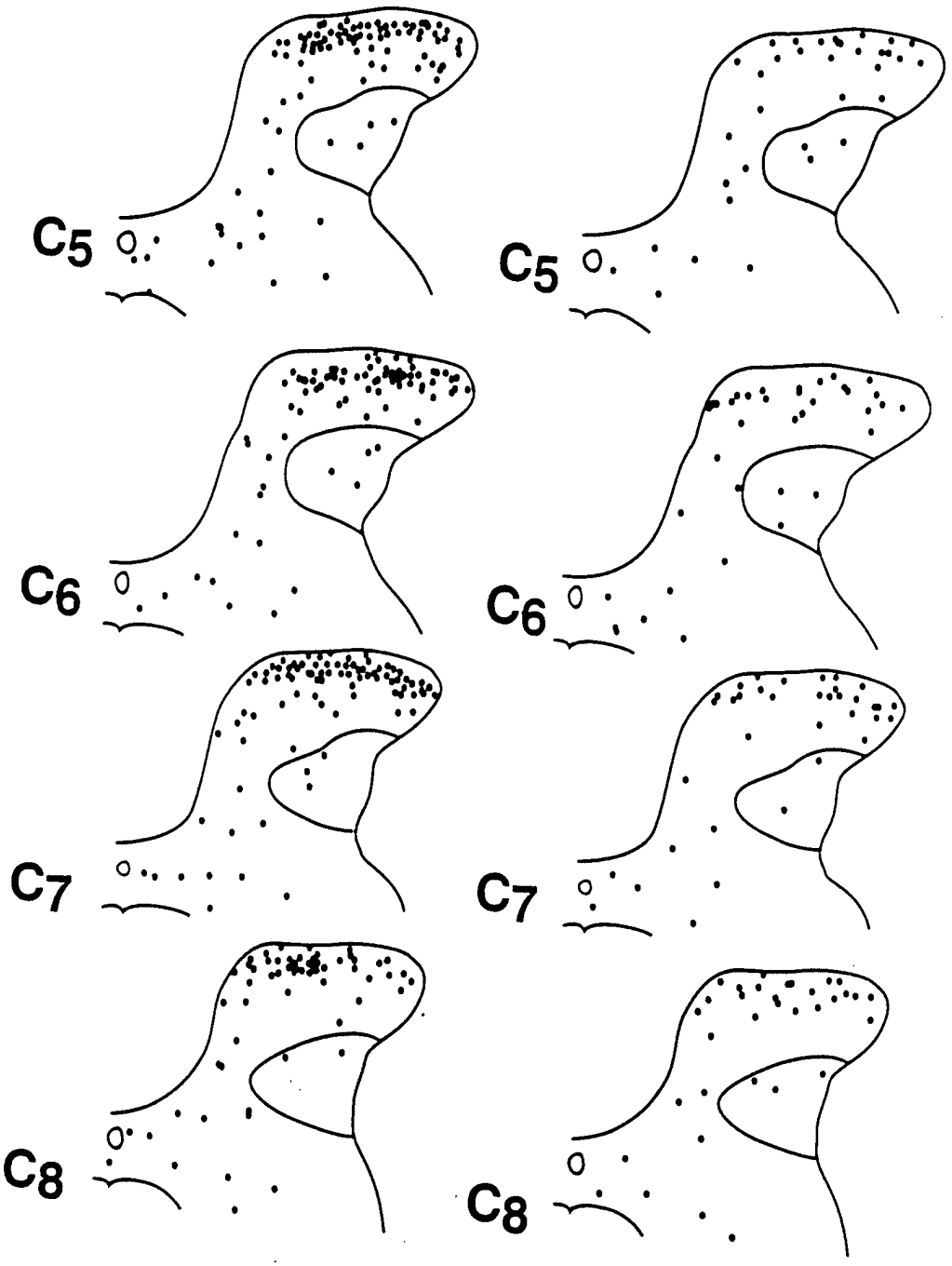

Figure 4.

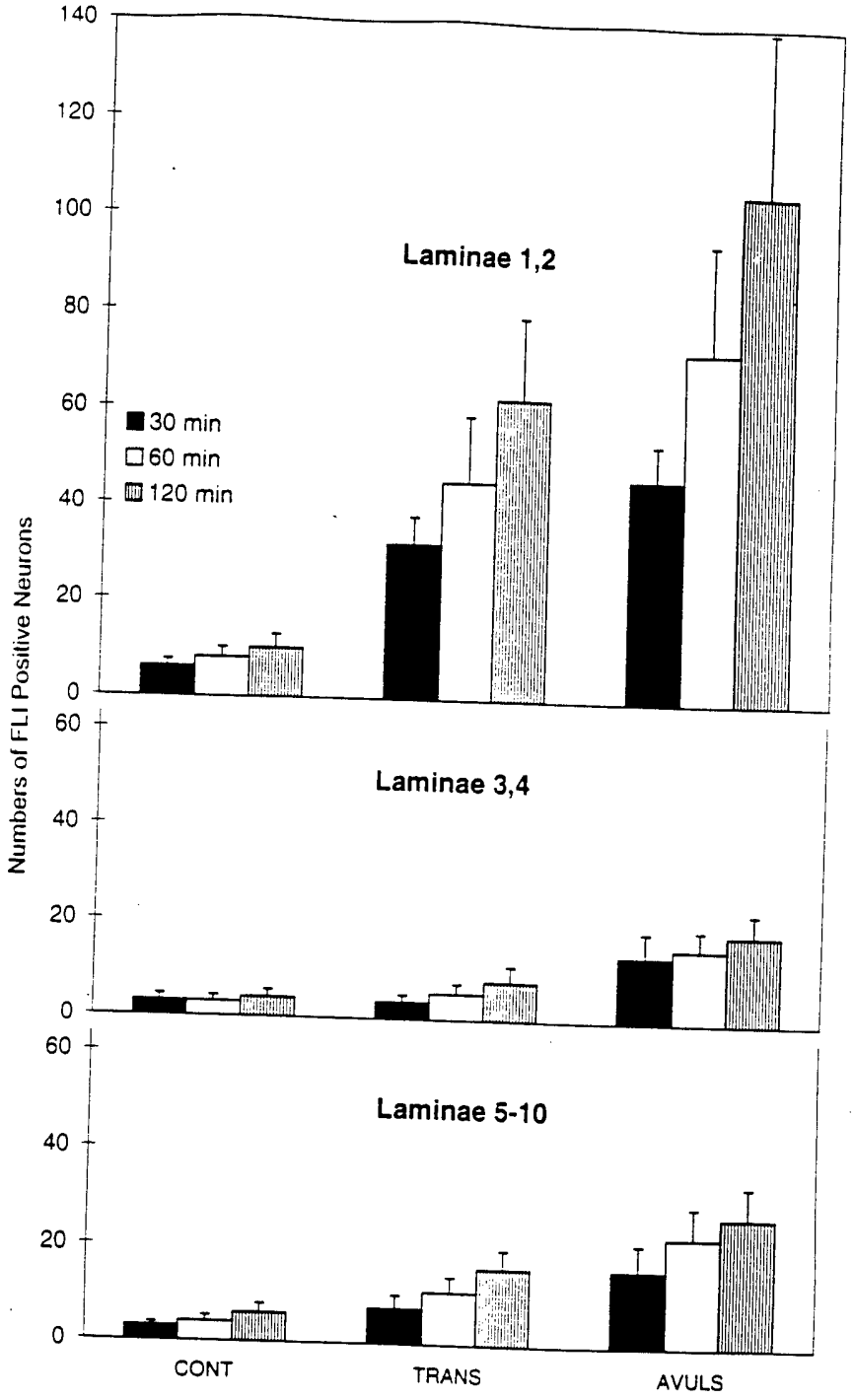
Numbers of FLI Positive Neurons
Laminae 1,2
30 min
60 min
120 min
Laminae 3,4
Laminae 5-10
CONT
TRANS
AVULS

IV. A QUANTITATIVE MODEL FOR INDUCING AVULSIVE INJURIES OF THE BRACHIAL PLEXUS NERVE IN RATS

INTRODUCTION

Avulsion injuries occur in motor vehicle injuries and often in the newborn (1) and may lead to permanent disabilities. The potential for loss of both sensory and motor function, with little or no recovery, makes this an important focus of development of new therapeutic approaches. This injury, which involves both the peripheral and central nervous systems, is somewhat unique. Experimental approaches have suffered from the lack of a quantitative model that does not require a surgical procedure. The method developed here has advantages in that the injury is caused by limb acceleration as occurs in human patients.

Currently, there are several procedures for inducing motor root avulsions. Intervertebrally, the use of a microhemostat forceps may be employed to apply pressure directly to the surgically exposed nerve (2-4). Avulsion may also be induced extravertebrally by separating the peripheral nerve in question from all the surrounding adipose and connective tissue, and applying a "steady, moderate traction" away from the intervertebral foramina with the animal secured. While these methods do indeed result in ventral root avulsion, two problems arise. First, the applied force does not accurately simulate an impact force, which is how many of these injuries occur. Rather than the sharp staccato of an impact, the nerves are avulsed with a gradually increasing force. This could decrease the future usefulness of any knowledge gained from these studies. Second, the methods have too much of a qualitative character, which is a problem for collating and/or comparing the results of collaborative efforts in this area. Similar studies could potentially give completely different results based on such difficult-to-quantify factors as the rate of force application or the amount of

pressure in a nerve and its rate of change.

We created an apparatus that could affect ventral root avulsions in the limbs of rats with the idea of overcoming these shortcomings. This apparatus is easily reproducible by other researchers and provides a definite, quantifiable relationship between impact energy and avulsion.

MATERIALS AND METHODS

The avulsion apparatus was constructed to accommodate 300-gram male Sprague-Dawley rats. The device consists of a plastic tube with an inner diameter of 5.5 cm, a thickness of 0.5 cm, and length of 24.7 cm. The tube has a slightly elliptical hole on the bottom that is approximately 4 cm in diameter and 4 cm off center. Two rectangular plastic stands at 4 cm hold the tube 17.5 cm above the benchtop.

To use this apparatus, rats were anesthetized using sodium pentobarbital and then pushed through the tube until the hole was lined up with the forelimb. Then, the forelimb was manually worked through the hole so that the entire forelimb, except the shoulder, was outside of the tube. The forelimb was then positioned just above a rectangular aluminum rod of 35 cm length attached to one of the plastic stands via a hinge. A circular aluminum stick 35 cm in length with hash marks at every centimeter was soldered onto the other end of the rod, 32 cm away. The rod acted as the lever through which energy was transferred from the point of actual impact to the forelimb of the rat. The end attached to the plastic stand acted as the fulcrum and the opposite end with the measuring stick was where the impact occurred.

After the rat was secured in the tube, the forelimb was tied right above the elbow to a hole in the aluminum rod 8 cm away from the hinge using suture material, where it received the impact

force at a theoretical factor of four. Finally, doughnut-shaped iron weights of known mass were combined and dropped down the circular measuring stick from a height of 30 cm. The experiment was run four times, using masses of 250, 350, 450, and 550 g.

Following a period of two hours, the rats were observed for signs of paralysis, then perfused with formaldehyde. A laminectomy was performed and nerves C5-T1 were inspected for sign of avulsion. Samples of the ventral roots were taken for further analysis.

RESULTS

The rats subjected to the 250 g and 350 g weights were not paralyzed and showed no signs of brachial plexus avulsion. The rat that was injured with the 350 g weight was unable to move the affected arm and upon laminectomy, complete avulsion of nerves C6 and C7 was observed along with extensive hemorrhaging near the spinal cord. The rat subjected to the 450 g weight showed similar hemorrhaging and avulsion of nerves C5, C6, and C7.

DISCUSSION

With the use of sufficiently heavy weights, the apparatus was able to induce avulsive injuries in laboratory rats. The energy was delivered to the forelimb of the rat indirectly and very suddenly, possibly similar to the manner in which avulsion occurs in automobile accidents.

The conditions causing avulsion can be quantified in the form of potential energy (mass times gravity times height). In the case of the 450 g weight, 1.323 Joules of energy were theoretically delivered to the limb. The actual value is probably smaller because of inefficiencies introduced by the machine. Losses due to friction may occur at the hinge of the aluminum rod or where the weights

slide down the measuring stick. We attempted to minimize these losses by making sure the joint felt loose and the lever could be lowered and raised with minimal resistance. Also, care was taken to ensure that the weights did not fit tightly around the measuring stick. The suture material is another possible inefficiency in this mechanism, since it probably undergoes mechanical strain and absorbs some of the energy in the process.

Energy transferred to the actual nerves is a fraction of the total energy delivered to the arm; muscle, bone, and connective tissue absorb most of the energy. Whether or not avulsion occurs can depend to a certain degree on the muscular strength and bone mass of the rat. Heavier weights ensure that enough energy will be transferred to the nerves to obtain the desired result. Right now it is unknown whether the nerves absorb the brunt of the energy first, with other factors coming into play later. More direct measurements of stress (i.e., on the nerve itself) are necessary.

This model for inducing avulsion is not only more realistic than others but also easy to reproduce. The apparatus used here can be constructed in about two days' time by a reasonably skilled technician.

REFERENCES

1. Vbachs JM, Slooff AC, Peeters LL. Obstetric antecedents of surgically treated obstetric brachial plexus injuries. Br J Obstet Gynecol 1995;102:813-817.

2. Bertelli JA, Osal D, Mira JC. Median nerve neurotization by peripheral nerve grafts directly into implanted spinal cord: Anatomical behavioral and electrophysiological evidence of sensorimotor recovery. Brain Res 1994;644:1590-159.

3. Bertelli JA, Mira JC. Brachial plexus repair by peripheral nerve grafts directly into the spinal cord in rats. J Neurosurg 1994;81:107-114.

4. Zhao S, Pang Y, Beuerman RW, et al. Expression of *c-fos* protein in the spinal cord after brachial plexus injury: A comparison of root avulsion with distal nerve transection. Submitted.

V. CENTRAL MECHANISMS IN CHRONIC PAIN

INTRODUCTION

Support for a project entitled, "Central Mechanisms in Chronic Pain," was approved originally for funding under the US Army Medical Research and Development Command Cooperative Agreement to complement studies currently underway on Chapter 5, "Repair and Regeneration of Peripheral Nerve Damage," Co-PIs: R. Beuerman, D. Kline and A. Sumner. The project proposed to study the central nervous system mechanisms that are related to peripheral nerve injury and underlie the conversion from states of acute pain to states of chronic debilitating pain.

SUMMARY

Central Mechanisms Study (Year 1)

The specific aims of the study were 1) to demonstrate that interhemispheric connections are necessary for establishing a state of chronic pain, 2) to demonstrate that interhemispheric connections are necessary for maintaining a state of chronic pain, and 3) to identify the anatomical sites and potential mechanisms that underlie the conversion from a state of acute pain to a state of chronic neuropathic pain.

For this, albino rats were subjected to surgical transection of the corpus callosum prior to the initiation of a deafferentation stimulus, dorsal rhizotomy. The rats were then observed for preservation of normal behavior or for the onset of autotomy, a constellation of behavioral changes including self mutilation believed to be associated with chronic pain.

Based upon the proposed hypothesis, we predicted that the rats undergoing callosotomy

would not develop autotomous behavior. This result would establish the corpus callosum as an essential component in a neuronal circuit that is critical for the augmentation and maintenance of nociceptive signals at the level of perception, the thalamus. Sustained neuronal activity then would be predicted to provide the basis for neuronal changes responsible for internally generated pain.

In fact, as described in last year's progress report, animals undergoing callosotomy prior to dorsal rhizotomy did develop autotomous behavior. Unlike animals in which the corpus callosum had not been sectioned, which began self mutilation between 24 hours and 6 weeks post-rhizotomy, animals with a transected corpus callosum never self mutilated before 90 days post-rhizotomy. Although this result was suggestive that the corpus callosum does play a role in the generation of central pain, the fact that, unexpectedly, not all rats that underwent dorsal rhizotomy without prior callosal sectioning developed autotomy indicated that this observation would require statistical verification. The number of animals and the funding available that would have been necessary to continue with the planned experiments was insufficient to proceed. The direction of the subsequent studies was therefore modified during the second year of the study.

Peripheral Mechanisms Study (Year 2)

The treatment of pain related to nerve injury was studied during the second year of support in the hope of elucidating mechanisms that produce pain following nerve injury. We chose to study the role of a new medication, gabapentin, in pain induced by inflammation, because of its clinically demonstrated efficacy in the treatment of neuropathic pain, its favorable side effect profile, and its anecdotal efficacy in clinically reducing pain in conditions that were not clearly of neuropathic origin. It was predicted that by comparing the response to treatment of inflammatory pain with that

induced by nerve injury, we could shed additional light on mechanisms responsible for pain related to nerve injury. Since pain associated with nerve injury has been correlated to the quantity of membrane-associated sodium channels during this study, we chose, in addition, to study alterations in concentrations of sodium channels within dorsal root ganglia and peripheral nerves of albino rats following subcutaneous injections of complete Freund's adjuvant (CFA).

GABAPENTIN STUDY

In the initial study, the effect of gabapentin on pain induced by inflammation was studied in albino rats using paw withdrawal latencies, tail-flick, and hotplate techniques. Following baseline threshold determinations, a subcutaneous injection of CFA was administered into one volar forepaw. Withdrawal latencies were determined following subcutaneous administration of gabapentin, carbamazepine, ibuprofen, morphine, or saline.

Methods and Materials

Pain responses were measured in albino Sprague-Dawley rats. The latency to paw withdrawal, to tail-flick, and to hotplate aversion were the determinants of pain threshold. Rats weighing between 250-350 g were housed two animals to a cage. For testing the rats were placed in Plexiglas chambers on a glass plate and were allowed to acclimate to their surroundings for a minimum of 5 minutes. The animals were allowed free range of activity within the chamber. The glabrous surface of each of the paws was stimulated in succession through the glass plate using a halogen heat source. The latency of paw withdrawal from the onset of stimulation was measured automatically using an IITC analgesiometer (IITC Life Science, Inc., Woodland Hills, CA). The

stimulus was automatically discontinued after 10.7 seconds to avoid tissue damage. Each paw was stimulated 4 times during each testing session. Baseline pain thresholds were determined in 3 separate testing sessions on 3 separate days. Tail-flick latency was measured in a group of 12 rats. Morphine sulfate (10 mg/kg), ibuprofen (40 mg/kg) or gabapentin (40 mg/kg) was administered subcutaneously to each rat. The order of drug administration was randomized with at least 4 days between drugs. Baseline latency was measured immediately before and at 15, 30, 60, 90, and 120 minutes after administration of drug. For the tail-flick test, the stimulus was discontinued after 12 seconds to avoid tissue damage. The same 12 rats were tested for hotplate analgesia immediately before and 45 minutes after drug administration. The rats were placed on the hotplate surface that was set at 52°C. The rats were removed from the hotplate surface when they licked a hindpaw, jumped, or if they did not respond after 30 seconds. The time from stimulus onset to removal from the hotplate was recorded.

Following baseline threshold determinations for paw withdrawal latency, the rats were anesthetized with a combination of ketamine (60 mg/kg) and xylazine (8 mg/kg). One forepaw of each rat received a subcutaneous injection of 0.25 ml of complete Freund's adjuvant (CFA; *Mycobacterium tuberculosis*; Sigma) suspended in an oil:saline (1:1) emulsion (0.5 mg *Mycobacterium*/ml emulsion) using a sterile tuberculin syringe. The rats were then weighed and allowed to recover from anesthesia. Pain thresholds were measured on 5 separate days during the week following CFA injection. Either gabapentin (20-160 mg/kg) or normal saline was administered by subcutaneous injection 1 hour prior to each testing session. Ibuprofen (100 mg/kg) was given as a positive treatment control. Carbamazepine (40 mg/kg) was used as a negative treatment control.

To confirm that the route of administration and drug absorption was adequate to produce a

response, 2 groups of 11 rats were subjected to subcutaneous injections of 5% formalin in isotonic saline into the plantar surface of one hindpaw 30 minutes after receiving a subcutaneous injection of either gabapentin (160 mg/kg) or normal saline. Time spent in licking, lifting, and biting the injected paw was monitored for 90 minutes following the formalin injection and recorded at 5 minute intervals.

Results and Conclusions

In contrast to gabapentin's previously described efficacy in altering pain thresholds in the chronic constriction injury and formalin injection models of neuropathic pain and its anti-allodynic effect following nerve root ligation, we demonstrated no effect on paw withdrawal latencies associated with CFA-induced inflammation or on baseline hotplate or tail-flick response.

We concluded that gabapentin has no effect on pain initiated by CFA-induced inflammation. We proposed that gabapentin's effect in the treatment of neuropathic pain may be mediated through modulation of peripheral mechanisms related to the altered function of ion channels in damaged neurons. Such a mechanism suggests that improved nociceptive pain in clinical reports may have an underlying neuropathic component that is reduced by gabapentin. The results of this study were presented at the annual meeting of the American Federation of Medical Research in New Orleans and a paper is currently in press in *Analgesia*.

SODIUM CHANNEL STUDIES

Complete Freund's Adjuvant Study

To study the hypothesis generated in the gabapentin experiments, we chose to study

alterations in concentrations of sodium channels within dorsal root ganglia and peripheral nerves of albino rats following subcutaneous injections of CFA and chronic constriction injury (CCI) in order to establish a relationship between sodium channel concentration and hypersensitivity induced by inflammation and by nerve injury. The results from experiments in which hypersensitivity was induced by CFA injection show that the production of sodium channels is dramatically increased in dorsal root ganglia within 24 hours of paw injection.

Methods and Materials

Pairs of rats were anesthetized with a combination of ketamine (60 mg/kg) and xylazine (8 mg/kg). One hindpaw of each rat received a subcutaneous injection of 0.5 ml of complete Freund's adjuvant (CFA; *Mycobacterium tuberculosis*; Sigma) suspended in an oil:saline (1:1) emulsion (0.5 mg *Mycobacterium*/ml emulsion) using a sterile tuberculin syringe. The hindlimb contralateral to the injected paw provided an internal control. Rats were allowed to survive in pairs for 4, 24, 48, and 72 hours, 1 and 2 weeks, and 1, 2, and 6 months after CFA injection. An additional pair of rats received a 0.5-ml subcutaneous injection of normal saline or incomplete Freund's adjuvant as a treatment control. Prior to sacrifice, pain thresholds were measured by determining the latency to paw withdrawal from a thermal stimulus and were compared to control values that had been determined in an earlier study. The rats were then given a lethal dose of pentobarbital sodium (200 mg) and perfused transcardially with 0.9% saline followed by 4% paraformaldehyde in 0.1 M phosphate buffer, pH 7.6. The tissue was allowed to fix for 1 hour. The dorsal root ganglia and portions of the sciatic and medial plantar nerves were then dissected bilaterally from each animal. The nerve fibers and dorsal root ganglia were teased apart and fixed on poly-L-lysine coated slides

with 4% paraformaldehyde/0.1 M phosphate buffered saline (PBS) for 15 minutes. After rinsing in 0.1 M PBS, the slides were immersed in 0.1 M PBS/0.3% Triton X-100 (Sigma)/10% normal goat serum for a minimum of 1 hour. The tissue was then incubated overnight at room temperature with a site-specific, anti-sodium channel antibody (EO3) (dilution 1:100) (1). For controls, the anti-sodium channel antibody was preblocked with the peptide antigen (1 μl of peptide per 2 μl of antibody). After rinsing in 0.1 M PBS, the tissue was incubated for at least 1 hour at room temperature with lissamine rhodamine-labeled goat antirabbit immunoglobulin G. The slides were then rinsed in 0.1 M PBS, dried, coverslipped, and viewed with an Olympus BH2 epifluorescence microscope.

Results

Behaviorally, paw withdrawal latencies begin to decrease within 4 hours following CFA injection. Minimum latencies are seen at 24 hours post-injection and then within 14 days return to baseline levels. When survival times are extended beyond 14 days, paw withdrawal latencies continue at or marginally above baseline levels. Data from 6 month survival post-injection are pending but are not predicted to be different from baseline latencies.

Immunocytochemistry reveals sodium channels in high density at nodes of Ranvier in all samples of peripheral nerve. As described previously, sodium channel-specific labeling was seen at low levels within control dorsal root ganglia. On the injected side, however, an increase in sodium channel labeling is seen in dorsal root ganglia as early as 24 hours following CFA injection. Within 48 hours, during the early functional recovery, virtually all neurons of the dorsal root ganglia segmentally associated with the injected paw are intensely labeled. Except for the nuclear region,

the neuronal cytoplasm labels uniformly. At 72 hours post-injection, labeling remains intense but there is a suggestion of heterogeneity within the ganglia such that the larger cellular profiles appear less intensely labeled when compared to smaller profiles. The distribution of labeling within individual neurons remains constant. At 1 week post-injection, the paw withdrawal latencies have almost returned to baseline levels and the heterogeneity of ganglion labeling is clear. The labeling appears to be more intense in the smaller profiles. This pattern persists through the 1 month survival but labeling begins to diminish by 2 months post-injection. At 6 months after the CFA injection, sodium channel labeling has almost returned to control levels. Sodium channel labeling following injections of either saline or incomplete Freund's adjuvant as treatment controls is indistinguishable from that seen in untreated controls.

Conclusions

We concluded that sodium channel production is significantly increased in dorsal root ganglia following the injection of CFA. This increase is not reflected in concomitant increases in sodium channel labeling in either contralateral dorsal root ganglia or in peripheral nerve. The time of onset of the reduction of the paw withdrawal latency and sodium channel augmentation strongly indicates that sodium channels play a role in the acute maintenance of neuronal hypersensitivity during inflammation. The mechanism by which sodium channel augmentation occurs is not known. It is possible that the pain initiated by the original injection and the reduction of receptor thresholds results in repetitive neuronal firing and the stimulation of genes that are responsible for sodium channel production (2). Although repetitive neuronal firing and the opening of metabatropic glutamate receptors has been proposed as a mechanism for turning on gene expression and neuronal

plasticity in the spinal cord (3,4), glutaminergic synapses have not been identified in dorsal root ganglia. Thus, the signal for sodium channel augmentation in dorsal root ganglia may come from repetitive membrane depolarizations resulting from peripheral receptor generation of action potentials or through the stimulation of extracellular mediators, including nerve growth factor, that are released during the inflammatory response (2,5-8) and are transported to the neuronal perikaryon. The augmentation of sodium channels in dorsal root ganglia could then play a role in maintaining the inflammatory hyperpathic response (9) necessary for monitoring wound healing. The apparent prolonged augmentation of sodium channels in the smaller neurons would be consistent with the maintenance of C-fiber activity thought to subserve pain vigilance. That the reduction of sodium channel production follows the return to normal thresholds for paw withdrawal suggests that the sodium channels are maintained by the mediators of the inflammatory response.

Of particular interest is that sodium channel augmentation is dramatic and consistently occurs within 24 hours of the introduction of the inflammatory agent. However, unlike pain of neuropathic origin, traditional blockers of voltage-dependent sodium channels typically are clinically ineffective in treating pain induced by inflammation (10). One possibility is that the sodium channels augmented during inflammation are of different subtypes than those produced in response to nerve injury. Indeed, since the EO3 antibody identifies a conserved segment of all sodium channels, sodium channels of all subtypes are labeled with this antibody. Since each sodium channel subtype may respond differently to different therapeutic interventions (11), further identification of channel subtypes must be made. Alternatively, sodium channel subtypes may be produced in different proportions in response to a given stimulus resulting in different activation parameters (12,13). Different ratios of ion channel populations could provide the basis for the prolonged periods of

ectopic firing seen following nerve injury compared to the transient augmentation of hypersensitivity seen in inflammation. Third, in contrast to sodium channels that are produced in response to nerve injury, which must be functional and rapidly integrated into growing neuronal processes for the restoration of generator and encoding zones of sensory nerve terminals (12), all of the sodium channels labeled in response to an inflammatory stimulus may not be integrated within neuronal membranes or may only be precursors to functional, subtype-specific sodium channels that are formed in anticipation of potential neuronal damage and used transiently to enhance the efficacy of neuronal transmission. The uniform cytoplasmic distribution of labeling potentially supports this suggestion. In addition, the distribution of sodium channels is likely to be important in determining their accessibility to therapeutic chemical blockade and thus may partially explain the difference in clinical response. Hypersensitivity seen in acute inflammation, however, suggests that at least some of the sodium channels are functional and serve to enhance the efficacy of neuronal transmission (2,14) through the dorsal root ganglion to the spinal cord. Although less likely, sodium channel augmentation during inflammation may serve as a mechanism for endogenous pain suppression by inserting voltage-dependent sodium channels into the perikaryal membranes of dorsal root ganglion cells to enhance membrane permeability and serve as a current sink to decrease the centrally projected signal. In either case, the results of this study thus provide a basis for exploring novel therapeutic alternatives for the treatment of pain through modulation of sodium channel activity.

The results of this study will presented at the annual meeting of the American Pain Society in New Orleans and is currently being prepared for submission to *Nature*.

CONTINUING STUDIES

Chronic Constriction Injury

Chronic constriction injury has been studied in only 2 rats to date. The results indicate that at 2 weeks post-injury there is a significant increase in the density of sodium channels at the site of the ligation but not within the dorsal root ganglia nor in control sections of peripheral nerve. These preliminary results support the prediction that there are important mechanistic differences in the production of hypersensitivity induced by inflammation and nerve injury. In addition, these mechanisms are related in some way to the regulation of the production and distribution of sodium channels within hyperactive neurons. These differences are likely to provide the basis for distinctions recognized in clinical treatment and in the production of chronic pain states seen following nerve injury. Recognition and delineation of the signals mediating the different responses will be important issues for investigation in future studies to provided possibilities for preemptive treatment of pain following nerve injury and for new and more effective options in the treatment of pain associated with inflammation.

REFERENCES

1. England JD, Happel LT, Kline DG, et al. Sodium channel accumulation in humans with painful neuromas. Neurology 1996;47: 272-276.

2. D'Arcangelo G, Paradiso K, Shepherd D, et al. Neuronal growth factor regulation of two different sodium channel types through distinct signal transduction pathways. J Cell Biol 1993;122: 915-921.

3. Coderre TJ. The role of excitatory amino acid receptors and intracellular messengers in persistent nociception after tissue injury in rats. Mol Neurobiol 1993;7:229-246.

4. Lipton SA, Rosenberg PA. Excitatory amino acids as a final common pathway for neurologic disorders. New Engl J Med 1994;330:613-622.

5. O'Lague PH, Huttner SL. Physiological and morphological studies of rat pheochromocytoma cells PC12 chemically fused and grown in culture. Proc Natl Acad Sci USA 1980;77:1701-1705.

6. Rudy B, Kirschenbaum B, Rukenstein A, et al. Nerve growth factor increases the number of functional Na channels and induces TTX-resistant Na channels in PC12 pheochromocytoma cells. J Neurosci 1987;7:1613-1625.

7. Mandel G, Cooperman SS, Maue RA, et al. Selective induction of brain type II Na^+ channels by nerve growth factor. Proc Natl Acad Sci USA 1988;85: 924-928.

8. Pollock JD, Krempin M, Rudy B. Differential effects of NGF, FGF, EGF, cAMP and dexamethasone on neurite outgrowth and sodium channel expression in PC12 cells. J Neurosci 1990;10: 2626-2637.

9. Zhang J-M, Song X-J, LaMotte RH. An in vitro study of ectopic discharge generation and adrenergic sensitivity in the intact, nerve-injured rat dorsal root ganglion. Pain 1997;72:51-57.

10. Gould HJ III, Gould TN, Reeb CS, et al. The effect of gabapentin on inflammatory pain in rats. Analgesia, in press.

11. Omana-Zapata I, Khabbaz MA, Hunter JC, et al. Tetrodotoxin inhibits neuropathic ectopic activity in neuromas, dorsal root ganglia and dorsal horn neurons. Pain 1997;72:41-49.

12. Devor M, Lomazov P, Matzner O. In: Touch, Temperature, and Pain in Health and Disease: Mechanisms and Assessments, Progress in Pain Research and Management. Boivie J, Hansson P, Lindblom U, eds. Seattle: IASP Press, 1994;3: 207-230.

13. Waxman SG, Kocsis JD, Black JA. Type III sodium channel mRNA is expressed in embryonic but not adult spinal sensory neurons, and is reexpressed following axotomy. J Neurophysiol 1994;72:466-470.

14. Study RE, Kral MG Spontaneous action potential activity in isolated dorsal root ganglion neurons from rats with a painful neuropathy. Pain 1996;65:235-242.

Sodium channel accumulation in humans with painful neuromas

Article abstract—Painful neuromas from 16 patients were examined using site-specific antisodium channel antibodies employed in immunocytochemical and radioimmunoassay methods. Normal sural nerves from six of these patients served as controls. Immunocytochemistry showed abnormal segmental accumulation of sodium channels within many axons in the neuromas. Dense immunolocalization was especially apparent within the axonal tips. Radioimmunoassay confirmed a significantly greater density of sodium channels in the neuromas as compared with the sural nerves. Thus, sodium channels accumulate abnormally within the axons of neuromas in humans. This alteration of the sodium channels may underlie the generation of axonal hyperexcitability and the resulting abnormal sensory phenomena (pain and paresthesias), which frequently occur after peripheral nerve injury.

NEUROLOGY 1996;47:272–276

J.D. England, MD; L.T. Happel, PhD; D.G. Kline, MD; F. Gamboni, PhD; C.L. Thouron; Z.P. Liu, MD; and S.R. Levinson, PhD

Peripheral nerve trauma may result in the formation of a neuroma, a tangled mass of regenerating axons embedded within the connective tissue of a nerve trunk. The axons within a neuroma not only fail to reinnervate their original targets, but may also develop abnormal electrical hyperexcitability.[1,2]

In human neuromas, the development of ectopic hyperexcitability within sensory axons is likely to be a major cause of neuroma-associated pain and dysesthesias. Clinical evaluation of patients with painful neuromas and routine histologic analysis of excised neuromas have not identified the factors responsible for this pain. Because the ability of an axon to generate an action potential depends ultimately on the distribution and properties of voltage-gated ion channels, especially voltage-gated sodium channels, a potential cause of ectopic axonal hyperexcitability could be an abnormal redistribution of ion channels within injured axons. A particularly attractive hypothesis is that aberrant axonal electrical hyperexcitability is, in part, caused by an abnormal accumulation of sodium channels along injured or regenerating axons.[2-5]

This report describes the changes in the sodium channels which characterize painful neuromas in humans. These findings are correlated with what is currently known about the remodeling of axonal membranes within neuromas.

Methods. *Patients.* The study group consisted of 16 patients with painful traumatic neuromas selected from a large population of patients with peripheral nerve injuries seen at the Louisiana State University School of Medicine, New Orleans. Each patient was evaluated clinically and electrophysiologically (EMG/nerve conduction study) by a team of neurologists and neurosurgeons. The pain of each patient's nerve injury was graded subjectively on a scale from 1+ to 4+ (table). For each of the 16 patients in this study, surgical treatment of the neuroma was believed to offer the best chance for pain relief or nerve regeneration. Thus, each patient underwent surgical excision of the neuroma. In some cases, sural nerve autografts were interposed within the resected nerve segment.

Preparation of antisodium channel antibody. A site-directed antibody was raised to a highly conserved region found in all known vertebrate sodium channels, including those of human neuronal tissues. This segment (TEEQKKYYNAMKKLGSKK) resides in a putative intracellular loop connecting domains III and IV in the alpha subunit of the sodium channel. The synthetic peptide coding for this segment was conjugated to a keyhole-limpet hemocyanin carrier and used to immunize rabbits through regular injections. The resultant high-titer antisera were processed using an immunoaffinity column to which the immunizing peptide had been immobilized, yielding a highly pure and concentrated preparation of antisodium channel antibodies. The specificity of the antibody preparation was demonstrated by the quantitative elimination

Table *Sodium channel density and painfulness of neuromas*

Patient	Specimen	NaCh*,	Pain
1	C5 neuroma	23.5	+
2	Normal nerve	23.7	−
3	Middle trunk neuroma	25.8	+
4	C5–upper trunk neuroma	26.3	+
5	Femoral neuroma and	28.6	+
	normal nerve	9.6	−
6	Upper trunk neuroma	30.1	+
7	Axillary neuroma and	30.6	+
	normal nerve	12.6	−
8	C6 neuroma	31.0	+
9	C5 neuroma	31.0	++
10	C7 neuroma	31.2	+
11	Superficial radial neuroma	32.7	++
12	Brachial plexus neuroma	32.9	+++
13	Medial cord neuroma and	48.3	++
	normal nerve	20.4	−
14	Sural neuroma	48.3	+++
15	Sciatic neuroma (distal segment)	67.2	++++
	Sciatic neuroma (proximal segment)	25.4	++++
	and normal nerve	16.2	−
16	Sciatic neuroma and	74.2	+
	normal nerve	20.1	−

* Sodium channel density in picomol per gram of wet weight.

− = no pain; + = mild pain; ++ = moderate pain; +++ = severe pain; ++++ = very severe pain.

of antibody binding by preincubation with either pure sodium channel or synthetic peptide in a sensitive radioimmunoassay (RIA)[6] and in immunocytochemical preparations (figure 1d).

Immunocytochemistry. Immunocytochemical methods were performed in accordance with described procedures.[5,6] After reaction with tissue, the antisodium channel antibody was visualized with lissamine rhodamine-labeled goat antirabbit immunoglobulin G. For control slides, the primary antisodium channel antibody was preblocked with the peptide antigen (1 μl of peptide per 2 μl of antibody overnight at 4° C). Labeled specimens were examined with either an Olympus BH2 epifluorescence microscope or a Leica laser scanning confocal microscope.

Radioimmunoassay. Neuroma or sural nerve specimens were weighed and then homogenized in 0.1 mol/liter sodium phosphate buffer (pH 7.5) and 1% Lubrol PX. They were then centrifuged at 45,700*g* for 25 min, and the pellets were discarded. The supernatants were denatured by adding 1% SDS and 2.5% betamercaptoethanol and boiling for 2 min. After cooling, they were dialyzed against 0.1 mol/liter sodium phosphate buffer at room temperature for 24 hr. The extracts were retrieved and diluted in 0.1 mol/liter sodium phosphate buffer (pH 7.5), 1% bovine serum albumin, 0.1% Lubrol, and 0.021% egg phosphatidylcholine (Sigma, grade V) to a concentration of <10 mg wet tissue per 100 μl. Samples (100 μl per tube) were incubated with the antisodium channel antibody diluted to 1:2,000 for 1 hr at room temperature. Twenty microliters of iodine-125–labeled purified eel sodium channel (17 fmol or 30,000 cpm; specific activity = 1.06 mCi/nmol; 1 Ci = 37 Gbq) was then added to each tube and incubated another 2 hr at room temperature. Antibody–antigen complexes were solid phase precipitated by adding 100 μl of Tachisorb-R (Calbiochem #575544) and incubating with gentle shaking for 2 hr at room temperature. Samples were washed with 0.1 mol/liter sodium phosphate buffer, 1% bovine serum albumin, 0.1% Lubrol, and 0.02% egg phosphatidylcholine (Sigma, grade V) (1.25 ml per tube) and then centrifuged at 3,700*g* for 5 min. The pellets were resuspended in the same buffer and recentrifuged at 3,700*g* for another 5 min. The supernatants were discarded, and the radioactivity of the pellets was determined using a gamma counter. Concentrations of sodium channels were calculated with reference to a standard curve determined by using known quantities of highly purified eel sodium channel.

Results. *Immunocytochemistry.* Seventeen neuromas from 16 patients (one patient had two specimens) and six sural nerves from six of these patients were examined immunocytochemically.

In the sural nerves, sodium channel-specific immunoreactivity (IR) was seen only at nodes of Ranvier. Unmyelinated axons exhibited no specific IR anywhere along their axolemma. These results in human sural nerves are identical to those found using similar immunohistochemical studies in fish posterior lateral line nerves.[5,6] Although electrophysiologic and biochemical studies demonstrate some voltage-gated sodium channels along normal unmyelinated and internodal axolemma, the density of these sodium channels is too low to be visualized immunocytochemically with antisodium channel antibodies.[5,6]

All neuromas showed abnormally intense sodium channel-specific IR within many axons. This IR was seen in large-diameter (>1 μm) and small-diameter (<1 μm) axons, although larger axons with dense IR were more frequently encountered. The IR was always nonuniform in distribution, occurring in patches of variable density along the axons. Of special note, this dense specific IR usually appeared along demyelinated or unmyelinated segments of axolemma. When myelinated fibers were seen, focal accumulation of sodium channels was observed only at normal nodes of Ranvier. Some of the most intense immunolabeling was seen at the neurite tips, and these axonal endings were always devoid of a myelin sheath. Within neuromas there was considerable individual axon variability of IR, with some axons showing many patches of intense IR and other axons (even neighbors) showing no IR. Even in the most intensely labeled neuromas, no more than 30 to 40% of all axons showed sodium channel-specific IR. Although all neuromas exhibited abnormal sodium channel-specific IR within many axons, there was considerable variability in terms of the number and intensity of axons stained within individual neuromas. Only minimal nonspecific immunofluorescence was seen when the primary antisodium channel antibody was preblocked with peptide, confirming the specificity of the above-noted IR. Figure 1 provides examples of these immunocytochemical observations.

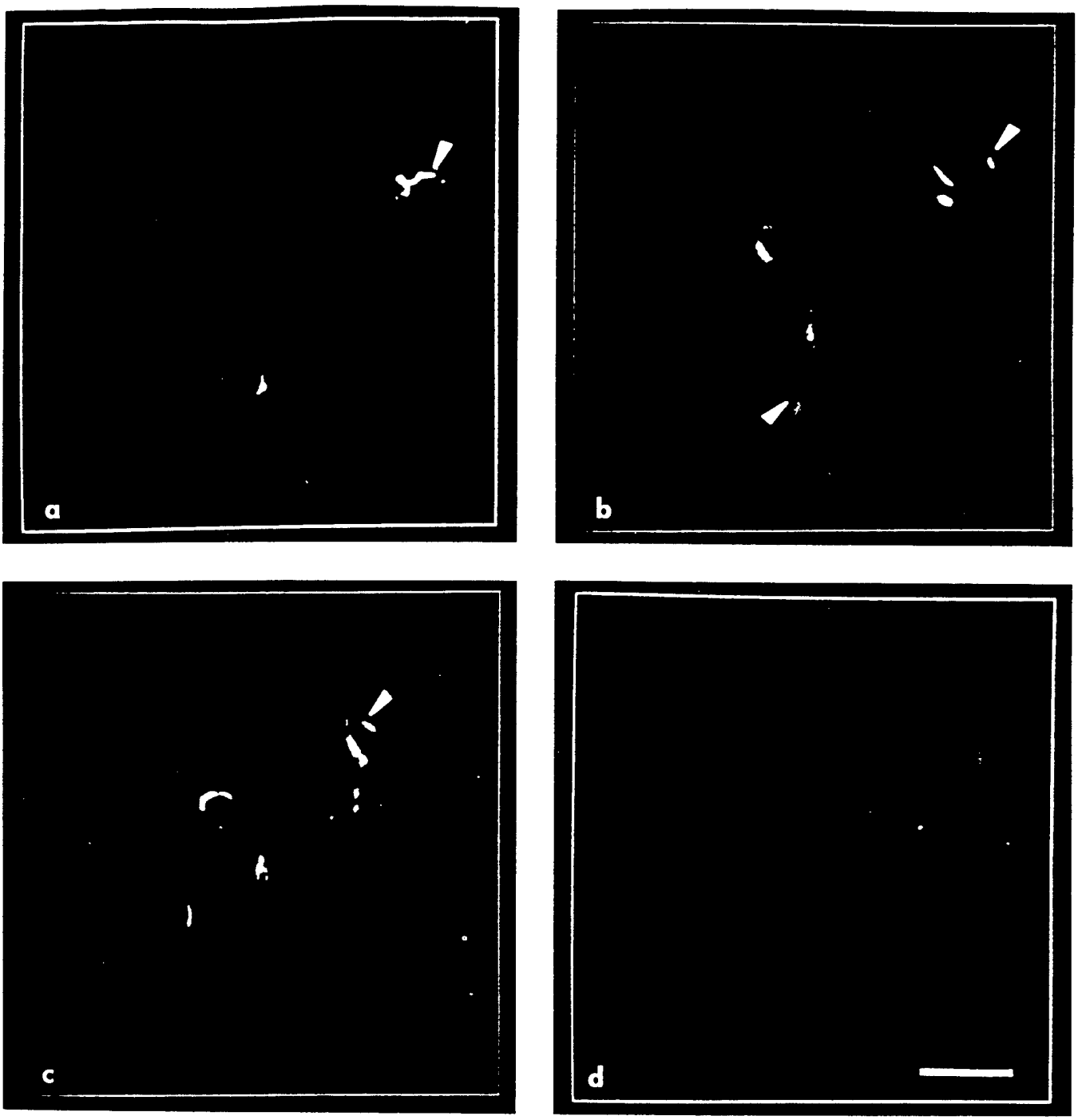

Figure 1. Sodium channel immunocytochemistry of neuromas. (a, b, c) Distinct segments of sodium channel-specific immunoreactivity are present throughout the axons of these neuromas. Also note the intense immunoreactivity present in several axonal tips (arrowheads). (d) Control showing the nonspecific immunofluorescence that occurs when the primary antisodium channel antibody is preblocked with peptide. Scale bar = 10 μm.

Radioimmunoassay. Sixteen neuromas from 15 of the patients (one patient had two specimens) and six sural nerves were examined using RIA. Portions of all of these specimens had been examined immunocytochemically (see prior discussion). For each specimen the concentration of sodium channels was calculated and expressed as picomol per gram of wet weight. The Mann-Whitney U test was used for statistical analysis of the two populations. RIA data demonstrated a significantly greater ($p = 0.0075$) sodium channel density in neuromas (median = 28.6; mean ± SEM = 32.5 ± 3.7 picomol per gram) as compared with sural nerves (median = 18.2; mean ± SEM = 17.1 ± 2.2 picomol per gram). The true density of axonal sodium channels within these neuromas was probably even greater because neuromas contain far more nonneural tissue than normal nerve. Figure 2 graphically illustrates the sodium channel density for each specimen. The variance of the normal nerves was much less than that of the neuromas, and there was very little overlap between the two populations. These population differences are consistent

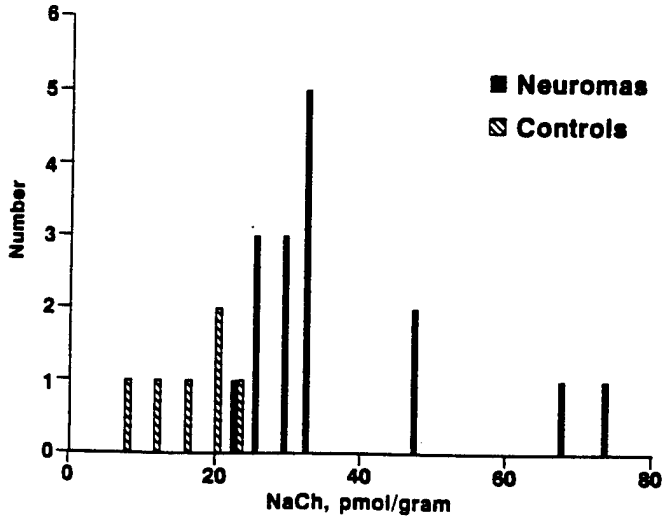

Figure 2. Frequency histogram of the sodium channel density in neuromas and control nerves. The neuromas, as a group, had a significantly greater concentration of sodium channels as compared with the control nerves (see text).

with the expected biologic variability of the sodium channel density, which was greater for the neuromas. Matched pairs of specimens were available from five patients (i.e., neuroma and sural nerve from the same patient). In each case, the neuroma contained a significantly greater density of sodium channels than the sural nerve. All RIA data are provided in the table, in which the neuromas are ordered according to their sodium channel density (i.e., from lowest to highest) and their degree of pain is provided. By inspection, one can ascertain a trend in the direction of greater pain for neuromas with greater concentrations of sodium channels. These data suggest a positive correlation between the density of sodium channels within neuromas and their degree of pain.

Discussion. This study shows that sodium channels accumulate abnormally within the axons of human painful neuromas. This work extends and corroborates the findings of several animal studies of nerve injury.[3-5] Immunocytochemical analysis of neuromas of the lateral line nerve of the fish *Apteronotus*[3] and focally injured nerve fibers of the lateral line nerve of *Carassius auratus* (goldfish)[5] have shown sodium channel accumulation at the endings of injured axons. Devor et al.[4] immunolocalized sodium channels at the electron microscopic level in neuromas produced in rats. Sodium channel accumulation occurred in preterminal axolemma, which was either demyelinated or unmyelinated, as well as in neuroma end bulbs. The large-diameter (>1 μm) axons within the neuromas acquired excess sodium channels only after myelin was stripped from their internodal axolemma. Many of these axons contained distinct patches of heavy sodium channel immunolabeling. These findings are concordant with our observations in human neuromas and, thus, may be a general feature of neuromas.

The accumulation of sodium channels within the axons of neuromas may be due to several factors. Sodium channels are synthesized in neuron cell bodies and transported down axons by microtubule-based fast axoplasmic transport.[5,7] When the cell bodies of the squid giant fiber lobe are dissociated from their giant axons and maintained in culture, sodium channels amass within the somata.[7] This observation suggests that the axonal membrane normally serves as a "sink" for sodium channels synthesized within the cell body and that its removal by axotomy causes sodium channels to accumulate in the remaining viable membrane. After injury to axons, sodium channels, which are continuously transported down axons, would be expected to accumulate at the nerve fibers' distal segments. Concordant with this hypothesis are studies demonstrating that block of fast axoplasmic transport decreases ectopic electrical activity in injured peripheral nerves.[2]

Local demyelination of axons within neuromas may be another factor that permits focal accumulation of sodium channels. In our study and previous studies[3-5] of traumatic nerve injury, when sodium channels were found in large axons (>1 μm diameter), the axolemma was devoid of myelin. Demyelination of axons, even when not accompanied by axotomy, permits the insertion of sodium channels along previously internodal axolemma.[6] Taken together, these observations indicate that changes of the regional axonal environment at the site of injury may act to change the distribution of sodium channels.

An important question regarding the accumulation of sodium channels within neuromas is whether this accumulation is relevant to the pathophysiology of pain associated with neuromas. Neuromas certainly may serve as a generator of painful impulses.[1,2] Wall and Gutnick[1] were the first to demonstrate that some afferent fibers originating in a neuroma develop spontaneous electrical hyperexcitability. This axonal spontaneous hyperexcitability and the sensitivity of neuromas to mechanical and chemical stimuli are now indisputable facts.[2,8] The prevalence of such ectopic axonal hyperexcitability varies with nerve fiber type and with the time since nerve injury, but it is nearly always present. At peak activity, an average of 28% of all injured fibers fire spontaneously and an even higher percentage exhibit abnormal mechanosensitivity.[2] Because the axolemmal distribution of sodium channels largely determines the regions of electrical excitability in normal axons, an altered distribution or quantity of such channels is a likely cause of ectopic impulse generation in injured axons.[2-5,8]

Besides the immunologic evidence supporting abnormal accumulation of sodium channels within neuromas, pharmacologic and mathematical models support this concept. Local anesthetics such as lidocaine and mexiletine, which selectively block sodium channels, have been studied in animals and humans with peripheral nerve injury. In humans with neuromas, pain can be decreased by local infiltration of lidocaine into the subcutaneous tissues surrounding the

neuroma.[9] In rats with experimental neuromas, intravenous infusion of both lidocaine and mexiletine can completely abolish the spontaneous afferent activity arising within neuromas without blocking nerve conduction itself.[10] Matzner and Devor[8] showed that the sodium channel blockers tetrodotoxin and lidocaine stop neuroma firing by suppressing the process of impulse initiation without blocking impulse propagation. In contrast, veratridine, which increases sodium conductance, accelerates ectopic firing.[8] Taken together, these pharmacologic studies provide strong evidence that the generator potential associated with ectopic neuroma firing sites is encoded into an impulse train by a process that depends on voltage-sensitive sodium channels. Mathematic models suggest that excess membrane sodium conductance plays a major role in promoting axonal hyperexcitability. The Hodgkin-Huxley equation was used to predict the effects of altering maximal sodium conductance (g_{Na+max}) on the process of repetitive neuronal firing.[2] This model shows that increasing g_{Na+max}, without changing any other membrane variable, decreases the threshold current necessary to evoke repetitive firing. This change in membrane properties renders the membrane hyperexcitable. Although changes in other membrane properties may occur in the axons within neuromas, these data indicate that accumulation of excess sodium channels is sufficient to cause ectopic axonal hyperexcitability.

The accumulation of sodium channels within injured axons may be a feature common to all varieties of peripheral nerve trauma, especially those which give rise to neuromas. It is likely to be a major cause of ectopic axonal hyperexcitability. When injured sensory fibers develop hyperexcitability, the perception of pain and paresthesias likely occurs[2,4,5]; however, the entire explanation for neuroma-associated pain is, undoubtedly, more complicated than this. The membrane remodeling that allows a redistribution of sodium channels probably causes changes in other membrane-associated proteins, as well. In particular, other ion channels may undergo changes in distribution, quantity, or function. If alterations of voltage-sensitive potassium channels or calcium channels occur, axonal membrane electrical properties could be affected in a complex manner. Peripheral nerve injury should also trigger changes in the CNS such as postsynaptic amplification of afferent barrages and central sensitization, in which normally nonpainful afferent input is perceived as painful.[2] These other factors notwithstanding, further investigation of ion channel distribution and function within damaged axons should provide a better understanding of the basis for the abnormal electrical excitability that frequently develops after peripheral nerve trauma. Modification of ion channel distribution or function may prove to be a particularly fruitful approach to the treatment of pain in diseases of the peripheral nervous system.

From the Departments of Neurology (Drs. England, Happel, and Liu), Neurosurgery (Drs. Happel and Kline), and Anatomy (Ms. Thouron), Louisiana State University School of Medicine, New Orleans, LA; and the Department of Physiology (Drs. Gamboni and Levinson), University of Colorado School of Medicine, Denver, CO.

Supported by grants from the National Institutes of Health (NS15879 to S.R.L.), the United States Department of Defense (DAMD 17-93-V-3013 to J.D.E., L.T.H., and D.G.K.), and a Neuroscience Incentive Grant from the Louisiana State University Neuroscience Center (J.D.E. and L.T.H.).

Presented in part at the 47th Annual Meeting of the American Academy of Neurology, Seattle, WA, May 1995.

Received August 29, 1995. Accepted in final form November 13, 1995.

Address correspondence and reprint requests to Dr. John D. England, Department of Neurology, Louisiana State University School of Medicine, 1542 Tulane Avenue, New Orleans, LA 70112-2822.

References

1. Wall PD, Gutnick M. Properties of afferent nerve impulses originating from a neuroma. Nature 1974;248:740–743.
2. Devor M, Lomazov P, Matzner O. Sodium channel accumulation in injured axons as a substrate for neuropathic pain. In: Boivie J, Hansson P, Lindblom U, eds. Touch, temperature, and pain in health and disease: mechanisms and assessments, progress in pain research and management. Vol 3. Seattle: IASP Press, 1994:207–230.
3. Devor M, Keller CH, Deerinck TJ, Levinson SR, Ellisman MH. Na^+ channel accumulation on axolemma of afferent endings in nerve end neuromas in *Apteronotus*. Neurosci Lett 1989; 102:149–154.
4. Devor M, Govrin-Lippmann R, Angelides K. Na^+ channel immunolocalization in peripheral mammalian axons and changes following nerve injury and neuroma formation. J Neurosci 1993;13:1976–1992.
5. England JD, Gamboni F, Ferguson MA, Levinson SR. Sodium channels accumulate at the tips of injured axons. Muscle Nerve 1994;17:593–598.
6. England JD, Gamboni F, Levinson SR, Finger TE. Changed distribution of sodium channels along demyelinated axons. Proc Natl Acad Sci USA 1990;87:6777–6780.
7. Brismar T, Gilly WF. Synthesis of sodium channels in the cell bodies of squid giant axons. Proc Natl Acad Sci USA 1987;84: 1459–1463.
8. Matzner O, Devor M. Hyperexcitability at sites of nerve injury depends on voltage-sensitive Na^+ channels. J Neurophysiol 1994;72:349–359.
9. Chabel C, Jacobson L, Russell LC, Burchiel KJ. Pain responses to perineuromal injection of normal saline, gallamine, and lidocaine in humans. Pain 1989;36:321–325.
10. Chabal C, Russell LC, Burchiel KJ. The effect of intravenous lidocaine, tocainide, and mexiletine on spontaneously active fibers originating in rat sciatic neuromas. Pain 1989;38:333–338.

MICROSCOPY RESEARCH AND TECHNIQUE 34:445–451 (1996)

Immunocytochemical Investigations of Sodium Channels Along Nodal and Internodal Portions of Demyelinated Axons

JOHN D. ENGLAND, S. ROCK LEVINSON, AND PETER SHRAGER

Department of Neurology, Louisiana State University School of Medicine, New Orleans, Louisiana 70112 (J.D.E.); Department of Physiology, University of Colorado School of Medicine, Denver, Colorado 80262 (S.R.L.); Department of Physiology, University of Rochester Medical Center, Rochester, New York 14642 (P.S.)

KEY WORDS Ion channels, Neural conduction, Antibodies, Schwann cell, Doxorubicin, Lysolecithin

ABSTRACT Voltage-gated sodium channels are largely localized to the nodes of Ranvier in myelinated axons, providing the physiological basis for saltatory conduction. Studies using anti-sodium channel antibodies have shown that along demyelinated axons sodium channels form new distributions. The nature of this changed distribution appears to vary with the time course and mechanism of demyelination. In chronic demyelination, sodium channels increase in number and redistribute along previously internodal axon segments. In chronic demyelination produced by doxorubicin, the increase in sodium channels appeared independently of Schwann cells, suggesting increased neuronal synthesis. In acute demyelination produced by lysolecithin new clusters of sodium channels developed but only in association with the edges of remyelinating Schwann cells, which appeared to control the distribution and mobility of the channels. These findings affirm the plasticity of sodium channels in demyelinated axons and are relevant to understanding how these axons recover conduction.

INTRODUCTION

The sodium channel is a transmembrane protein which mediates the voltage-dependent sodium permeability of electrically excitable membranes. The presence of sodium channels is of obvious importance for the generation and propagation of action potentials along axolemma. The distribution of sodium channels along myelinated axons is nonuniform since they are largely localized to the nodes of Ranvier (Chiu, 1980; Ellisman and Levinson, 1982; Neumcke and Stampfli, 1982; Ritchie and Rogart, 1977; Waxman and Ritchie, 1993). This nodal localization of sodium channels provides one of the physiological bases for saltatory conduction. In contrast to these unchallenged observations regarding the localization of sodium channels in myelinated axons, little is known regarding the distribution of sodium channels in demyelinated axons. Such information is important because the resumption of axonal conduction appears the basis for recovery in many demyelinating diseases (Albers et al., 1985; Smith and Hall, 1980; Sumner, 1981). The recent availability of antibodies specifically directed against sodium channels has provided new and refined methods for examining sodium channels along demyelinated axons.

DISTRIBUTION OF SODIUM CHANNELS ALONG MYELINATED AXONS

In normal myelinated axons sodium channels are largely localized to the axolemma at nodes of Ranvier. The most recent electrophysiological and biochemical studies demonstrate an axolemmal sodium channel density of ~ 1,000 to 2,000/μm^2 at the nodes of Ranvier compared with a density of 40 to 80/μm^2 in the internodal segments (Chiu, 1980, 1987; Ellisman and Levinson, 1982; Neumcke and Stampfli, 1982; Ritchie and Rogart, 1977; Shrager, 1989; Waxman and Ritchie, 1993). Immunocytochemical studies such as those illustrated in Figures 1 and 2a have provided clear-cut proof of the nodal clustering of sodium channels.

The mechanisms underlying the segregation of sodium channels at nodes of Ranvier are not well understood. The observation that nodal-specific axolemmal specialization can develop independently of myelination suggests that intrinsic axonal factors immobilize sodium channels at nodes of Ranvier, perhaps independently of glial cell contact (Ellisman, 1979; Wiley-Livingston and Ellisman, 1980). Of particular interest in this regard is the protein, ankyrin, which links certain transmembrane proteins with the cytoskeleton in several types of cells, including erythrocytes and neurons (Baines, 1990). One isoform of ankyrin not only localizes to nodes of Ranvier (Kordeli et al., 1990) but also binds to the voltage-gated sodium channel (Srinivasan et al., 1988). These findings provide indirect support for the hypothesis that sodium channels are restricted to the node by their linkage to ankyrin, which associates with the internal cytomatrix via spectrin (Baines, 1990). The particular role played by glial cells in determining or refining nodal clustering of sodium channels is not known, but in one experimental model using co-cultures of sensory neurons and Schwann cells, the clustering of sodium channels on axons appeared to be related to Schwann cell contact (Joe and Angelides,

Received February 13, 1995; accepted in revised form March 20, 1995.

Address reprint requests to John D. England, M.D., Department of Neurology, Louisiana State University Medical Center, 1542 Tulane Avenue, New Orleans, LA 70112.

Fig. 1. Sodium channel localization along myelinated axons from the dorsal column of eel (*Electrophorus electricus*) spinal cord using a polyclonal anti-sodium channel antibody. **a:** Partially mechanically desheathed myelinated fiber showing sodium channel-specific immunostaining at the node of Ranvier (arrows). Bar = 1 μm. **b:** Completely mechanically desheathed fiber showing that sodium channel-specific immunostaining is still restricted to the nodal zone despite antibody access to internodal axolemma (arrows). Bar = 1 μm. **c:** Myelinated fiber reacted with antibody pre-adsorbed with purified sodium channel. The lack of immunostaining confirms antibody specificity for sodium channels. Bar = 1 μm. (Reproduced from Ellisman and Levinson, 1982, with permission of the authors and National Academy of Sciences.)

1992). Even if initial nodal clustering of sodium channels can occur independently of glial cell contact, glial cell-axon interactions could reshape and refine the final distribution of sodium channels. A major possibility is that the density of sodium channels could be suppressed along axolemma ensheathed by Schwann cells.

In the peripheral nervous system Schwann cell processes are closely apposed to the axolemma at nodes of Ranvier, and in the central nervous system astrocyte processes have a similar perinodal anatomy (Berthold and Rydmark, 1983; Hildebrand, 1971; Raine, 1984; Sims et al., 1991; Waxman and Black, 1984). These relationships are so specific that Schwann cell processes (in the PNS) and perinodal astrocyte processes (in the CNS) should be considered integral parts of the node of Ranvier. Thus, in the central nervous system, perinodal astrocytes are important components of the node of Ranvier even though oligodendrocytes provide myelin for the central axons. Both Schwann cells and astrocytes contain sodium channels. Glial sodium channels were documented first in cultured Schwann cells and astrocytes (Bevan et al., 1985; Chiu et al., 1984; Nowak et al., 1987; Shrager et al., 1985), but recent immunohistochemical studies have confirmed that sodium channels are expressed in situ by astrocytes and Schwann cells (Black et al., 1989a,b; Ritchie et al., 1990). Why sodium channels exist within these glial cells is not known. One theory is that these satellite cells may function as ancillary sites for the synthesis of sodium channels, which are then transferred to nodal axolemma (Bevan et al., 1985; Gray and Ritchie, 1985; Shrager et al., 1985). Since neurons produce and transport sodium channels independently of glial cells (Brismar and Gilly, 1987; England et al., 1994; Lombet et al., 1985), axonal sodium channels most likely do not arise exclusively or primarily from satellite cells. Thus, the significance of glial associated sodium channels is currently unknown.

DISTRIBUTION OF SODIUM CHANNELS ALONG DEMYELINATED AXONS

Demyelination is the primary pathophysiologic process in several important diseases of the nervous system. Examples include multiple sclerosis and the demyelinating peripheral neuropathies. In these diseases, at least acutely, most of the symptoms and signs are due to demyelinative conduction block along affected axons. Although remyelination and the re-establishment of saltatory conduction can restore function, many of these diseases are characterized by incomplete remyelination. This is especially true for demyelinative diseases of the central nervous system such as multiple sclerosis where limited remyelination occurs (McDonald, 1974, 1977). The well-established fact that patients with multiple sclerosis often exhibit considerable remission after an attack (despite persistent central nervous system demyelination) suggests that some chronically demyelinated axons can recover conduction, perhaps in a continuous manner (McDonald, 1974, 1977). In view of this possibility, several investigators have been interested in exploring how sodium channels might be reorganized along demyelinated ax-

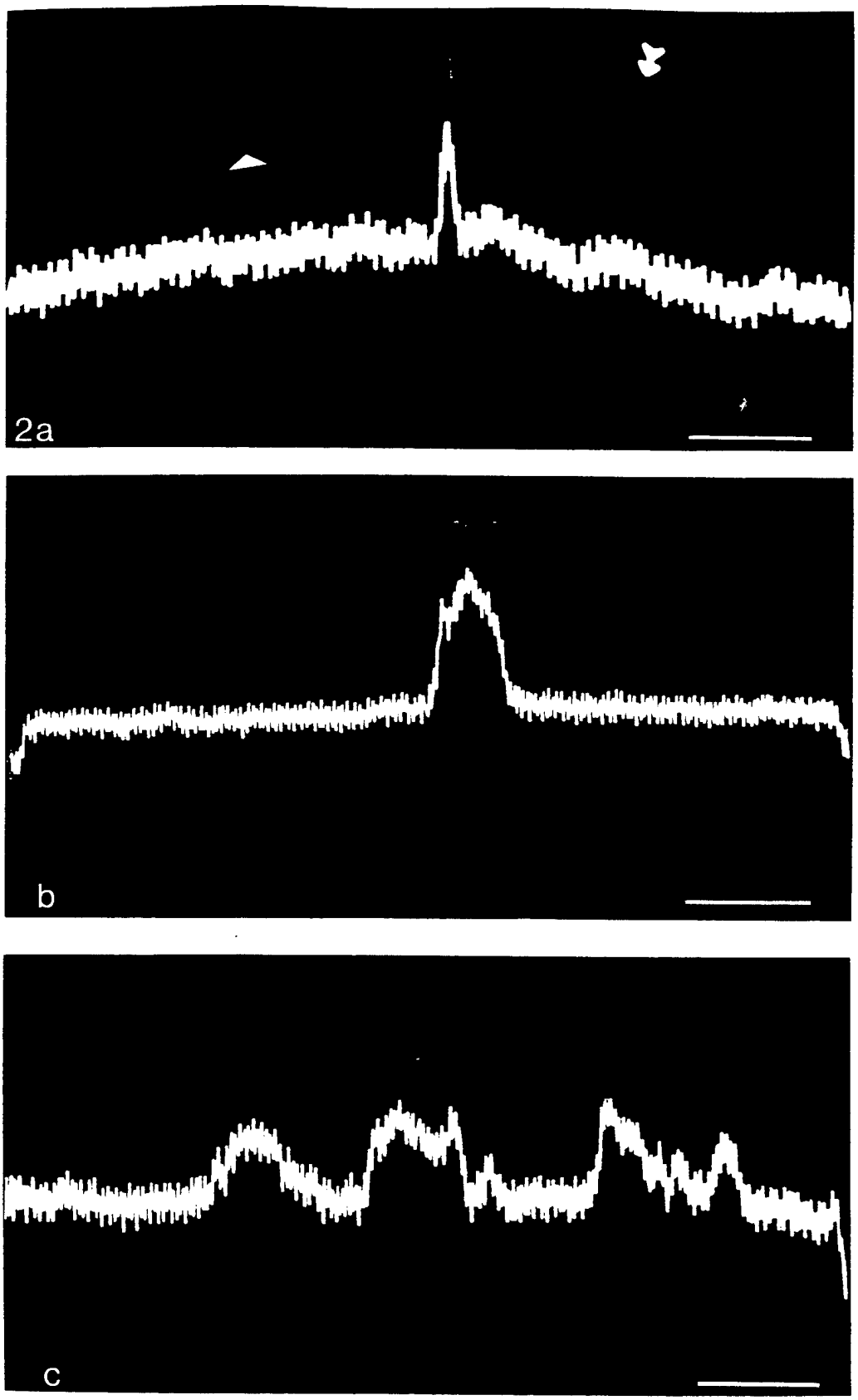

Fig. 2. Sodium channel localization along lateral line nerve axons from *Carassius auratus* using a polyclonal anti-sodium channel antibody. In a, b, and c the top image is the fluorescence photomicrograph and the bottom image is the digitized representation showing the relative pixel intensity along the axons. **a:** Normal myelinated axon. Note the discrete peak of immunoreactivity at the node of Ranvier, the lower level of nonspecific fluorescence of the myelin (arrow), and the virtually undetectable nonspecific fluorescence of mechanically desheathed internodal axon (arrowhead). **b:** Demyelinated axon at 14 days after injection of doxorubicin with one segment of intense immunoreactivity. **c:** Demyelinated axon at 21 days after injection of doxorubicin with multiple segments of intense immunoreactivity. Bars = 50 μm. (Reproduced from England et al., 1990, with permission of the authors and National Academy of Sciences.)

ons. Knowing how these channels are affected by demyelination is important to understanding why demyelinated axons fail to conduct impulses or, conversely, how some might recover conduction.

SUBACUTE AND CHRONIC DEMYELINATION

Several toxins which specifically demyelinate nerve are known. Using them, one can create a well-defined in vivo experimental model of demyelinated nerve which is well suited for investigating the resulting modulations of axonal sodium channels.

In vivo intraneural microinjection of doxorubicin, a DNA intercalating agent, causes delayed subacute demyelination by killing Schwann cells (England et al., 1988, 1990). In the posterior lateral line nerve of *Carassius auratus* (goldfish) this agent results in extensive segmental demyelination of axons starting at 12 to 14 days postinjection. Using a well-characterized polyclonal antibody directed against sodium channels, immunocytochemical studies have revealed new distributions of sodium channels along some of these demyelinated axons (England et al., 1990). The formation of the new distributions of sodium channels occurred concomitantly with the evolution of segmental demyelination, being evident by days 14 and 21 after injection. The segments of immunoreactivity specific for sodium channels ranged in length from 35 to 72 μm, much longer than nodes of Ranvier, which are approximately 1 μm in length. Several demyelinated axons (especially at days 21 to 28 after injection) showed multiple regions of specific immunoreactivity, each extending over relatively long stretches of bare axolemma (Fig. 2). These changes occurred along axons surrounded only by Schwann cell basal lamina without Schwann cell cytoplasm or myelin, implying that the new patches of sodium channels arose from within the axons themselves. Additionally, the length and location of the sodium channels indicated placement into previously internodal axolemma.

An important issue is whether such new distributions of sodium channels arise from the redistribution of already existing sodium channels at nodes of Ranvier or from the synthesis of new sodium channels. Evidence in favor of the synthesis of new sodium channels is available from radioimmunoassay (RIA) studies. RIA demonstrated a significant increase in the number of sodium channels in doxorubicin-demyelinated lateral line nerves of *C. auratus* (England et al., 1990, 1991). At days 14 and 28 after doxorubicin treatment there was approximately a three- to four-fold increase of sodium channels in the demyelinated nerves (Fig. 3). The time course of this phenomenon exactly paralleled that of the sodium channel distribution changes seen immunocytochemically (England et al., 1990). Taken together, these studies strongly suggest that new sodium channels are inserted into demyelinated axolemma.

Other studies have suggested a redistribution of sodium channels along demyelinated axons. For instance, Bostock and Sears demonstrated short segments of continuous conduction along axons demyelinated by diphtheria toxin (Bostock and Sears, 1976, 1978), and ferric ion-ferrocyanide (FeFCN) staining

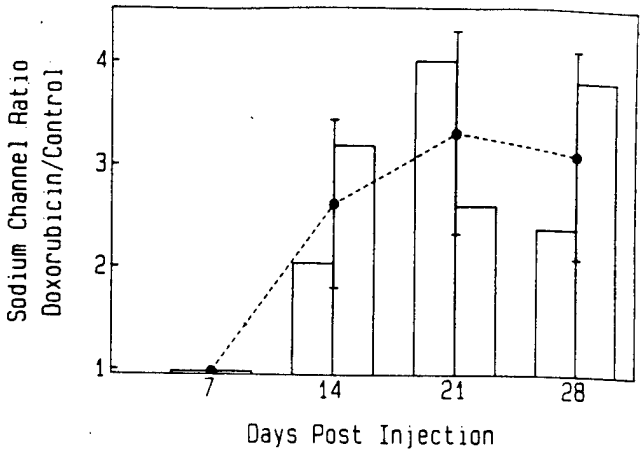

Fig. 3. Time course of the change in sodium channel quantity in nerves demyelinated by doxorubicin. Each column represents the ratio of the sodium channel concentration per wet weight demyelinated nerve/sodium channel concentration per wet weight control nerve for pooled nerve preparations. A total of 88 demyelinated nerves and an equal number of control nerves were analyzed by radioimmunoassay. The mean ratios (●) ± S.D. are shown. (Reproduced from England et al., 1991, with permission of the authors and Elsevier Science B.V.)

suggested a reorganization of axon membrane in rat demyelinated peripheral nerve fibers (Foster et al., 1980). More recently, increased sodium channel densities (assessed by tritiated saxitoxin binding) have been documented in the hypomyelinated brain of the mutant mouse *shiverer*, which has a deletion of the myelin basic protein gene (Noebels et al., 1991), as well as within the demyelinated brain lesions of human multiple sclerosis (Moll et al., 1991). Interestingly, the magnitude of these increases in sodium channels (two- to four-fold) closely approximates the values found in the RIA studies of doxorubicin-demyelinated nerves (England et al., 1991). Collectively, these data suggest that chronic demyelination in general causes a similar increase in the number of axonal sodium channels.

Although the above-noted studies are all consistent with the placement of new sodium channels along chronically demyelinated axons, the source of these channels is not known. The two major possibilities are that these sodium channels are synthesized within the neuron cell bodies or within glial cells. Sodium channels are quite clearly synthesized in neuron cell bodies (Brismar and Gilly, 1987) and transported within axons by fast axoplasmic transport (Lombet et al., 1985). In nerves demyelinated by doxorubicin, sodium channels increase despite the fact that Schwann cells die, suggesting a neuronal source for the new channels (England et al., 1990, 1991). Closely related work has demonstrated that excess sodium channels accumulate in afferent endings in nerve end neuromas (Devor et al., 1989) and within the tips of injured axons (England et al., 1994), further implying that new sodium channel distributions can arise solely from neuronal mechanisms. Since some astrocytes and Schwann cells contain sodium channels (Bevan et al., 1985; Black et al., 1989a,b; Chiu et al., 1984; Nowak et al., 1987; Ritchie

Fig. 4. Sodium channel clustering in remyelinating axons following intraneural microinjection of lysolecithin. **A:** Aggregates of sodium channels form at the edges of a Schwann cell, 14 days postinjection. **B:** Two sodium channel clusters associated with different Schwann cells appear to fuse, forming a new node of Ranvier, also at 14 days postinjection. **C:** Two new nodes of Ranvier separated by a short internode, 60 days postinjection. Bars = 10 μm. (Panel C reproduced from Dugandzija-Novakovic et al., 1995, with permission of the Society for Neuroscience.)

et al., 1990; Shrager et al., 1985), one must, at the least, consider the possibility that these glial cells provide demyelinated axons with new sodium channels. Additionally, neuronal synthesis of sodium channels and glial transport of sodium channels to axons may both occur. Using a polyclonal anti-sodium channel antibody, Black et al. have demonstrated patches of increased sodium channel density along rat spinal cord axons demyelinated by ethidium bromide/irradiation (Black et al., 1991); however, this immunostaining occurred only at axonal sites in contact with astrocyte or Schwann cell processes. The association of astrocytes with sodium channels along demyelinated central nervous system axons is somewhat surprising since it is the oligodendrocytes which provide myelin in the central nervous system. But, as previously noted, some astrocytes are normally closely apposed to central axons at the perinodal region. Astrocytes, instead of oligodendrocytes, appear to have an intimate association with sodium channels in central axons. In a few other experimental systems the development of sodium channel clusters in axolemma appeared to depend upon glial-axonal contact (Black et al., 1985; Hildebrand and Waxman, 1983; Rosenbluth, 1985; Rosenbluth and Blakemore, 1984). Thus, glial cells may provide or promote the expression of sodium channels along some chronically demyelinated axons. Their exact contribution requires further study.

ACUTE DEMYELINATION

Intraneural microinjection of lysolecithin causes acute demyelination (Hall and Gregson, 1971). The initial damage to myelin is visible within a few hours postinjection, progressing to complete demyelination of some axons within a few days. Proliferation of Schwann cells also occurs within a few days, and remyelination is evident by 9 to 10 days postinjection. This acute demyelination and rapid remyelination is, thus, much different than the chronic demyelination and incomplete remyelination which follows doxorubicin injection (England et al., 1988).

Using a site-directed polyclonal anti-sodium channel antibody, sodium channel clustering has been studied along rat sciatic axons demyelinated by intraneural injection of lysolecithin (Dugandzija-Novakovic et al., 1995). Demyelination developed rapidly, and by 7 days postinjection many axons exhibited long stretches of complete demyelination. At this stage clusters of sodium channels were rarely seen, appearing only at heminodes (marking the transition from myelinated to demyelinated axon at the injection site) and occasionally in the middle of a demyelinated axonal segment (presumably representing original nodal clusters). Beginning at approximately 8 days, proliferating Schwann cells adhered to demyelinated axons, and clusters of sodium channels were found at the edges of the Schwann cells (Fig. 4A). When the Schwann cells elongated, the clusters of sodium channels seemed to move with them along the axon. As the Schwann cells continued to move toward one another, their associated clusters of sodium channels were forced together in the ever decreasing length of axon separating the Schwann cell processes. Eventually the clusters of sodium channels associated with two apposing Schwann cells appeared to fuse, forming new nodes of Ranvier (Fig. 4B and C). Thus, at least in this model of acute demyelination, sodium channel aggregation and mobility are presumably linked to or controlled by remyelinating Schwann cells.

Previous investigators have studied the electrophysiological changes which occur along axons after acute demyelination. Rat ventral root axons were demyelinated by lysolecithin and examined using the electrophysiological technique of external longitudinal current analysis (Smith et al., 1982). New discrete foci of inward axonal current were seen as early as 4 days after application of lysolecithin, at which time remyelination or other morphological evidence of nodal formation were not yet present. These investigators suggested that these discrete foci of inward current were destined to become new nodes of Ranvier; therefore, they named them "phi" siological nodes or "ϕ"-nodes. Perhaps these "ϕ nodes" are the electrophysiological correlate of the sodium channel clusters seen immunocytochemically (Dugandzija-Novakovic et al., 1995) although why the electrophysiological foci were seen earlier (4 days) than the immunocytochemical clusters (8 days) is not known. Whether "ϕ nodes" require Schwann cell influence for their formation or arise de novo is also not known.

Entirely different electrophysiological results were documented along rat ventral root axons acutely demyelinated by diphtheria toxin (Bostock and Sears, 1976, 1978). Using the same technique of external longitudinal current analysis, Bostock and Sears recorded inwardly directed membrane currents over relatively long stretches of demyelinated axons, suggesting continuous conduction. Why axons acutely demyelinated by lysolecithin should develop discrete foci of inward current (suggesting discrete foci of sodium channels), whereas axons acutely demyelinated by diphtheria toxin should develop long segments of continuous conduction (suggesting long segments of internodal sodium channels) is an unresolved issue.

Sodium channel redistribution in demyelination may vary not only with the time course of this process (acute, subacute, and chronic) but also with the mechanism of demyelination. Resolution of these issues will require complementary electrophysiological and immunocytochemical studies. Understanding these processes in full will also require identification of the molecular interactions which determine aggregation of sodium channels within the axonal membrane.

ACKNOWLEDGMENTS

We thank Ms. Cathy A. England for secretarial assistance. This work was supported by grants from the National Institutes of Health (NS01272 to J.D.E., NS15879 to S.R.L., and NS17965 to P.S.) and the United States Department of Defense (DAMD17-93-V-3013 to J.D.E.).

REFERENCES

Albers, J.W., Donofrio, P.D., and McGonagle, T.K. (1985) Sequential electrodiagnostic abnormalities in acute inflammatory demyelinating polyradiculopathy. Muscle Nerve, 8:528–539.

Baines, A.J. (1990) Ankyrin and the node of Ranvier. TINS, 13:119–121.

Berthold, C., and Rydmark, M. (1983) Electron microscopic serial section analysis of nodes of Ranvier in lumbosacral spinal roots of the cat: Ultrastructural organization of nodal compartments in fibres of different sizes. J. Neurocytol., 12:475–505.

Bevan, S., Chiu, S.Y., Gray, P.T.A., and Ritchie, J.M. (1985) The presence of voltage-gated sodium, potassium and chloride channels in rat cultured astrocytes. Proc. R. Soc. Lond. (Biol.), 225:229–313.

Black, J.A., Sims, T.J., Waxman, S.G., and Gilmore, S.A. (1985) Membrane ultrastructure of developing axons in glial cell deficient rat spinal cord. J. Neurocytol., 14:79–104.

Black, J.A., Friedman, B., Waxman, S.G., et al. (1989a) Immunoultrastructural localization of sodium channels at nodes of Ranvier and perinodal astrocytes in rat optic nerve. Proc. R. Soc. Lond. (Biol.), 238:38–57.

Black, J.A., Waxman, S.G., Friedman, B., et al. (1989b) Sodium channels in astrocytes of rat optic nerve in situ: Immuno-electron microscopic studies. Glia, 2:353–369.

Black, J.A., Felts, P., Smith, K.J., Kocsis, J.D., and Waxman, S.G. (1991) Distribution of sodium channels in chronically demyelinated spinal cord axons: Immuno-ultrastructural localization and electrophysiological observations. Brain Res., 544:59–70.

Bostock, H., and Sears, T.A. (1976) Continuous conduction in demyelinated mammalian nerve fibres. Nature, 263:786–787.

Bostock, H., and Sears, T.E. (1978) The internodal axon membrane: Electrical excitability and continuous conduction in segmental demyelination. J. Physiol., 280:273–301.

Brismar, T., and Gilly, W.F. (1987) Synthesis of sodium channels in the cell bodies of squid giant axons. Proc. Natl. Acad. Sci. U.S.A., 84:1459–1463.

Chiu, S.Y. (1980) Asymmetry currents in the mammalian myelinated nerve. J. Physiol., 309:499–519.

Chiu, S.Y. (1987) Sodium and potassium currents in acutely demyelinated internodes of rabbit sciatic nerves. J. Physiol., 391:631–649.

Chiu, S.Y., Shrager, P., and Ritchie, J.M. (1984) Neuronal-type Na^+- and K^+-channels in rabbit cultured Schwann cells. Nature, 311: 156–157.

Devor, M., Keller, C.H., Deerinck, T.J., Levinson, S.R., and Ellisman, M.H. (1989) Na^+ channel accumulation on axolemma of afferent endings in nerve end neuromas in Apteronotus. Neurosci. Lett., 102:149–154.

Dugandzija-Novakovic, S., Koszowski, A.G., Levinson, S.R., and Shrager, P. (1995) Clustering of Na^+ channels and node of Ranvier formation in remyelinating axons. J. Neurosci., 15:492–503.

Ellisman, M.H. (1979) Molecular specializations of the axon membrane at nodes of Ranvier are not dependent upon myelination. J. Neurocytol., 8:719–735.

Ellisman, M.H., and Levinson, S.R. (1982) Immunocytochemical localization of sodium channel distributions in the excitable membranes of Electrophorus electricus. Proc. Natl. Acad. Sci. U.S.A., 79:6707–6711.

England, J.D., Rhee, E.K., Said, G., and Sumner, A.J. (1988) Schwann cell degeneration induced by doxorubicin (Adriamycin). Brain, 111: 901–913.

England, J.D., Gamboni, F., Levinson, S.R., and Finger, T.E. (1990) Changed distribution of sodium channels along demyelinated axons. Proc. Natl. Acad. Sci. U.S.A., 87:6777–6780.

England, J.D., Gamboni, F., and Levinson, S.R. (1991) Increased numbers of sodium channels form along demyelinated axons. Brain Res., 548:334–337.

England, J.D., Gamboni, F., Ferguson, M.A., and Levinson, S.R. (1994) Sodium channels accumulate at the tips of injured axons. Muscle Nerve, 17:593–598.

Foster, R.E., Whalen, C.C., and Waxman, S.G. (1980) Reorganization of the axon membrane in demyelinated peripheral nerve fibers: Morphological evidence. Science, 210:661–663.

Gray, P.T., and Ritchie, J.M. (1985) Ion channels in Schwann and glial cells. Trends Neurosci., 8:411–415.

Hall, S.M., and Gregson, N.A. (1971) The in vivo and ultrastructural effects of injection of lysophosphatidyl choline into myelinated peripheral nerve fibres of the adult mouse. J. Cell Sci., 9:769–789.

Hildebrand, C. (1971) Ultrastructural and light-microscopic studies of the nodal region in large myelinated fibres of the adult feline spinal cord white matter. Acta. Physiol. Scand. (Suppl.), 364:43–71.

Hildebrand, C., and Waxman, S.G. (1983) Regional node-like membrane specializations in non-myelinated axons of rat retinal nerve fiber layer. Brain Res., 258:23–32.

Joe, E., and Angelides, K. (1992) Clustering of voltage-dependent sodium channels on axons depends on Schwann cell contact. Nature, 356:333–335.

Kordeli, E., Davis, J., Trapp, B., and Bennett, V. (1990) An isoform of ankyrin is localized at nodes of Ranvier in myelinated axons of central and peripheral nerves. J. Cell Biol., 110:1341–1352.

Lombet, A., Laduron, P., Mourre, C., Jacomet, Y., and Lazdunski, M. (1985) Axonal transport of the voltage-dependent Na^+ channel protein identified by its tetrodotoxin binding site in rat sciatic nerves. Brain Res., 345:153–158.

McDonald, W.I. (1974) Remyelination in relation to clinical lesion of the central nervous system. Br. Med. Bull., 30:186–189.

McDonald, W.I. (1977) Acute optic neuritis. Br. J. Hosp. Med., 18:42–48.

Moll, C., Mourre, C., Lazdunski, M., and Ulrich, J. (1991) Increase of sodium channels in demyelinated lesions of multiple sclerosis. Brain Res., 556:311–316.

Neumcke, B., and Stampfli, R. (1982) Sodium currents and sodium-current fluctuations in the rat myelinated nerve fibers. J. Physiol., 329:163–184.

Noebels, J.L., Marcom, P.K., and Jalilian-Tehrani, M.H. (1991) Sodium channel density in hypomyelinated brain increased by myelin basic protein gene deletion. Nature, 352:431–434.

Nowak, L., Ascher, P., and Berwald-Netter, Y. (1987) Ionic channels in mouse astrocytes in culture. J. Neurosci., 7:101–109.

Raine, C.S. (1984) On the association between perinodal astrocyte processes and the node of Ranvier in the CNS. J. Neurocytol., 13: 21–27.

Ritchie, J.M., and Rogart, R.B. (1977) Density of sodium channels in mammalian myelinated nerve fibers and nature of the axonal membrane under the myelin sheath. Proc. Natl. Acad. Sci. U.S.A., 74: 211–215.

Ritchie, J.M., Black, J.A., Waxman, S.G., and Angelides, K.J. (1990) Sodium channels in the cytoplasm of Schwann cells. Proc. Natl. Acad. Sci. U.S.A., 87:9290–9294.

Rosenbluth, J. (1985) Intramembranous particle patches in myelin-deficient rat mutant. Neurosci. Lett., 62:19–24.

Rosenbluth, J., and Blakemore, W.F. (1984) Structural specializations in cat of chronically demyelinated spinal cord axons as seen in freeze-fracture replicas. Neurosci. Lett., 48:171–177.

Shrager, P. (1989) Sodium channels in single demyelinated mammalian axons. Brain Res., 483:149–154.

Shrager, P., Chiu, S.Y., and Ritchie, J.M. (1985) Voltage-dependent sodium and potassium channels in mammalian cultured Schwann cells. Proc. Natl. Acad. Sci. U.S.A., 82:948–952.

Sims, T.J., Gilmore, S.A., and Waxman, S.G. (1991) Radial glia give rise to perinodal processes. Brain Res., 549:25–36.

Smith, K.J., and Hall, S.M. (1980) Nerve conduction during peripheral demyelination and remyelination. J. Neurol. Sci., 48:201–219.

Smith, K.J., Bostock, H., and Hall, S.M. (1982) Saltatory conduction precedes remyelination in axons demyelinated with lysophosphatidyl choline. J. Neurol. Sci., 54:13–31.

Srinivasan, Y., Elmer, L., Davis, J., Bennett, V., and Angelides, K. (1988) Ankyrin and spectrin associate with voltage-dependent sodium channels in brain. Nature, 333:177–180.

Sumner, A.J. (1981) The physiological basis for symptoms in Guillain-Barre syndrome. Ann. Neurol. (Suppl.), 9:28–30.

Waxman, S.G., and Black, J.A. (1984) Freeze-fracture ultrastructure of the perinodal astrocyte and associated glial junctions. Brain Res., 308:77–87.

Waxman, S.G., and Ritchie, J.M. (1993) Molecular dissection of the myelinated axons. Ann. Neurol., 33:121–136.

Wiley-Livingston, C.A., and Ellisman, M.H. (1980) Development of axonal membrane specializations defines nodes of Ranvier and precedes Schwann cell myelin elaboration. Dev. Biol., 79:334–355.

Pergamon

PII: S0197-0186(96)00075-7

Neurochem. Int. Vol. 30, Nos 4/5, pp. 401–410, 1997

0197-0186/97 $17.00 + 0.00

TUMOR NECROSIS FACTOR-ALPHA AND INTERLEUKIN-1 INDUCE ACTIVATION OF MAP KINASE AND SAP KINASE IN HUMAN NEUROMA FIBROBLASTS

GANG LU,[1] ROGER W. BEUERMAN,[1]* SHURUM ZHAO,[2] GUANG SUN,[1] DOAN H. NGUYEN,[1] SUSAN MA[1] and DAVID G. KLINE[2]

[1]LSU Eye Center and [2]Department of Neurosurgery, Louisiana State University Medical Center School of Medicine, New Orleans, Louisiana, U.S.A.

(*Received 29 March 1996; accepted 4 June 1996*)

Abstract—Two cytokines, tumor necrosis factor-alpha (TNF-α) and interleukin-1 (IL-1), which are released by macrophages during the early inflammatory phase of nerve injury, are known to induce activation of mitogen-activated protein kinase (MAPK) and stress-activated protein kinase (SAPK), which locate at different signal transduction pathways and are involved in cell cycle G_0/G_1 transition and cellular proliferation in human fibroblasts. Activation of these two protein kinases by the cytokines may stimulate fibroblast proliferation in damaged nerves and thereby play a role in the formation of a neuroma, a disorganized mass of tissue that interferes with neural regeneration and repair. To investigate the possibility that this mechanism is operative in neuroma formation, we used cultured, serum-starved fibroblasts from surgically removed human neuromas stimulated with TNF-α and/or IL-1α and IL-1β, and measured the activation of MAPK and SAPK using myelin basic protein (MBP) and human c-Jun (1–169) glutathione S-agarose transferase (GST) fusion protein as substrates. For comparison, neuroma fibroblast cultures were also stimulated with phorbol 12-myristate 13-acetate (PMA) and platelet-derived growth factor-AB (PDGF-AB), a potent activator for MAPK. TNF-α and both forms of IL-1 produced a rapid activation of MAPK, with a peak at 15 min for TNF-α stimulation, and a peak at 30 min for IL-1 stimulation. TNF-α combined with either IL-1α or IL-1β produced a synergistic effect on the activation of MAPK. The increases in MAPK induced by TNF-α and IL-1 were similar to the increases induced by PMA and PDGF-AB. To confirm the presence of MAPK, immunoprecipitation and immunoblotting were carried out on experimental and control lysates. TNF-α and IL-1 also increased activation of SAPK, but to a lesser extent than MAPK. PMA and PDGF-AB were also much less effective in stimulating activation of SAPK. Our findings indicate that TNF-α and IL-1 activate parallel signal transduction pathways in human neuroma fibroblasts, and that they are relatively stronger activators of MAPK than of SAPK. Previous studies have convincingly demonstrated that MAPK and SAPK are involved in human fibroblast proliferation. The results of our study suggest that TNF-α and IL-1 may play a role in frustrating functional nerve regeneration after injury by stimulating these two kinases, which, in turn, leads to fibroblast proliferation and formation of neuromas. © 1997 Elsevier Science Ltd. All rights reserved

Injury to peripheral nerve initiates a series of cellular reactions that include invasion of the injury site by inflammatory cells and activation and transformation of the neural fibroblasts and Schwann cells. Interruption of the vascular supply and the associated cellular damage allow macrophages and other cells of immune origin to gain easy access to the interior of the nerve (Frisén *et al.*, 1993; Venezie *et al.*, 1995). Macrophages secrete large amounts of cytokines, in particular tumor necrosis factor-alpha (TNF-α). The environment in which this occurs (the interior of the damaged nerve) is somewhat sequestered from the extra-neural space and there is ample opportunity for the fibroblasts and Schwann cells therein to be exposed to cytokines or other cell signaling molecules.

An undesirable consequence of nerve damage is the development of a neuroma, which prevents neural growth and functional recovery. A neuroma consists of a disorganized mass of connective tissue made up largely of fibroblasts and their collagen products. Cytokines, which can be damaging or stimulatory to fibroblasts, may be involved in neuroma formation, but their role, if any, is unclear. The purpose of this study was to examine the response of human neuroma

*To whom all correspondence should be addressed at: LSU Eye Center, 2020 Gravier Street, Suite B, New Orleans, LA 70112, U.S.A.

fibroblasts to cytokines and to determine if a growth or proliferative response could be identified.

TNF-α (cachectin), a product of stimulated monocytes and macrophages, is a 17 kDa polypeptide that binds to two specific receptors (55 and 80 kDa) and mediates a wide range of biological activities (Vilcek and Lee, 1991). In human fibroblasts, the 55 kDa receptor is the major functional receptor for TNF-α (Tartaglia and Goeddel, 1991). Interleukin-1 occurs in the form of two polypeptides, IL-1α and IL-1β, which are distinct gene products with molecular weights of 17 kDa. However, they recognize the same cell surface receptors and share various biologic activities. There are two types of receptors for IL-1: receptor type I, a major functional receptor, of which the 25 kDa cytoplasmic portion is essential for signaling, and receptor type II, a smaller protein that is unimportant in signal transduction (Sims *et al.*, 1993). Both TNF-α and IL-1 are proinflammatory cytokines and induce some similar biological effects, particularly those associated with local and systemic inflammatory processes, but they share only 3% of their primary amino acid structure and have entirely different receptors (Dinarello, 1991). TNF-α and IL-1 have been shown to stimulate fibroblast proliferation, modulate reparative functions following tissue injury, and accelerate wound healing (Dinarello, 1991; Schmidt *et al.*, 1982; Sugarman *et al.*, 1985; Vilcek *et al.*, 1986; Vilcek and Lee, 1991).

Previous studies have demonstrated that TNF-α and IL-1 activate several protein kinases, including MAPK, in human fibroblasts, indicating that these two cytokines may share a cytoplasmic component of a signal transduction pathway (Guy *et al.*, 1991). Activation of MAPK is an absolute requirement for triggering the fibroblast proliferative response and cell cycle progression (Meloche, 1995; Pagès *et al.*, 1993). Recent studies have confirmed that, in some types of cells, TNF-α and IL-1 also induce activation of a novel protein kinase, stress-activated protein kinase (SAPK), which is part of a signal transduction cascade related to, but distinct from, the MAPK pathway (Brach *et al.*, 1993; Kyriakis *et al.*, 1994; Sánchez *et al.*, 1994; Sluss *et al.*, 1994; Westwick *et al.*, 1994; Whitmarsh *et al.*, 1995). Activated MAPK and/or SAPK can translocate into the nucleus and regulate the early response genes *c-jun* and *c-fos*, which are activated prior to the G_0/G_1 cell cycle transition. Neutralizing antibodies to *c-jun* or *c-fos* are capable of abolishing cell cycle progression in human fibroblasts.

In the present study, we stimulated fibroblasts cultured from human neuroma tissues with TNF-α and IL-1 and found that both protein kinases, MAPK and SAPK, were activated in the stimulated cells. For activation of MAPK, the effect of a combination of TNF-α and either IL-1α or IL-1β was synergistic. PMA and PDGF-AB increased activation of MAPK, but had only weak effects on SAPK. These results suggest that TNF-α and IL-1 may trigger fibroblast proliferation and accelerate the early stages of neuroma formation after injury to peripheral nerve.

EXPERIMENTAL PROCEDURES

Materials

Human recombinant TNF-α (3.3×10^4 units/μg), IL-1α (1×10^4 units/μg), IL-1β (1×10^4 units/μg), and platelet-derived growth factor isoform-AB (PDGF-AB) were purchased from Upstate Biotechnology Incorporated (UBI, Lake Placid, NY, U.S.A.). Anti-MAPK rabbit polyclonal antibody covalently coupled to protein A agarose by dimethylpimelimidate; anti-human MAPK polyclonal antibody, which recognizes 42 and 44 kDa isoforms of MAPK; and human c-Jun (1–169) GST fusion protein were also purchased from UBI. Protein transfer membrane was obtained from Amersham (England). [γ-^{32}P]ATP (800 Ci/mmol) and ^{125}I-protein A (58.67 mCi/mg) were obtained from ICN (Irvine, CA, U.S.A.). Sodium pyrophosphate, trichloroacetic acid, *b*-glycerolphosphate, and *b*-mercaptoethanol were purchased from Aldrich Chemical Co. (Milwaukee, WI, U.S.A.). Dulbecco's modified Eagle's medium (D-MEM) and fetal bovine serum were obtained from Gibco BRL, Life Technologies, Inc. (Grand Island, NY, U.S.A.). PMA and all other reagents were purchased from Sigma (St Louis, MO, U.S.A.).

Cell culture and cytokine treatment

Human neuroma tissues obtained from surgical patients were cut into pieces and cultured in D-MEM containing 20% fetal bovine serum, 100 units/ml penicillin, and 100 μg/ml streptomycin, and maintained at 37°C in a humidified atmosphere of air with 5% CO_2. The cells were used at passages two to six. In each passage, about 1×10^6 cells were seeded in 100 mm polystyrene tissue culture dishes and allowed to grow to confluence. The medium was changed to serum-free medium for 24 h prior to experimental manipulation. The quiescent cells were stimulated by adding 10 ng/ml TNF-α, 3 ng/ml IL-1α, or 3 ng/ml IL-1β or a combination of TNF-α and IL-1α or IL-1β. In another experiment, PDGF-AB (10 ng/ml) was added to the culture medium, and the cells were incubated for 15 min at 37°C, or PMA (300 ng/ml) was added to the medium and the cells were incubated for 10 min at 37°C. Control cells were cultured in the same fashion but were not stimulated with cytokines.

MAPK in vitro *assay*

Experimental and control cells were washed three times in ice-cold phosphate-buffered saline, then scraped into 500 μl of ice-cold lysis buffer containing 50 mM *b*-glycerolphosphate (pH 7.4), 7 mM NaF, and 0.3 mM EDTA. The cell lysate was collected into a pellet pestle tube (Kontes) and centrifuged at 5000 rpm for 5 min at 4°C. The pellets were ground, then centrifuged again at 12,000 rpm for 15 min at

4°C. The supernatant was collected into Eppendorf microcentrifuge tubes and stored at −70°C for analysis. The protein concentration was measured with BCA protein assay reagent (Pierce, Rockford, IL, U.S.A.).

MAPK activity was determined with the use of myelin basic protein (MBP) as substrate. In this procedure, 15 μl of cell extract, 10 μl (2 μg/μl) MBP, 15 μl reaction buffer mixture containing 70 mM *b*-glycerolphosphate, 10 mM NaF, 0.6 mM EDTA, 15 mM $MgCl_2$, 2 mM dithiothreitol, 2 μCi [γ-^{32}P]ATP, and 10 μM ATP were added. The tubes were vortexed gently and incubated for 10 min at 30°C. The reaction was stopped by placing 20 μl aliquots of the kinase assay mixture onto 2 × 2 cm squares of P81 phosphocellulose papers, which were then washed in 0.75% phosphoric acid for 15 min with three changes of buffer. After the papers were rinsed in acetone for 5 min, each paper was transferred into a scintillation vial and radiolabel incorporation was determined by liquid scintillation counting. The remaining reaction mixture was mixed with 15 μl of 2X Laemmli's sample buffer, boiled for 5 min, and subjected to 10% SDS–PAGE. The gel was washed extensively in a washing buffer containing 1% sodium pyrophosphate and 5% trichloroacetic acid, then dried for autoradiography.

Immunocomplex MAPK assay

Experimental and control cells were washed three times with ice-cold phosphate-buffered saline, then lysed in 500 μl of lysis buffer containing 50 mM *b*-glycerolphosphate (pH 7.4), 7 mM NaF, 0.3 mM EDTA, 10 μg/ml pepstatin, and 10 μg/ml aprotinin. The cell lysates were centrifuged at 12,000 rpm in an Eppendorf microcentrifuge tube for 15 min at 4°C. The supernatant (300 μl) was collected and incubated with protein A-agarose rabbit polyclonal antibody to MAPK for 2 h at 4°C. After centrifugation, the supernatant was removed, the bead-antibody–antigen complex was washed twice with lysis buffer, and the complex was resuspended in 20 μl of substrate (MBP, 2 μl/ml). The reaction was started by adding 20 μl of the reaction buffer mixture containing 5 μCi [γ-^{32}P]ATP and 10 μM ATP, and the samples were incubated for 10 min at 37°C. The reaction was stopped by the addition of 20 μl of 2X Laemmli's sample buffer. The samples were boiled for 5 min and subjected to 10% SDS–PAGE. After electrophoresis, the gel was dried and autoradiography was performed. Band densities were determined by scanning with a StrataScan 7000 (StrataGene, CA, U.S.A.).

Immunoblotting

Equal volumes of lysate were subjected to 10% SDS–PAGE. After electrophoresis, the proteins were transferred to a membrane using transfer buffer containing 20 mM Trisma (base) (pH 8.6), 120 mM glycine, and 20% (V/V) methanol. The membrane was washed with PBS (pH 7.4), blocked with freshly prepared PBS containing 3% nonfat dry milk, and subsequently probed with rabbit polyclonal antibody to MAPK diluted 1:200 in PBS nonfat milk buffer overnight at 4°C. The next day, the membrane was washed with PBS buffer. For detection of antibody, the membrane was incubated in PBS nonfat milk buffer containing ^{125}I-protein A (1 μCi/ml) for 2 h at room temperature, washed three times in PBS buffer, dried, and exposed to x-ray film at −70°C.

Solid-phase JNK assay

A previously described method (Hibi *et al.*, 1993) was modified slightly and adapted for this experiment. Briefly, cultured cells were lysed with a buffer containing 25 mM HEPES (pH 7.7), 0.3 M NaCl, 1.5 mM $MgCl_2$, 0.2 mM EDTA, 0.1% Triton X-100, 0.5 mM DTT, 20 mM *b*-glycerolphosphate, 0.1 mM Na_3VO_4, 2 μg/ml leupeptin, and 100 μg/ml PMSF. The lysates were diluted in buffer containing 25 mM HEPES (pH 7.7), 75 mM NaCl, 2.5 mM $MgCl_2$, 0.1 mM EDTA, 0.05% Triton X-100, 0.5 mM DTT, 20 mM *b*-glycerolphosphate, 0.1 mM Na_3VO_4, 2 μg/ml leupeptin, and 100 μg/ml PMSF. Diluted cell lysates (300 μl with 30 μg protein) were mixed with 5 μl of c-Jun GST agarose suspension and incubated with gentle agitation for 2 h at 4°C, then pelleted by centrifugation. The complexes were washed three times with HEPES binding buffer (20 mM HEPES, pH 7.7; 50 mM NaCl; 2.5 mM $MgCl_2$; 0.1 mM EDTA, and 0.05% Triton X-100), resuspended in 20 μl of kinase buffer (20 mM HEPES, pH 7.6; 20 mM $MgCl_2$; 20 mM *b*-glycerolphosphate; 20 mM *p*-nitrophenyl phosphate; 0.1 mM Na_3VO_4; 2 mM DTT) containing 20 μM ATP and 3 μCi [γ-^{32}P]ATP, and incubated for 20 min at 30°C. The reaction was terminated by adding 20 μl of 2X Laemmli's sample buffer and the samples were subjected to 10% SDS–PAGE. After electrophoresis the gel was washed with washing buffer for staining and autoradiography. The band density of phosphorylated c-Jun GST fusion protein was determined by scanning densitometry.

RESULTS

Kinetics of MAPK activation

MAPK phosphorylates MBP *in vitro* as a specific substrate. By measuring the ability of lysates from experimental and control cells to phosphorylate MBP, we determined the ability of cytokines alone and in combination to activate MAPK in human neuroma fibroblasts. To determine optimal concentrations and contact time for stimulation, we initially measured the activity of MAPK in a concentration series following stimulation by TNF-α and IL-1. In this system, a peak of MAPK activation was reached for TNF-α at 10 ng/ml (Fig. 1(A)). This concentration is consistent with previous reports that cytokines in low concentration can stimulate proliferation and mediate various cellular functions of fibroblasts (Hattori *et al.*, 1993; Sugarman *et al.*, 1985; Vilcek *et al.*, 1986). The profile for Il-1α appeared to have two peaks, one at 1 ng and one at 100 ng; however, in preliminary experiments involving stimulation with IL-1α and TNF-α in combination, 3 and 6 ng of IL-1α gave similar results, and, therefore, 3 ng was chosen for use in subsequent experiments. As seen in Fig. 1(B), the peak at 6 ng was only slightly and non-significantly greater than the value at 3 ng. (Although we also saw a peak at 100 ng, this concentration is probably not physiological.) The time-dependent study of MAPK activation showed

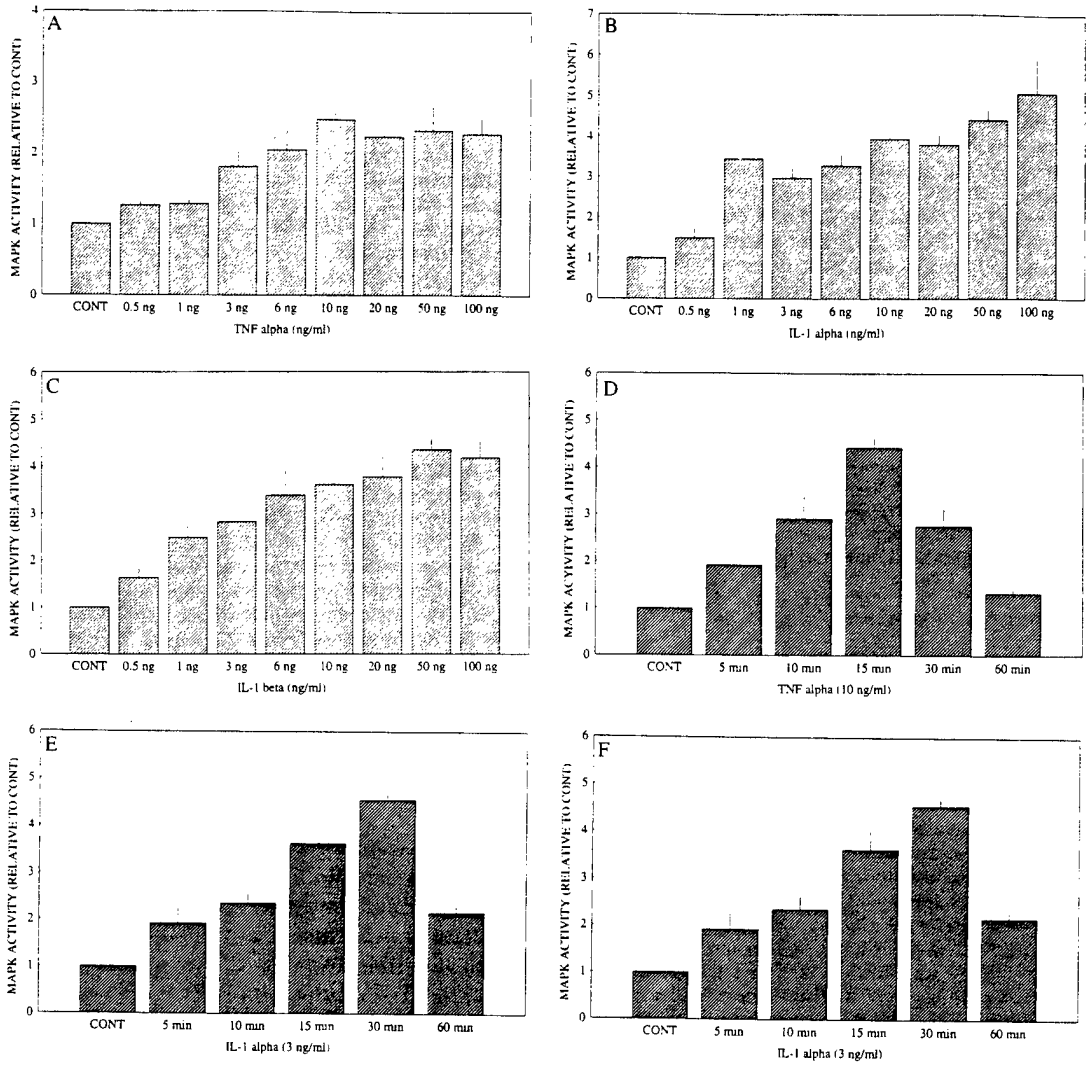

Fig. 1. TNF-α and IL-1 activation of MAPK in human neuroma fibroblasts. (A) TNF-α, (B) IL-1α, and (C) IL-1β concentration-dependent responses. (D) TNF-α, (E) IL-1α, and (F) IL-1β time kinetics. Human neuroma fibroblasts were grown to confluence and incubated in serum-free medium for 24 h, then stimulated for 15 min with TNF-α or IL-1 in doses ranging from 0.5 to 100 ng ml. For the time kinetics studies, cells were treated with 10 ng/ml TNF-α or 3 ng/ml IL-1 and harvested at different time points. The activity of MAPK in the lysates was determined as described in Experimental Procedures. Three independent tests were repeated in each experiment. Values are expressed as means $\pm$ standard errors. CONT, control.

that TNF-α induced a rapid activation of MAPK; the level was maximal at 15 min, then declined to control level at 1 h (Fig. 1(D)). For IL-1α and IL-1β stimulation, MAPK activity was maximal at 30 min (a slight delay from the peak with TNF-α), and declined by 60 min (Fig. 1(E) and (F)).

TNF-α and IL-1 activation of MAPK in human neuroma fibroblasts

We evaluated MAPK activation produced by TNF-α and IL-1, individually and in combination, using a 15 min stimulation period. PMA and PDGF-AB, two

known activators of MAPK, were selected as positive controls. PMA is a potent activator of MAPK, exerting its effect by phosphorylation of protein kinase C and Raf-1 signal transduction pathways. We used 300 ng/ml of PMA, which produced maximal stimulation in the human neuroma fibroblasts (data not shown). PDGF-AB, a major functional isoform of platelet-derived growth factor that also stimulates fibroblast proliferation (Meyer-Ingold and Eichner, 1995), was used at a concentration of 10 ng/ml. PDGF-AB is an intrinsic tyrosine MAPK activator and the signal transduction pathway and mitogenic effects are well documented (Lubinus *et al.*, 1994; Marshall, 1995; Valius and Kazlauskas, 1993). Following the 15 min stimulation period, the lysates from experimental and control cells were reacted with substrate (MBP) and reaction buffer containing [γ-^{32}P]ATP for 10 min. Phosphorylation of MBP was used as the measure of MAPK activity in the lysates.

The results showed that treatment with either TNF-α or IL-1 alone increased activation of MAPK nearly 2.5-fold, compared with control. Samples treated with a combination of TNF-α and IL-1 showed a 3.5-fold increase in the phosphorylation of MBP, an increase greater than that produced by either cytokine alone (Fig. 2). The increase resulting from stimulation by the two cytokines together was also greater than that produced by PDGF-AB and was similar to that produced by PMA, which was the most potent activator used in our study. These results demonstrated that TNF-α and IL-1 are individually capable of activating MAPK and also that stimulation with the two cytokines together produces a synergistic effect that further enhances MAPK activation. Statistical analysis of the results from 8 to 11 independent repetitions showed that activation by TNF-α and IL-1α together was significantly greater than activation by either one alone ($p<0.0001$). Activation by TNF-α and IL-1β was also greater than activation by TNF-α alone ($p<0.001$), but was not significantly different from activation by IL-1β ($p=0.051$).

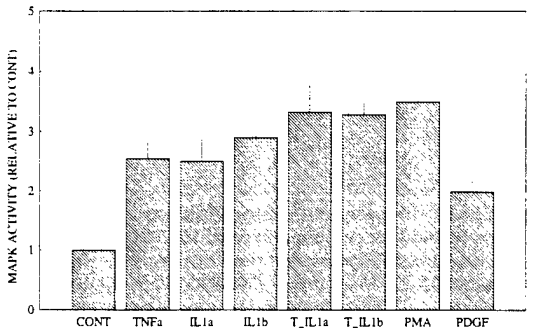

Fig. 2. MAPK activity in human neuroma fibroblasts treated with either TNF-α, IL-1, or a combination of the two; PMA; or PDGF-AB. Serum-starved cells were treated with 10 ng/ml TNF-α and/or 3 ng/ml IL-1 for 15 min, 300 ng/ml PMA for 10 min, or 10 ng/ml PDGF-AB for 15 min. Eight to 11 independent experiments were repeated with TNF-α and IL-1, and three with PMA and PDGF-AB. The lysates from experimental and control cells were reacted with substrate (MBP) and reactivation buffer containing [γ-^{32}p]ATP for 10 min. Phosphorylation of MBP was measured to determine MAPK activity in the lysates. The combination of TNF-α and IL-1α produced significantly greater MAPK activation than either one alone ($P<0.0001$). Activation by TNF-α and IL-1β combined was significantly greater than that produced by TNF-α alone ($p<0.001$), but not significantly different from that produced by IL-1β alone ($p=0.051$). Values are expressed as means ± standard errors. CONT, control; T—IL1a, TNF-α plus IL-1α; T—IL1b, TNF-α plus IL-1β.

We undertook to demonstrate activation of MAPK more specifically, in that it is possible that some other protein kinase could potentially phosphorylate MBP, the substrate used in this study. To this end, immunoprecipitation of MAPK from experimental and control lysates was carried out with protein A-agarose bound to rabbit polyclonal antibody to MAPK, and the resulting immunocomplex was reacted with MBP and reaction buffer containing [γ-^{32}P]ATP. Following electrophoresis, the densities of the phosphorylated MBP bands were calculated. It was found that, after stimulation with TNF-α, IL-1α, and Il-1β, MAPK levels were 4.5-, 2.3- and 3-fold higher than control levels, respectively. The combination of TNF-α and IL-1α and the combination of TNF-α and IL-1β produced 5.5- and 6-fold higher levels, respectively, compared with controls. PMA stimulation produced 7-fold higher levels, and PDGF-AB produced 5-fold higher levels, compared with controls (Fig. 3). Thus, activation of MAPK and the synergistic effect of the combination of TNF-α and IL-1 were confirmed in these experiments.

We analysed MAPK by immunoblotting with a polyclonal antibody that recognizes both the 42 and the 44 kDa isoforms. Activation of MAPK requires phosphorylation on the threonine and serine residues, which changes the electrophoretic mobility. In untreated control cells, the 42 kDa band was seen, but the 44 kDa band was somewhat stronger. In the lysate from the cytokine-treated cells (Fig. 4), however, the 44 kDa band was considerably more intense than the 42 kDa band. This type of molecular weight shift is consistent with MAPK activation.

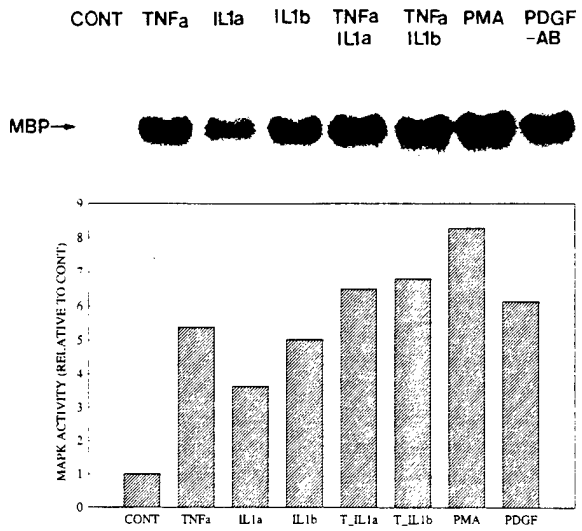

Fig. 3. Immunoprecipitation analysis of MAPK activity. (Top) The lysates from experimental and control cells were immunoprecipitated with protein A-agarose bound to rabbit polyclonal antibody to MAPK, and the resulting immunocomplexes were washed, resuspended, and mixed with reaction buffer containing MBP and [γ-^{32}P]ATP for 10 min at 30°C. The reaction was stopped by the addition of 2X Laemmli's sample buffer, after which the samples were boiled for 3 min and subjected to 10% SDS–PAGE. (Bottom) The phosphorylated MBP bands were scanned and the densities of the bands were calculated and plotted as a histogram. CONT, control; T—IL1a, TNF-α plus IL-1α; T—IL1b, TNF-α plus IL-1β.

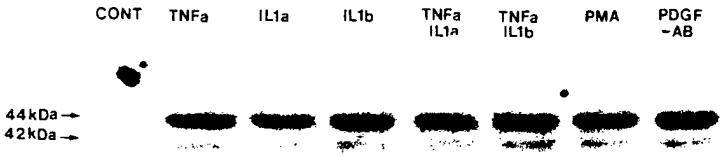

Fig. 4. Immunoblot analysis of human neuroma fibroblast lysates. Lysates from experimental and control cells were analysed as previously described. Equal volumes of the lysates were subjected to 10% SDS–PAGE. After electrophoresis, the protein was transferred onto nitrocellulose membranes then probed with an anti-MAPK antibody that recognizes both the 44 and 42 kDa isoforms of MAPK. The immunocomplexes on the membrane were detected with ^{125}I-labeled protein A and imaged by autoradiography. CONT, control.

TNF-α and IL-1 activation of JNK/SAPK signaling pathway

Recent studies have found that in some cell types, TNF-α and IL-1 activate a distinct signal transduction pathway, the JNK/SAPK signaling pathway, which is thought to be responsible for phosphorylation of the transactivating domain of the c-Jun protein *in vivo* and is an upstream regulator of activation of the *c-jun* gene. Phosphorylated c-Jun homodimers have potent AP-1 activity and control the expression of a number of genes.

To determine if TNF-α and IL-1 induce activation of the JNK pathway in human neuroma fibroblasts, solid-phase protein kinase assays were carried out using a GST fusion protein containing amino acids 1-169 of c-Jun. This c-Jun GST fusion protein is bound through its GST moiety to glutathione (GSH)-agarose beads to generate an affinity matrix for identification of c-Jun binding proteins. The c-Jun amino-terminal kinase binds to a specific region within the c-Jun transactivation domain and phosphorylates serine 63 and serine 73. After binding and SDS–PAGE, an increase in phosphorylated c-Jun GST was found in lysates treated with TNF-α, IL-1α, or IL-1β. IL-1β alone and IL-1β in combination with TNF-α phosphorylated the protein more efficiently than any of the other cytokines or combinations used in this study. Control lysa-

tes, as well as those involving PMA and PDGF stimulation, showed only weak phosphorylation of c-Jun GST (Fig. 5).

DISCUSSION

Our results demonstrate that TNF-α and IL-1 activate MAPK in human neuroma fibroblasts. Previous studies have shown that these cytokines share many common biological activities, despite the fact that they are structurally unrelated and bind to different cell surface receptors (Dinarello, 1991). This phenomenon could be explained by sharing of a common segment of a signal transduction pathway. Two-dimensional gel electrophoresis has demonstrated that both TNF-α and IL-1 increase phosphorylation of a specific group of at least 23 proteins and decrease phosphorylation of 10 additional proteins, whereas other cytokines do not exhibit this effect (Guy *et al.*, 1991; Guy *et al.*, 1992). Because the TNF-α and IL-1 receptors lack intrinsic kinase activity, the cytokines bind to their receptors and initiate a signaling cascade by phosphorylation of intracellular protein kinases, including protein kinase C, protein kinase A, phospholipase C, MAPK, and SAPK (Brenner *et al.*, 1989; Mizel, 1990; Saklatvala, 1995; Sluss *et al.*, 1994; Vietor *et al.*, 1993; Vilcek and Lee, 1991; Whitmarsh *et al.*, 1995). The receptor for PDGF-AB does have intrinsic tyrosine kinase activity (Lubinus *et al.*, 1994; Valius and Kazlauskas, 1993), and PMA is a potent tumor promoter and strong MAPK activator (Gause *et al.*, 1993; Srinivasan and Begum, 1994). In our study, both induced a large increase in activation of MAPK, but only weak activation of SAPK, and the increase in MAPK activation stimulated by TNF-α and IL-1 was similar to that produced by PMA and PDGF-AB. These results indicate that TNF-α and IL-1 are relatively potent stimulators of MAPK in these cells.

MAPK can phosphorylate a large number of proteins after they are activated. These proteins, which include c-Fos, Elk-1, and c-Myc, are often regulatory in nature and are located in the cytoplasm and the nucleus (Saklatvala, 1995). Moreover, upstream proteins of the MAPK cascade, including NGF receptor, EGF receptor, PTP2C, SOS, Raf-1, and MEK, are also good substrates for MAPK (Cano and Mahadevan, 1995; Seger and Krebs, 1995). Cytoskeletal elements, such as MAP-1, MAP-2, and MAP-4, are

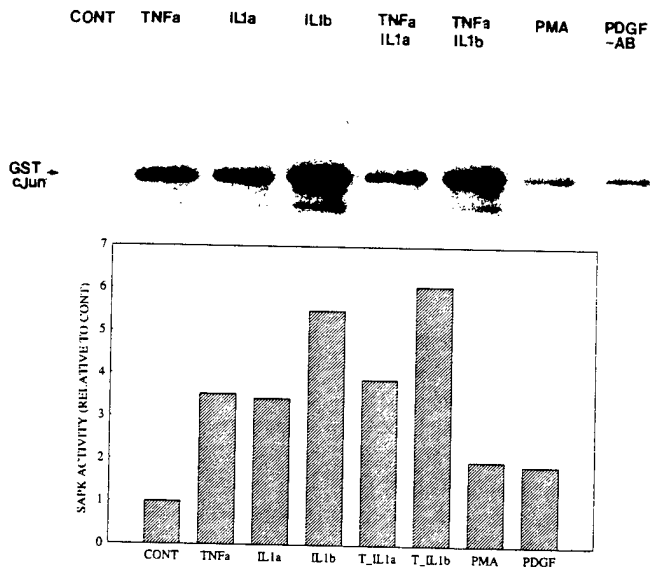

Fig. 5. Determination of SAPK activity with solid-phase protein kinase assay. (Top) Experimental and control cell lysates were diluted to a volume of 300 μl containing 30 μg protein. The lysate solution was mixed with agarose-conjugated human c-Jun (1–169) GST fusion protein and incubated with gentle agitation for 2 h at 4°C, then pelletted. After washing, the pellets were resuspended and incubated in kinase buffer containing [γ-^{32}P]ATP for 20 min at 30°C. The reaction was terminated by adding 2X Laemmli's sample buffer and the samples were subjected to 10% SDS–PAGE. Following electrophoresis, the gel was washed and imaged by autoradiography. (Bottom) Radioactivity incorporated into the bands of c-Jun GST was measured by densitometry and the results were plotted as a histogram. CONT, control; T—IL1a, TNF-α plus IL-1α; T—IL1b, TNF-α plus IL-1β.

also substrates for MAPK (Saklatvala, 1995; Seger and Krebs, 1995); phosphorylation of these proteins regulates cytoskeletal rearrangements and cellular morphology.

Usually, activation of MAPK is involved in the cell cycle G_0/G_1 transition and is directly correlated with cellular proliferation (Boulton *et al.*, 1990; Meloche, 1995). However, in some types of cells, such as neurons, activation of MAPK is unrelated to cell proliferation (Qui and Green, 1992; Traverse *et al.*, 1992). MAPK activation in PC12 cells causes cellular differentiation that is frequently accompanied by cessation of proliferation (Cowley *et al.*, 1994). Some forms of PDGF are potent activators of MAPK in human fibroblasts; the isoforms PDGF-AB and PDGF-BB elicit a strong mitogenic response, whereas PDGF-AA is not a major functional isoform and does not have a significant effect on DNA synthesis in the cells (Lubinus *et al.*, 1994; Meyer-Ingold and Eichner, 1995). Both TNF-α and IL-1 have been shown to promote MAPK activation and also to promote DNA synthesis in fibroblasts. In fact, these activities of the two cytokines have been most convincingly demonstrated in studies of fibroblasts (Guy *et al.*, 1991; Vietor *et al.*, 1993; Vilcek *et al.*, 1986; Schmidt *et al.*, 1982). Data from our study substantiate the finding that TNF-α and IL-1 may accelerate cell proliferation following activation of MAPK. However, our study also shows that TNF-α and IL-1 activate MAPK synergistically, which may be due to binding of the cytokines to different receptors affecting a common target kinase. TNF-α and IL-1 show many synergistic functions (Dinarello, 1991; Vilcek and Lee, 1991), and these cytokines have been found in wound fluid and plasma after injury (Grayson *et al.*, 1993; Wells *et al.*, 1992), which suggests that they have intrinsic secondary relationships to one another.

TNF-α and IL-1 activate SAPK in human neuroma fibroblasts, a signal transduction pathway thought to be distantly related to the MAPK pathway. Two SAPK isoforms (46 kDa $SAPK_1$ and 55 kDa $SAPK_2$) have been identified. SAPK can activate transcriptional activity of *c-jun* by phosphorylation of the c-Jun NH_2-terminal domain at serine 63 and 73 (Hibi *et al.*, 1993; Kyriakis *et al.*, 1994). MAPK and SAPK are similar in that both require dual phosphorylation at threonine and serine within subdomain VIII for activation (Cano and Mahadevan, 1995); however, upstream protein kinases are distinct. For downstream substrates, although MAPK also phosphorylates c-Jun, phosphopeptide mapping has indicated that phosphorylation occurs at a C-terminal site on Ser-243 that is inhibitory (Minden *et al.*, 1994). In our study, activation of SAPK was induced by TNF-α and IL-1 binding to their receptors and mediating a distinct signaling transduction pathway.

Cytokines affect both MAPK and SAPK (Saklatvala, 1995); however, the transcriptional control site is thought to be a physiologically significant target of their signaling transduction pathways (Whitmarsh *et al.*, 1995). Several studies have demonstrated that MAPK induces activation of *c-fos* and SAPK activates *c-jun*. Both *c-fos* and *c-jun* are components of the AP-1 transcription factor complex, which is capable of forming homodimers and heterodimers with various other members of the Jun–Fos family (Angel and Karin, 1991). TCF and Elk-1 can also be substrates for both MAPK and SAPK. Phosphorylation of Elk-1 by these kinases leads to increased TCF at SRE (serum response element) and increased transcriptional activity, which contributes to increased *c-fos* expression by activating the *c-fos* promoter associated with SRE (Whitmarsh *et al.*, 1995). Increased expression of Fos and Jun proteins is essential for activation of AP-1. Studies have also demonstrated that TNF-α-stimulated fibroblast proliferation requires activation of *c-jun*/AP-1 (Brach *et al.*, 1993). In our study, TNF-α and IL-1 increased activation of MAPK and SAPK, which would, in turn, promote fibroblast proliferation by increasing *c-fos* and *c-jun* activity.

TNF-α and IL-1 are secreted by macrophages in the peripheral and central nervous systems, and the levels of these cytokines have been shown to increase dramatically in plasma 24–48 h after peripheral nerve injury (Wells *et al.*, 1992). In addition, cytokines can induce non-neuronal cells such as astrocytes, Schwann cells, and fibroblasts to produce NGF, which may facilitate the regeneration of injured axons (Carman-Krzan *et al.*, 1991; Lindholm *et al.*, 1987, 1988; Hattori *et al.*, 1993). Our results indicate that TNF-α and IL-1 induce activation of MAPK and SAPK in human neuroma fibroblasts and that these activated protein kinases may act to accelerate fibroblast proliferation, which clearly has a central role in neuroma formation. The results of this and other studies suggest that early inflammatory events may have an important role in the initiation of cellular events that could lead to neuroma formation. However, additional events, possibly including the lingering presence of inflammatory cells and the continued release of cytokines, must occur to maintain the activation of the fibroblasts beyond the role required for repair.

Acknowledgements—This work was supported in part by Department of the Army, Cooperative Agreement

DAMD17-93-V-3013 (this does not necessarily reflect the position or the policy of the government, and no official endorsement should be inferred), and United States Public Health Service grants EY04074 (R. W. B.) and EY02377 (Departmental Core Facility) from the National Eye Institute, National Institutes of Health, Bethesda, Maryland, U.S.A.

REFERENCES

Angel, P. and Karin, M. (1991) The role of Jun, Fos and the AP-1 complex in cell-proliferation and transformation. *Biochim. Biophys. Acta* **1072,** 129–157.

Boulton, T. G., Yancopoulos, G. D., Gregory, J. S., Slaughter, C., Moomaw, C., Hsu, J. and Cobb, M. H. (1990) An insulin-stimulated protein kinase similar to yeast kinases involved in cell cycle control. *Science* **249,** 64–67.

Brach, M. A., Gruss, H. J., Sott, C. and Herrmann, F. (1993) The mitogenic response to tumor necrosis factor alpha requires c-Jun/AP-1. *Mol. cell. Biol.* **13,** 4284–4290.

Brenner, D. A., O'Hara, M., Angel, P., Chojkier, M. and Karin, M. (1989) Prolonged activation of jun and collagenase genes by tumor necrosis factor-α. *Nature* **337,** 661–663.

Cano, E. and Mahadevan, L. C. (1995) Parallel signal processing among mammalian MAPKs. *Trends Biochem. Sci.* **20,** 117–122.

Carman-Krzan, M., Vig'e, X. and Wise, B. C. (1991) Regulation by interleukin-1 of nerve growth factor secretion and nerve growth factor mRNA expression in rat primary astroglial cultures. *J. Neurochem.* **56,** 636–643.

Cowley, S., Paterson, H., Kemp, P. and Marshall, C. J. (1994) Activation of MAP kinase is necessary and sufficient for PC12 differentiation and for transformation of NIH 3T3 cells. *Cell* **77,** 841–852.

Dinarello, C. A. (1991) Interleukin-1 and interleukin-1 antagonism. *Blood* **77,** 1627–1652.

Frisén, J., Risling, M. and Fried, K. (1993) Distribution and axonal relations of macrophages in a neuroma. *Neuroscience* **55,** 1003–1013.

Gause, K. C., Homma, M. K., Licciardi, K. A., Seger, R., Ahn, N. G., Peterson, M. J., Krebs, E. C. and Meier, K. E. (1993) Effects of phorbol ester on mitogen-activated protein kinase activity in wild-type and phorbol ester-resistant EL4 thymoma cells. *J. biol. Chem.* **268,** 16124–16129.

Grayson, L. S., Hansbrough, J. F., Zapata-Sirvent, R. L., Dore, C. A., Morgan, L. J. and Nicholson, M. A. (1993) Quantitation of cytokine levels in skin graft donor site wound fluid. *Burns* **19,** 401–405.

Guy, G. R., Chua, S. P., Wong, N. S., Ng, S. B. and Tan, Y. H. (1991) Interleukin 1 and tumor necrosis factor activate common multiple protein kinases in human fibroblasts. *J. biol. Chem.* **266,** 14343–14352.

Guy, G. R., Cao, X., Chua, S. P. and Tan, Y. H. (1992) Okadaic acid mimics multiple changes in early protein phosphorylation and gene expression induced by tumor necrosis factor or interleukin-1. *J. biol. Chem.* **267,** 1846–1852.

Hattori, A., Tanaka, E., Murase, K., Ishida, N., Chatani, Y., Tsujimoto, M. N., Hayashi, K. and Kohno, M. (1993) Tumor necrosis factor stimulates the synthesis and secretion of biologically active nerve growth factor in non-neuronal cells. *J. biol. Chem.* **268,** 2577–2582.

Hibi, M., Lin, A., Smeal, T., Minden, A. and Karin, M. (1993) Identification of an oncoprotein- and UV-responsive protein kinase that binds and potentiates the c-Jun activation domain. *Genes Dev.* **7,** 2135–2148.

Kyriakis, J. M., Banerjee, P., Nikolakaki, E., Dai, T., Rubie, E. A., Ahmad, M. F., Avruch, J. and Woodgett, J. R. (1994) The stress-activated protein kinase subfamily of c-Jun kinases. *Nature* **369,** 156–160.

Lindholm, D., Heumann, R., Hengerer, B. and Theonen, H. (1988) Interleukin 1 increases stability and transcription of mRNA encoding nerve growth factor in cultured rat fibroblasts. *J. biol. Chem.* **263,** 16348–16351.

Lindholm, D., Heumann, R., Meyer, M. and Thoenen, H. (1987) Interleukin-1 regulates synthesis of nerve growth factor in non-neural cells of rat sciatic nerve. *Nature* **330,** 658–659.

Lubinus, M., Meier, K. E., Smith, E. A., Gause, K. C., LeRoy, E. C. and Trojanowska, M. (1994) Independent effects of platelet-derived growth factor isoforms on mitogen-activated protein kinase activation and mitogenesis in human dermal fibroblasts. *J. biol. Chem.* **269,** 9822–9825.

Marshall, C. J. (1995) Specificity of receptor tyrosine kinase signaling: transient versus sustained extracellular signal-regulated kinase activation. *Cell* **80,** 179–185.

Meloche, S. (1995) Cell cycle reentry of mammalian fibroblasts is accompanied by the sustained activation of p44mapk and p42mapk isoforms in the G_1 phase and their inactivation at the G1/S transition. *J. cell. Physiol.* **163,** 577–588.

Meyer-Ingold, W. and Eichner, W. (1995) Platelet-derived growth factor. *Cell. Biol. Int.* **19,** 389–398.

Minden, A., Lin, A., Smeal, T., Dérijard, B., Cobb, M., Davis, R. and Karin, M. (1994) c-Jun N-terminal phosphorylation correlates with activation of the JNK subgroup but not the ERK subgroup of mitogen-activated protein kinases. *Mol. cell. Biol.* **14,** 6683–6688.

Mizel, S. B. (1990) Cyclic AMP and interleukin 1 signal transduction. *Immunol. Today* **11,** 390–391.

Pagès, G., Lenormand, P., L'Allemain, G., Chambard, J. C., Meloche, S. and Pouysségur, J. (1993) Mitogen-activated protein kinases p42mapk and p44mapk are required for fibroblast proliferation. *Proc. natn. Acad. Sci. USA* **90,** 8319–8323.

Qui, M. S. and Green, S. H. (1992) PC12 cell neuronal differentiation is associated with prolonged $p21^{ras}$ activity and consequent prolonged ERK activity. *Neuron* **9,** 705–717.

Saklatvala, J. (1995) Intracellular signalling mechanisms of interleukin 1 and tumour necrosis factor: possible targets for therapy. *Br. Med. Bull.* **51,** 402–418.

Sánchez, I., Húghes, R. T., Mayer, B. J., Yee, K., Woodgett, J. R., Avruch, J., Kyriakis, J. M. and Zon, L. I. (1994) Role of SAPK/ERK kinase-1 in the stress-activated pathway regulating transcription factor c-Jun. *Nature* **372,** 794–798.

Schmidt, J. A., Mizel, S. B., Cohen, D. and Green, I. (1982) Interleukin 1, a potential regulator of fibroblast proliferation. *J. Immunol.* **128,** 2177–2182.

Seger, R. and Krebs, E. G. (1995) The MAPK signaling cascade. *FASEB J.* **9,** 726–735.

Sims, J. E., Gayle, M. A., Slack, J. L., Alderson, M. R., Bird, T. A., Giri, J. G., Colotta, F., Re, F., Mantovani, A., Shanebeck, K., Grabstein, K. H. and Dower, S. K. (1993) Interleukin 1 signalling occurs exclusively via the type I receptor. *Proc. natn. Acad. Sci. USA* **90,** 6155–6159.

Sluss, H. K., Barrett, T., Dérijard, B. and Davis, R. J. (1994) Signal transduction by tumor necrosis factor mediated by JNK protein kinases. *Mol. cell Biol.* **14,** 8376–8384.

Srinivasan, M. and Begum, N. (1994) Stimulation of protein phosphatase-1 activity by phorbol esters. *J. biol. Chem.* **269,** 16662–16667.

Sugarman, B. J., Aggarwal, B. B., Hass, P. E., Figari, I. S., Palladino, M. A. Jr and Shepard, H. M. (1985) Recombinant human tumor necrosis factor-α effects on proliferation of normal and transformed cells *in vitro*. *Science* **230,** 943–945.

Tartaglia, L. A. and Goeddel, D. V. (1991) Two TNF receptors. *Immunol. Today* **13,** 151–153.

Traverse, S., Gomez, N., Paterson, H., Marshall, C. and Cohen, P. (1992) Sustained activation of the mitogen-activated protein (MAP) kinase cascade may be required for differentiation of PC12 cells: comparison of the effects of nerve growth factor and epidermal growth factor. *Biochem. J.* **288,** 351–355.

Valius, M. and Kazlauskas, A. (1993) Phospholipase C-γ1 and phosphatidylinositol 3 kinase are the downstream mediators of the PDGF receptor's mitogenic signal. *Cell* **73,** 321–334.

Venezie, R. D., Toews, A. D. and Morell, P. (1995) Macrophage recruitment in different models of nerve injury: lysozyme as a marker for active phagocytosis. *J. Neurosci. Res.* **40,** 99–107.

Vietor, I., Schwenger, P., Li, W., Schlessinger, J. and Vilcek, J. (1993) Tumor necrosis factor-induced activation and increased tyrosine phosphorylation of mitogen-activated protein (MAP) kinase in human fibroblasts. *J. biol. Chem.* **268,** 18994–18999.

Vilcek, J. and Lee, T. H. (1991) Tumor necrosis factor-new insights into the molecular mechanisms of its multiple actions. *J. biol. Chem.* **266,** 7313–7316.

Vilcek, J., Palombella, V. J., DeStefano, D. H., Swenson, C., Feinman, R., Hirai, M. and Tsujimoto, M. (1986) Fibroblast growth enhancing activity of tumor necrosis factor and its relationship to other polypeptide growth factors. *J. Exp. Med.* **163,** 632–643.

Wells, M. R., Racis, S. P. Jr and Vaidya, U. (1992) Changes in plasma cytokines associated with peripheral nerve injury. *J. Neuroimmunol.* **39,** 261–268.

Westwick, J. K., Weitzel, C., Minden, A., Karin, M. and Brenner, D. A. (1994) Tumor necrosis factor α stimulates AP-1 activity through prolonged activation of the c-Jun kinase. *J. biol. Chem.* **269,** 26396–26401.

Whitmarsh, A. J., Shore, P., Sharrocks, A. D. and Davis, R. J. (1995) Integration of MAP kinase signal transduction pathways at the serum response element. *Science* **269,** 403–407.

Shurun Zhao, Roger W. Beuerman,
and David G. Kline

NEUROTIZATION OF MOTOR NERVES INNERVATING THE LOWER EXTREMITY BY UTILIZING THE LOWER INTERCOSTAL NERVES

ABSTRACT

An animal model in the rat was developed to study the reinnervation of ventral roots contributing to lower-extremity nerves by use of intercostal nerves. Intercostal nerves and distal cauda equina roots were anastomosed, using a collagen tube and microsurgical technique. Most experimental animals could lift their previously paralyzed legs and could walk with a severe limp by 9 months postoperatively. Recordings of nerve action potentials (NAPs) and muscle action potentials (MAPs) indicated that the intercostal and sciatic nerves had some functional connections. Histologic analysis 12 months after repair demonstrated axonal regeneration extending from the intercostal nerves to and down lumbar ventral roots. Most of the regenerated fibers were moderately well-myelinated. Connections between the neurons of the anterior horn cells in the lower thoracic spinal cord and the reinnervated sciatic nerve were confirmed by retrograde tracer, using fast blue.

Intercostal nerves have been used for a number of years in an attempt to reinnervate the arm in very proximal brachial plexus stretch and avulsive injuries.[1-11] Although results vary from series to series, some 40 to 50 percent of patients do regain biceps/brachialis function. However, it has been difficult for such a neurotization procedure to provide more than one function. Patients recovering elbow flexion seldom gain shoulder abduction, even though the intercostal nerves are extended by grafts to axillary and/or suprascapular nerves.

The use of the intercostals for originating axons is one of several forms of neurotization used in the upper extremity. Neurotization techniques for the lower extremity are, to date, not as feasible as those for the upper extremity. This is, at least partly, due to the distance between the upper intercostal nerves and the femoral and sciatic nerves. In the current study, we designed an animal model of neurotization of lower-extremity nerves, by anastomosing ipsilateral and contralateral lower intercostal nerves to the ventral lumbar nerve roots of the cauda equina.

MATERIALS AND METHODS

SURGICAL TECHNIQUE. Ten healthy adult male Sprague-Dawley rats (weight: 270 to 330 g) were anesthetized by intraperitoneal injection with pentobarbital (4 mg/100 g). Atropine (0.12 ml) was given intramuscularly to inhibit bronchial secretions. Once anesthesia was satisfactory, the rats were intubated with an endotracheal tube, which was then connected to a small animal ventilator. Then, the rats were placed in a

Department of Neurosurgery, Louisiana State University Medical School, and LSU Lion's Eye Center, New Orleans, Louisiana *Reprint requests:* Dr. Kline, Dept. of Neurosurgery, 1542 Tulane Ave., New Orleans, LA 70112 Accepted for publication May 28, 1996

prone position. Under sterile conditions, an incision was made in the midline from thoracic vertebra 8 to lumbar vertebra 3. As the current experiments were designed to use the intercostal nerves on either the left or right sides, the incision was extended to the left (5 rats) and right (5 rats) at the thoracic 12 level. This was done at a left or right angle to the midline (Fig. 1). In this way, a "⊣" or "⊢" type incision was made.

The operation was then continued under the operating microscope. The paraspinal muscles were transacted at the thoracic 12 level and were also dissected away from the T8 through L2 lamina. A laminectomy was done between T8 and L2. This was carried out with both a mini-drill and a small rongeur. Intercostal muscles were then incised along the ribs. Care was taken to maintain the pleura and not to enter the thoracic cavity. The intercostal nerves of thoracic 9 to 12 on the right side (in 5 rats) or left side (in 5 rats) were carefully separated one by one, using microtweezers and scissors. The length of the intercostal nerves needed for the anastomosis depended on the distance between the outlets of the intercostal nerves and the ventral roots of the lower-extremity nerves. The intercostal nerves at the T9 and T10 levels were sectioned distal to the lateral cutaneous branch, and those at T11 and T12 were sectioned proximal to the lateral cutaneous branch. After all four intercostal nerves had been isolated, they were then tunneled under the paraspinal muscles, and the soft tissues were closed.

The dura at the level of L1 and L2 was opened at the midline. At the upper and lower ends of the opening, the dura was cut at a 90° angle, so an incision shaped as "I" was made. The sciatic and femoral nerves of the rat receive input from the spinal cord segments of lumbar 3 to 6 via their ventral and some posterior roots.[12] Dissections prior to these experiments showed that the nerve roots of L3 to L6 were approachable at an L-1 to L-2 intraspinal level. The exposed spinal cord was gently rotated with a moistened cotton-tipped applicator. The left ventral roots of L3 to L6 were identified, and cut with a pair of micro-

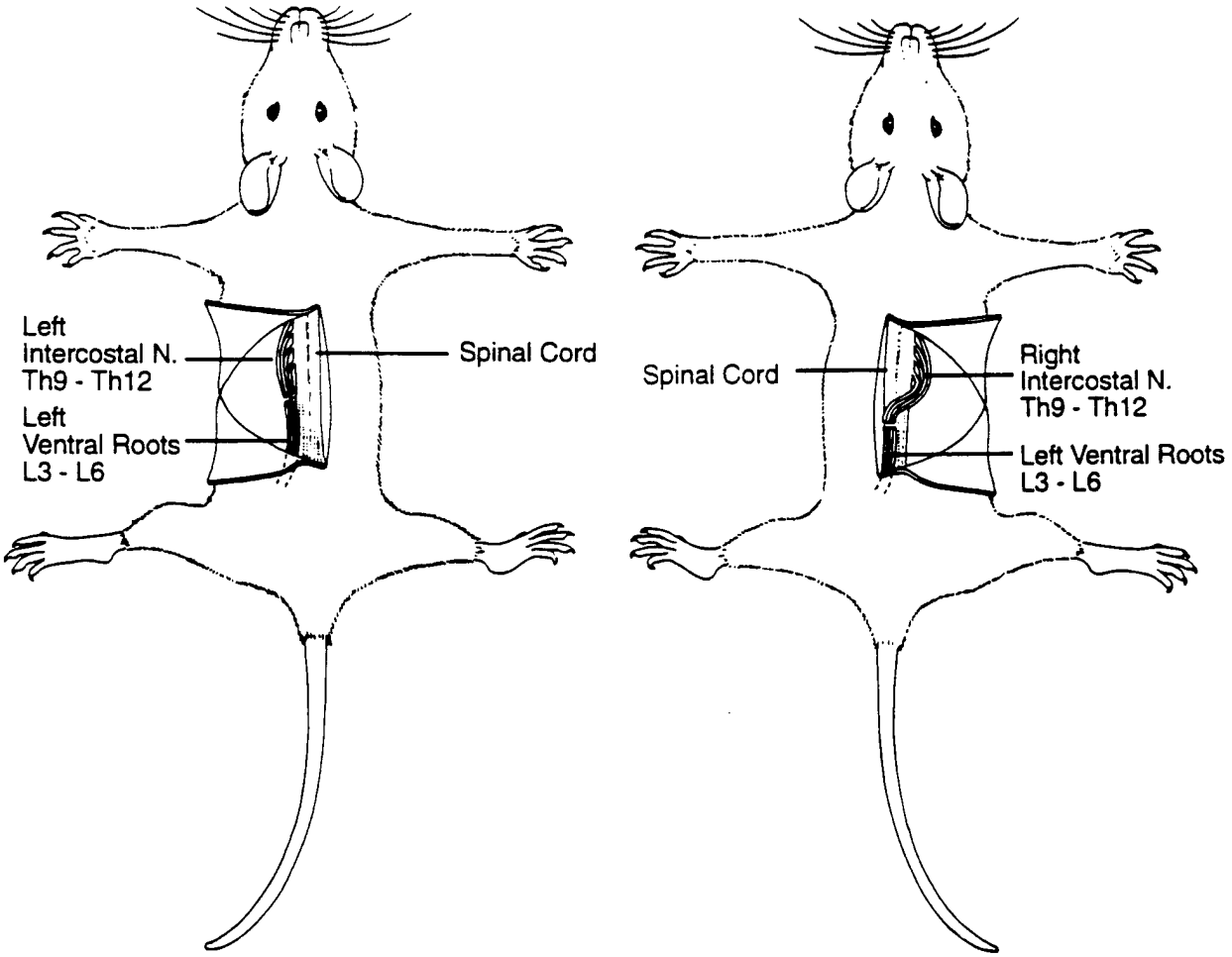

Figure 1. Schematic illustration depicts the method of connecting the intercostal nerves to the distal ventral roots leading to the sciatic and femoral nerves of the rat. A, Left intercostal nerves were connected to the left cauda equina distal ventral roots. B, Right intercostal nerves were connected to the left cauda equina distal ventral roots.

scissors below the transition region (TR) of the central and peripheral nervous system.[13] A collagen tube 1.5 mm in diameter and 12 mm in length (product of Colla-Tec, Inc.) was fixed with a 6-0 nylon suture to the ligament of the serratus dorsalis muscle. The position of the tube was between the upper end of L-1 and lower end of L-2 vertebrae. All the previously separated intercostal nerves and the dissected left L3 to L6 roots were trimmed at their ends, and carefully placed inside the tube with microtweezers through the openings at both ends of the tube.

The intercostal nerves and the ventral roots were adjusted, so that their ends were in contact. The intercostal nerves and ventral roots were fixed to either side of the tube with a 9-0 suture and to the muscles and ligaments beside the vertebrae (Fig. 2). Entubulation of the intercostal nerve and distal nerve roots prevented effective regeneration of axons from the transected proximal lumbar roots into the distal lumbar roots. The dural defect was then covered with a piece of subcutaneous fat. The superficial back muscles were closed with 4-0 chromic gut and the skin with 5-0 Mersilene sutures. Each animal was given a 0.5 ml subcutaneous injection of penicillin G and was kept in a warm room for 2 days, then returned to the routine animal care room in its cage.

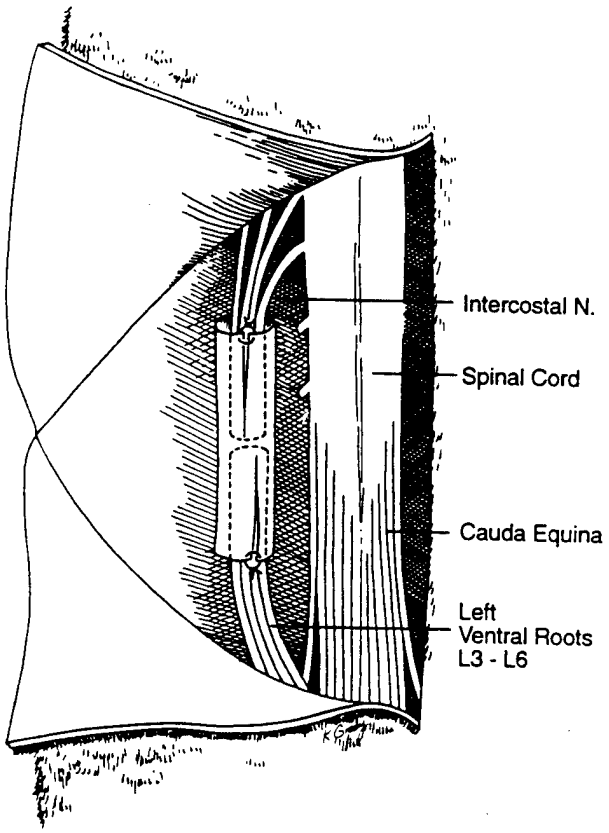

Figure 2. Schematic illustration of repair of intercostal nerves to the distal ventral roots.

Electrophysiologic Examinations. Twelve months after the operation, the animals were anesthetized with an injection of ketamine (40 mg/kg) intraperitoneally. An incision was made at the mid-thigh level on the left side using the operating microscope. Hamstring muscles were retracted to expose the sciatic complex. For nerve action potential (NAP) recording, the stimulating electrodes were bipolar platinum wire electrodes placed on the sciatic nerve. NAPs were recorded from the T9 to T12 intercostal nerves by using a bipolar platinum wire electrode. The distance between each of the bipolar electrodes was 0.5 cm. A ground electrode was placed in the rat's tail. Muscle action potentials (MAPs) were recorded from the muscles of legs of the rats by stimulation of the T9 to T12 intercostal nerves with bipolar platinum wire electrodes. Recording electrodes were two stainless steel needles inserted into the more distal leg muscles. The distance between the two sets of electrodes was 5 cm. A similar electrode was placed subcutaneously in the neck and was used as a ground electrode. Either a TECA TD20 electrophysiologic scope or a Gould 400 digital storage oscilloscope was used for recording. Stimulus was a square electric pulse; its duration was 0.05 ms and its intensity was 5 to 7 volts. At a bandwidth of 20 to 2000 Hz, NAP and MAP responses were recorded and replicated on the scope's X-Y plotter. While recording, the rectal temperature was maintained at 38°C by a heating pad.

Neuroanatomic and Histologic Studies. In the rats used for neuroanatomic studies, a fast blue (FB) solution (5 mg in 100 μl distilled water) was applied, according to the method of Aschoff and Hollander.[14,15] The fast blue solution was drawn into a small container made from a plastic tube. The sciatic nerve was freshly cut just proximal to its division into the peroneal, posterior tibial, and sural nerves, and immediately placed into the fast blue solution. Nerve and container were carefully sealed away from surrounding tissues by bone wax, which was softened by mineral oil. The nerve remained immersed in the solution for 90 min and was then removed. After FB application, the wounds were closed and the animals allowed to survive 72 to 96 hr. Then, the rats were anesthetized with pentobarbital and transcardially perfused for 3 to 5 min with saline (pH 7.2), followed by 8 percent paraformaldehyde (pH 5.6) for 5 to 10 min.

The thoracic spinal cord extending from T9 to T12 was then removed and placed at 4°C in a fixative containing 30 percent sucrose. The spinal cords were cut 12 hr later in serial transverse sections on a freezing microtome. Sections were mounted on glass slides for study of the spinal neurons under a fluorescent microscope. For the histologic studies, the rats were also perfused as above. The T9 to T12 intercostal nerves, L3 to L6 distal ventral roots, and sciatic nerve were removed, and kept in 2.5 percent glutaraldehyde

and 1 percent paraformaldehyde for 24 hr. Postfixation was by 1 percent osmium tetroxide. Tissue samples were then dehydrated with alcohol. Each nerve (or root) was embedded in 100 percent Epon and sectioned transversely with an ultramicrotome for light or electron microscopy. Semi-thin sections were stained with toluidine blue and basic fuchsin for light microscopy. The thin sections were stained with uranyl acetate and lead citrate, and examined using a 2168 Ultrastainer Carlsberg System (LKB Bromma).

RESULTS

The left lower extremity was completely paralyzed following operation. The rats could move around with their forelegs and right hind legs, but they dragged their left hind legs along. Respiratory function did not show any noticeable changes and urination recovered within a day. Surgery did not obviously affect the growth of the rats; their weight had increased to about 500 g when they were weighed 12 months later. The muscles on the left hind leg of some rats showed moderate atrophy. Three rats died during the 12-month period of study. Reasons for death were not entirely clear, but were probably pulmonary in origin. About 6 months later, the left lower extremity of some rats could move with respiration, and most rats could lift and walk with their left hind legs, although with quite a limp by 9 months after operation.

NAPs were recorded 12 months postoperatively. Most rats showed good responses (Fig. 3A). MAPs could be recorded from both flexor and extensor muscles of the thigh and lower legs. These MAP responses were surprisingly good (Fig. 3B); conduction velocities and amplitudes were close to those of normal controls.

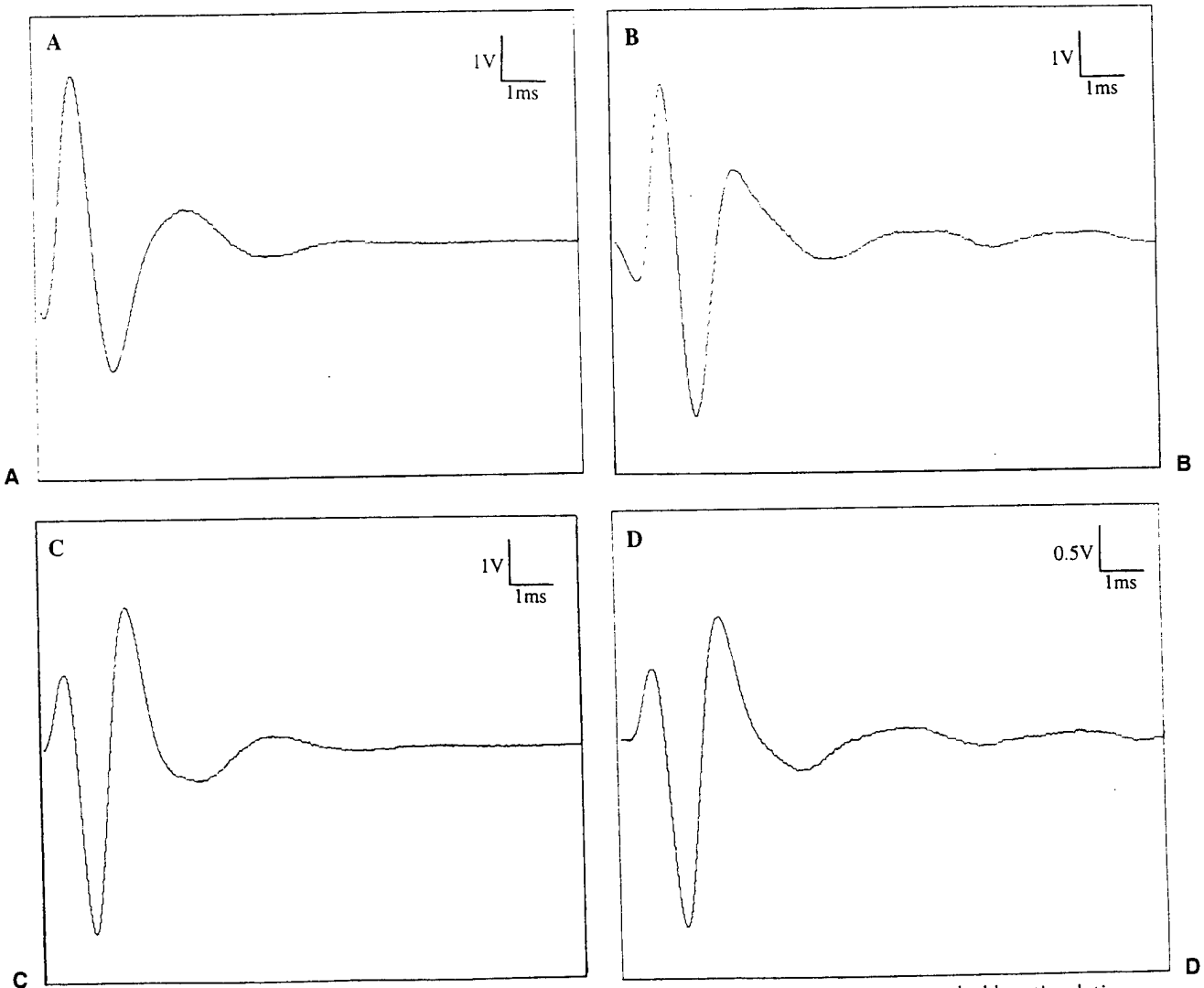

Figure 3. Nerve action potential (NAP) and muscle action potential (MAP) were recorded by stimulating intercostal nerves from a rat 12 months postoperatively. A, NAP recorded from sciatic nerve. Stimulus output is to the left of the tracing. B, MAP recorded from hamstring muscles. C, MAP recorded from flexor muscles of the hip. D, MAP recorded from gastrocnemius muscles.

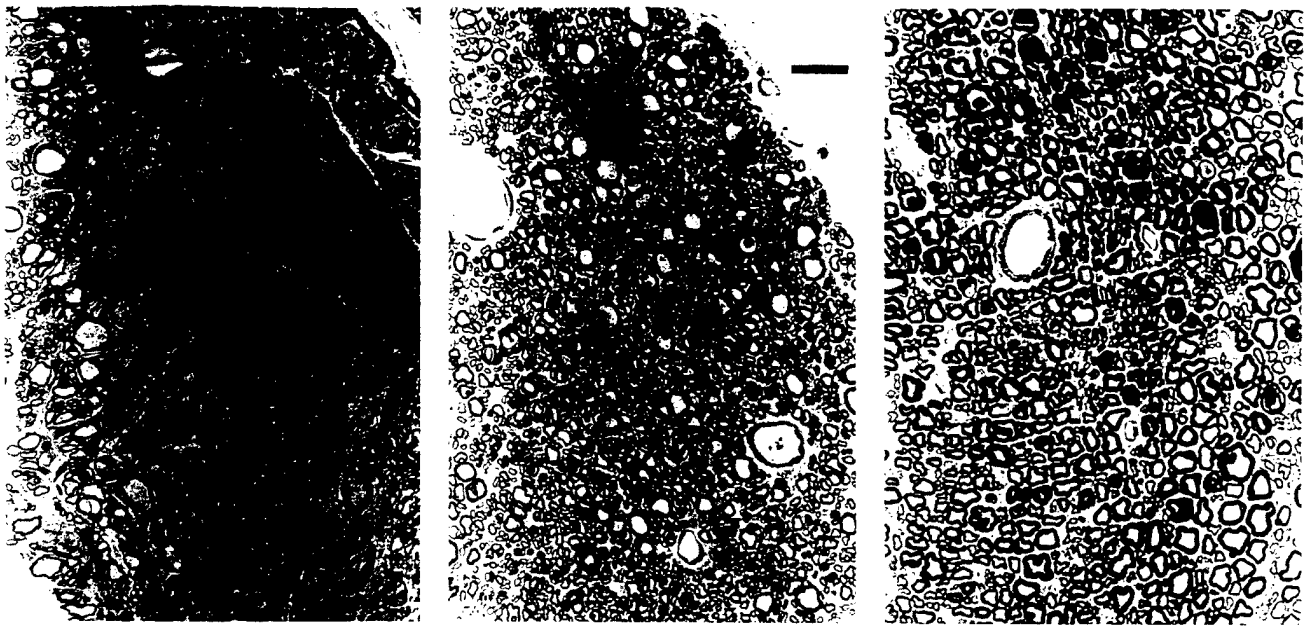

Figure 4. A, Photomicrograph of a transverse section of junctional area demonstrating the presence of regenerating nerve fibers in a rat sacrificed 12 months postoperatively. Regenerated nerve fibers are intermixed with degenerated fibers (magnification ×125). B, Photomicrograph of a transverse section of a distal ventral root showing extensive regeneration of intercostal nerve fibers into the nerve root (magnification ×125; bar length = 40 μm). C, Photomicrograph of a transverse section of sciatic nerve. Regenerated fibers are intermixed with intact sensory fibers (magnification ×125).

Figure 4 presents the histologic results from both peripheral nerves and cauda equina roots involved in the regenerative process. Extensive regeneration of nerve fibers can be seen originating from the intercostal nerves attached to the lower-extremity nerves. Electron microscopy indicated that distal to the junction of the intercostal nerves and lumbar 3 to 6 ventral roots, many regenerative nerve fibers were present. Myelinization was moderately mature (Fig. 5).

Results with fast-blue tracing showed that many neurons in the ventral horns of the thoracic spinal cord, extending from T9 to T12, contained fluorescent materials. It is presumed that these neurons contribute to the reconstructed sciatic nerve. Figure 6 is a microphotograph taken from the ventral horn of the thoracic spinal cord of a rat at a T10 to T11 level. This provided evidence that the nerve fibers in the reconstructed sciatic nerve were anatomically connected to these neurons.

DISCUSSION

Studies of the plasticity of the nervous system have been conducted on a wide range of species. The central nervous system has the capacity of adapting to severe changes in the arrangement of its outputs and inputs through the cross-anastomosis of peripheral nerves.[16–21] Intercostal nerves have been used to neuroticize patients with otherwise irreparable stretch injuries to the brachial plexus,[1–3,7–11,22,23] and the bladder.[24]

The intercostal nerves, especially the upper ones, are distant from the sciatic nerve and femoral nerve in the thigh. The current study showed, however, that it is possible to connect the lower intercostal nerves to sciatic and femoral nerve outflow, by anastomosing them to the ventral roots of the cauda equina. By 1 year postoperatively, there was regeneration of nerve

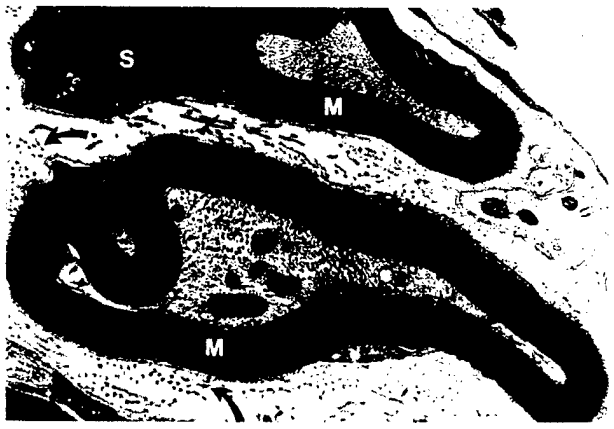

Figure 5. A, Electron micrograph of a portion of reinnervated ventral root 12 months postoperatively illustrating that the regenerated nerve fibers show normal configuration. Arrows = collagen; S = Schwann cell; M = myelinization of axons (magnification ×30000).

Figure 6. Microphotograph of the neurons in the anterior horn between the T10 to T11-level spinal cord marked by fast blue (FB) technique. The dye migrated from the proximal sciatic nerve, through the repair site, and then up the intercostal nerve(s) to the spinal cord.

fibers through the anastomosis and into more distal nerves. There was also some reversal of paralysis in the lower extremity of these rats. Such a technique, which connects the intercostal nerves to ventral lumbar roots, seems worthy of further study.

Mismatching of motor and sensory fibers from donor nerves with their pathways to recipient nerves leads to minimized useful functions.[25,26] For some mixed nerves, it has been assumed that only 10 percent (0.1) of the fibers are motor. The matching probability for the connection of motor fibers in two such mixed nerves is 0.01 ($p = 0.1 \times 0.1 = 0.01$).[26] In the current study, the intercostal nerves contain only 10 to 20 percent of motor nerve fibers[26]; on the other hand, the ventral roots have 100 percent motor fibers. Thus, the matching possibility for motor nerve fibers is, at most, 10 to 20 percent. As a result, anastomosis of the intercostal nerves to ventral roots has a higher matching possibility for motor fibers than the connection of intercostal nerves with mixed nerves, such as elements of the brachial plexus.

The motor elements of the lower intercostal nerves innervate several thoracic and abdominal muscles, such as the musculus intercostales externi and interni, musculus rectus abdominis, musculus obliquus internus abdominis, musculus transversus abdominis, and musculus obliquus externus abdominis. These lower intercostal nerves were considered as suitable donors, since they can provide at least two different muscle functions.[26] Narakas has indicated that a few hundred axons seem to be sufficient to reinnervate efficiently a poorly differentiated muscle like the biceps, but thousands are needed to restore the delicate balance of the small intrinsic muscles of the hand and to give them tactile gnosis.[1] Muscular activity of the lower extremity is much less delicate than that of the upper extremity. In addition, the technique used in the current study provides a higher matching possibility for motor fibers. Evidence has shown that the lower intercostal nerves can provide more motor nerve fibers than the upper intercostal nerves. Ploncard and Samardzic *et al.* have indicated that an intercostal nerve in the human contains about 500 to 700 motor nerve fibers,[4,22] but results from Schalow *et al.* suggest that this number is closer to 1000 to 2000.[26] The differences between the two studies arise because the former used upper intercostal nerves in their study, while the latter examined lower intercostal nerves.

The distance required for intercostal nerves to reach ventral roots, either ipsilateral or contralateral, is comparable. Thus, some reconnection to lower-extremity nerves can be achieved, using contralateral intercostal nerves. This would be useful when the ipsilateral intercostal nerves are dysfunctional, because of more proximal and unilateral spinal cord or

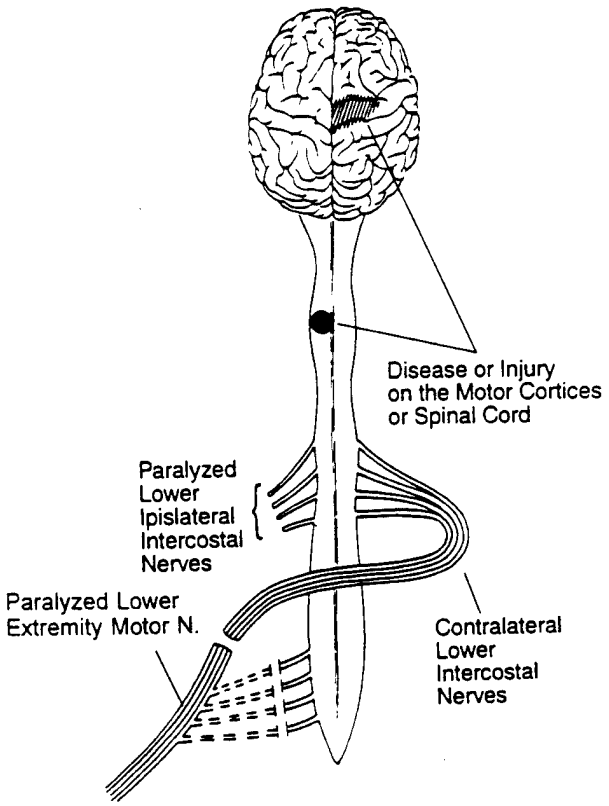

Figure 7. Schematic illustration depicts dysfunction of ipsilateral intercostal nerves because of more proximal spinal cord or contralateral cerebral injury. The contralateral intercostal nerves might be used to neuroticize lower-extremity nerves in such cases.

contralateral cerebral injury. Under such circumstances, contralateral intercostal nerves could be used to neuroticize lower-extremity nerves (Fig. 7). A suitable length of lower intercostal nerves can be directly attached to the cauda equina roots. This kind of grafting might be useful, if the intercostal nerves were used to bypass a distal spinal cord injury, cauda equina injury, or irreparable injuries to the pelvic plexus.

The current study was conducted on a lower animal, the rat, which is quite different from the human. Further studies need to be done on higher animals, such as the primate, before this technique can be applied to humans. To our knowledge, loss of lower intercostal function did not adversely affect abdominal-wall function in the rat. Nevertheless, this may be a more serious complications in higher animals or in humans.

REFERENCES

1. Narakas, A: Surgical treatment of traction injuries of the brachial plexus. Clin Orthopaed Rel Res 133:71, 1978
2. Tomita Y, Tasi TM, Burns I, *et al.*: Intercostal nerve transfer in brachial plexus injuries: An experimental study. Microsurgery 4:95, 1983
3. Dolenc V: Intercostal neurotization of the peripheral nerves in avulsing plexus injuries. Clin Plast Surg 11:143, 1984
4. Samardzic M, Antunovic V, Ioksimovic M, Bacetic D: Donor nerves in the reinnervation of brachial plexus. Neurolog Res 8:117, 1986
5. Sanardzic M, Grujicic D, Antunovic V, Ioksimovic M: Reinnervation of avulsed brachial plexus using the spinal accessory nerve. Surg Neurol 33:7, 1990
6. Samardzic M, Grujicic D, Antunovic V: Nerve transfer in brachial plexus traction injuries. J Neurosurg 76:191, 1992
7. Nagano A, Tsuyama N, Ochiai N, *et al.*: Direct nerve crossing with the intercostal nerve to treat avulsion injuries of the brachial plexus. J Hand Surg 14A:980, 1989
8. Friedman AH, Nunley JA II, Goldner RD, *et al.*: Nerve transposition for the restoration of elbow flexion following brachial plexus avulsion injuries. J Neurosurg 72:59, 1990
9. Akasaka Y, Hara T, Takahashi M: Free muscle transplantation combined with intercostal nerve crossing for reconstruction of elbow flexion and wrist extension in brachial plexus injuries. Microsurgery 12:346, 1991
10. Doi K, Sakai K, Kuwata N, *et al.*: Reconstruction of finger and elbow function after complete avulsion of the brachial plexus. J Hand Surg 5:797, 1991
11. Gu Y, Ma M: Nerve transfer for treatment of root avulsion of the brachial plexus: Experimental studies in a rat model. J Reconstr Microsurg 7:15, 1991
12. Hebel R, Stromberg MW: *Anatomy of the Laboratory Rat*. New York, Waverly Press, 1976, pp 133–135
13. Berthold CH, Carlstedt T, Coneliuson O: Anatomy of the nerve root at the central-peripheral transitional region. In Dyck PJ (ed): *Peripheral Neuropathy*. Philadelphia: W.B. Saunders, 1984, pp 156–170
14. Aschoff A, Holländer H: Fluorescent compounds as retrograde tracers compared with horseradish peroxidase (HRP). I. A parametric study in the central visual system of the albino rat. J Neurosci Methods 6:179, 1982
15. Illert M, Fritz N, Aschoff A, Holländer H: Fluorescent compounds as retrograde tracers compared with horseradish peroxidase (HRP). II. A parametric study in the peripheral motor system of the cat. J Neurosci Methods 6:199, 1982
16. Brinkman C, Porter R, Norman I: Plasticity of motor behavior in monkeys with crossed forelimb nerves. Science 220:438, 1983
17. Clark SA, Allard T, Jenkins WM, Merzenich MM: Receptive fields in the body-surface map in adult cortex defined by temporally correlated inputs. Nature 332:444, 1988
18. Vera CL, Lewin MG, Kase IC, Calderon MD: Central functional changes after facial-spinal-accessory anastomosis in man and facial-hypoglossal anastomosis in the cat. J Neurosurg 43:181, 1975
19. Seil FI: Tissue culture studies of neural plasticity. Rest Neurol Neurosci 1:1, 1989
20. Goldberger NE: Different patterns of recovery of motor function associated with different patterns of post-lesion axonal grows. In Seil FJ (ed): *Nerve, Organ and Tissue Regeneration: Research Perspectives*. New York: Academic Press, 1983, pp 155–463
21. Merill EG, Wall PD: Plasticity of connections in the adult nervous system. In Cotman CW (ed): *Neuronal Plasticity*. New York: Raven Press, 1978, pp 97–111
22. Ploncard P: A new approach to the intercostal-brachial anastomosis in the treatment of brachial plexus paralysis due to root avulsion: Late results. Acta Neurochir 61:281, 1982
23. Kawai H, Kawabata H, Masada K, *et al.*: Nerve repairs for traumatic brachial plexus palsy with root avulsion. Clin Orthop 237:75, 1988
24. Carlsson CA, Sundin T: Reconstruction of afferent and efferent nervous pathways to the urinary bladder in two paraplegic patients. Spine 5:37, 1980
25. Sunderland S: (Discussion) Functional specificity and somatotopic organization during peripheral nerve regeneration. In Jewett DL, McCarroll HR (ed): *Nerve Repair and Regeneration*. St. Louis: Mosby, 1980, p 113
26. Schalow G, Aho A, Lang G: Microanatomy and number of nerve fibers of the lower intercostal nerves with respect to a nerve anastomosis: Donor nerve analysis (IIV). Electromyogr Clin Neurophysiol 32:171, 1992

The authors express their gratitude to Mrs. Lia Pedroza for her technical assistance.

The Effect of Gabapentin on Inflammatory Pain in Rats

Harry J. Gould, III, Trevor N. Gould[1], Shea C. Reeb[2], and Dennis Paul
Departments of Neurology and Pharmacology
Louisiana State University Medical Center
New Orleans, Louisiana

Pages: 33
Figures: 9
Tables: None

[1] TNG is currently a student a Vanderbilt University, Nashville, TN.
[2] MSR is a teacher at Northshore High School in Slidell, LA.

Send Correspondence to: Harry J. Gould, III, M.D., Ph.D.
Department of Neurology
LSU Medical Center
1542 Tulane Avenue
New Orleans, LA 70112
Fax 504-568-7130

in press in Analgesia

1

RUNNING TITLE

Gabapentin in Inflammatory Pain

6

HJG is supported by US Army Medical Research Grant DAMD17-93-V-3013)

DP is supported by National Institute of Drug Abuse Grant (DA07379)

11

Some of these results were presented at the 1997 regional meeting of the American Federation for Medical Research in New Orleans, LA.

16 Gould, T.N.; Paul, D.J.; Gould, H.J., III. Analgesic effects of gabapentin on inflammatory pain in rat. J. Invest. Med., 45:6A; 1997.

ABSTRACT

Background. Gabapentin is a new anticonvulsant that has been used in the treatment of neuropathic pain. Anecdotal reports from patients who have been treated with gabapentin suggest that the range of efficacy in the management of pain may extend beyond neuropathic pain syndromes. The purpose of this study was to determine the effect of gabapentin on pain thresholds in rats with pain generated by infection-induced inflammation in an attempt to delineate the limits of gabapentin's role in producing analgesia.

Methods. The effect of gabapentin on pain induced by inflammation was studied in albino rats using paw withdrawal latencies, tail-flick, and hotplate techniques. Following baseline threshold determinations, a subcutaneous injection of complete Freund's adjuvant (CFA) was administered into one volar forepaw. Withdrawal latencies were determined following subcutaneous administration of gabapentin, carbamazepine, ibuprofen, morphine, or saline.

Results. In contrast to its previously described efficacy in altering pain thresholds in the chronic constriction injury and formalin injection models of neuropathic pain and its anti-allodynic effect following nerve root ligation, gabapentin has no effect on paw withdrawal latencies associated with CFA-induced inflammation or on baseline hotplate or tail-flick response.

Conclusions. Gabapentin has no effect on pain initiated by CFA-induced inflammation. Gabapentin's effect in the treatment of neuropathic pain may be mediated through modulation of peripheral mechanisms related to the altered function of ion channels in damaged neurons. Such a mechanism suggests that improved nociceptive pain in clinical reports may have an underlying neuropathic component that is reduced by gabapentin.

Keywords: Gabapentin, neuropathic pain, inflammatory pain, analgesia

INTRODUCTION

Anitconvulsant medications have frequently been used to treat neuropathic pain syndromes such as trigeminal neuralgia, post-herpetic neuralgia, and diabetic polyneuropathy [17, 42, 46, 70]. Gabapentin is a new anticonvulsant medication that has been released for use as add-on therapy in the treatment of refractory complex partial seizures. Because of its favorable side-effect profile [4, 49, 56], gabapentin has been tried and rapidly accepted by pain management specialists as an effective option for the treatment of many intractable neuropathic pain syndromes [17, 48, 59]. In our clinical experience, anecdotal reports from patients who have been treated with gabapentin for neuropathic pain suggest that the range of efficacy for gabapentin in the management of pain may extend beyond neuropathic pain syndromes. These patients report improvement in joint pain associated with arthritis and improvement in chronic low back pain.

Although gabapentin has been studied extensively [72, 73], its exact mechanism of action in general and its specific role in reducing the pain remains unknown. Recent studies in animals have shown that gabapentin reduces the pain thresholds in the chronic constriction injury (CCI) [3] and the nerve root ligature (Chung model) [36] models of neuropathic pain [32, 87, 88] and in the late-phase response of the formalin-induced inflammatory pain [22, 81] model [65]. The purpose of this study was to determine the effect of gabapentin on pain thresholds in rats with pain generated by infection-induced inflammation in an attempt to delineate the limits of gabapentin's role in producing analgesia. The results of this study provide a basis for comparison of gabapentin's

effect on pain thresholds that have been produced by different initiating mechanisms in the hope of identifying potential sites of action for this drug. Some of these results have been reported elsewhere [21].

METHODS

Pain responses were measured in albino Sprague-Dawley rats. The latency to paw withdrawal, to tail-flick, and to hotplate aversion were the determinants of pain threshold. Paw withdrawal latency was measured according to the protocol of Hargreaves et al. [26]. Rats weighing between 250-350 g were housed 2 animals to a cage. For testing the rats were placed in plexiglass chambers on a glass plate and were allowed to acclimate to their surroundings for a minimum of 5 minutes. The animals were allowed free range of activity within the chamber. The glabrous surface of each of the paws was stimulated in succession through the glass plate using a halogen heat source. The latency of paw withdrawal from the onset of stimulation was measured automatically using an IITC analgesiometer (IITC Life Science, Inc., Woodland Hills, CA). The stimulus was automatically discontinued after 10.7 seconds to avoid tissue damage. Each paw was stimulated 4 times during each testing session. Baseline pain thresholds were determined in 3 separate testing sessions on 3 separate days. Tail-flick latency was measured in a group of 12 rats. Morphine sulfate (10 mg/kg), ibuprofen (40 mg/kg) or gabapentin (40 mg/kg) was administered subcutaneously to each rat. The order of drug administration was randomized with at least 4 days between drugs. Baseline latency was measured immediately before and at 15, 30, 60, 90, and 120 minutes after administration of drug. For the tail-flick test, the stimulus was discontinued after 12 seconds to avoid tissue damage. The same 12 rats were tested for hotplate analgesia immediately before and 45 minutes after drug administration. The rats were placed on the hotplate surface that was set at 52°C. The

rats were removed from the hotplate surface when they licked a hindpaw, jumped, or if they did not respond after 30 seconds. The time from stimulus onset to removal from the hotplate was recorded.

Following baseline threshold determinations for paw withdrawal latency, the rats were anesthetized with a combination of ketamine (60 mg/kg) and xylazine (8 mg/kg). One forepaw of each rat received a subcutaneous injection of 0.25 ml of complete Freund's adjuvant (CFA; *Mycobacterium tuberculosis*; Sigma) suspended in an oil:saline (1:1) emulsion (0.5 mg *Mycobacterium*/ml emulsion) using a sterile tuberculin syringe. The rats were then weighed and allowed to recover from anesthesia. Pain thresholds were measured on 5 separate days during the week following CFA injection. Either gabapentin (20-160 mg/kg) or normal saline was administered by subcutaneous injection 1 hour prior to each testing session. Ibuprofen (100 mg/kg) was given as a positive treatment control. Carbamazepine (40 mg/kg) was used as a negative treatment control.

To confirm that the route of administration and drug absorption was adequate to produce a response, 2 groups of 11 rats were subjected to subcutaneous injections of 5% formalin in isotonic saline into the plantar surface of one hindpaw 30 minutes after receiving a subcutaneous injection of either gabapentin (160 mg/kg) or normal saline. Time spent in licking, lifting, and biting the injected paw was monitored for 90 minutes following the formalin injection and recorded at 5 minute intervals.

RESULTS

Baseline withdrawal latencies were determined in all rats on 3 separate occasions after 2 days of environmental acclimation and prior to experimental intervention. Paw withdrawal latencies ranged between 4-7 seconds. Figure 1 compares the mean baseline withdrawal latencies for forepaws and hindpaws. The latency of forepaw withdrawal was shorter (mean=5.05-5.12 sec.) than for hindpaw withdrawal (mean=5.56-5.77 sec.). There was no significant difference in withdrawal latencies between sides of the body. After CFA injection, the inflamed paw showed edema and erythema that involved the entire paw and frequently extended to the proximal forelimb. Behaviorally, the rats demonstrated reduced activity. There was significant guarding of the injected paw that was infrequently placed on the floor of the cage or testing chamber. The withdrawal latency for the injected paw on the day following CFA injection decreased to between 0.5-1.5 sec. with little change in the latency of the non-injected paws (Fig. 2). After the withdrawal latency was determined on 2 separate occasions, control injections of normal saline were administered prior to determining withdrawal latencies. A gradual and progressive increase in withdrawal latency of the injected paw continued but never returned to baseline levels of the non-injected paws during the period of study. Changes in the withdrawal latencies in the non-injected paws of the saline-treated controls were not significantly different from baseline.

The subcutaneous administration of gabapentin at 40 mg/kg had no effect on the physical appearance of the inflammatory response. Edema and erythema remained

unchanged. In addition, Figure 3 shows that the latencies of paw withdrawal to thermal stimulation in the gabapentin-treated rats were virtually identical to those of saline treated controls. Any difference between the gabapentin-treated group of rats and controls, although statistically significant was extremely small and was consistently of similar magnitude and in similar relationship to the control group for all days tested. This response was seen for each of the paws. The lack of analgesic effect with gabapentin was unrelated to the dose of gabapentin used in doses ranging between 20 mg/kg and 160 mg/kg (Fig. 4). Indeed, minimal differences between treated animals and controls were greater at doses of 20 mg/kg and 40 mg/kg than at doses of 80 mg/kg and 160 mg/kg and were more likely related to group differences than to a dose-response relationship. The effect of gabapentin on the inflammatory pain threshold was not significantly different when compared to the effect of ibuprofen depicted in Figure 4 or carbamazepine (40 mg/kg) depicted in Figure 5.

The effects of gabapentin, ibuprofen, and morphine in the tail-flick and hotplate tests are illustrated in Figures 6 and 7. Typically, the tail-flick and hotplate tests are sensitive to high-efficacy analgesics but insensitive to antiinflammatory drugs. Morphine produced a significant increase in tail-flick and hotplate latency whereas gabapentin and ibuprofen were virtually indistinguishable from baseline latencies.

In light of the negative response to gabapentin observed following the CFA injections and in the tail-flick and hotplate tests, the efficacy of our sample of gabapentin was subjected to formalin testing. Figure 8 depicts our data as depicted by Singh et al. [65], separating phase I (0-10 minutes) and phase II (10-90 minutes) and

shows that gabapentin produces a significant decrease in aversive behavior during phase II of the formalin test. The reduction in the phase II response is consistent with what would be predicted from Singh et al. [65] Figure 9 depicts the data in an expanded format to show in addition that gabapentin's effect in phase II occurs primarily between 40 and 80 minutes after the formalin injection. It should be noted that 10 of the 11 gabapentin-treated rats fell asleep, whereas only 2 of the 11 saline-treated rats slept during phase II of the formalin test. The data from rats sleeping more than 50% of phase II (1 rat from each group) were not used in the statistical analysis. The observation that a greater percentage of the gabapentin-treated rats were able to sleep than the saline-treated controls, suggests that gabapentin has either a strong antinociceptive or anxiolytic effect during phase II of the formalin test.

DISCUSSION

The results of this study show that gabapentin had little, if any, effect on pain responses associated with CFA-induced inflammation. In addition, there was no effect on baseline pain thresholds as measured by the tail-flick or hotplate test. These observations are consistent with the lack of response seen following carrageenan-induced paw edema [65] but is in contrast with the results of studies in which gabapentin increased pain thresholds in animals where pain was initiated either by loose ligature of a peripheral nerve [87, 88] or nerve root [32] or by subcutaneous injections of formalin [65]. The difference in response suggests that the mechanism of injury in both the CCI and Chung models and the formalin injection model alters neuronal function in a fashion unlike CFA-induced inflammation that allows gabapentin to have an effect.

Although each of the experimental models being considered has a component of inflammation associated with tissue damage in its implementation, only the CFA injection model is likely to maintain the integrity of nociceptive neurons. Inflammation produced by infectious mechansims augments the activity of peripheral neurons by reducing the threshold to firing of nociceptive neuronal elements. Chemoactive agents such as bradykinin, prostaglandins, leukotrienes, serotonin, adenosine and histamine that are released during the inflammatory response have been shown to reduce nociceptor and axonal firing thresholds without altering neuronal morphology [40, 55, 75, 82]. These substances are released in high concentrations in response to infection and local irritation. The release of inflammatory mediators has been thought to be

potentiated in conditions of neutrophilic proliferation and reduced pH [7, 25, 75] and through the activity of the sympathetic nervous system [6, 8, 37, 44, 52, 53, 60, 61, 64, 75, 77, 78]. In the formalin test, the initial irritation produced by subcutaneous injections of formalin with the subsequent release of chemoactive agents is of an inflammatory nature and is associated with rapidly increasing formalin concentrations in surrounding tissue during diffusion. Unlike the CFA-induced inflammation, the initial inflammatory effect in the formalin test is short-lived because the rapid penetration of formalin ultimately destroys surrounding tissues including the terminal elements of peripheral nerves, thus adding a neuropathic component to the pain elicited by formalin injection. Since the features of inflammation are likely to be present to varying degrees in each of the experimental models and the associated pain is refractory to treatment with gabapentin, it is unlikely that gabapentin produces its effect through modulation of these mechanisms.

In contrast, CCI produces nerve constriction and extensive demyelination beneath each of the ligatures [3] with a resulting increase in the spontaneous action potential activity in primary afferent fibers [11, 24, 34, 67, 90]. The increase in spontaneous activity has been related to alterations in ion channel function [18, 33, 74]. Loss of myelin from neuronal membranes due to injury results in an upregulation of sodium, potassium, and possibly calcium channels in the expanded, myelin-free regions or dorsal root ganglia resulting in hypersensitivity and increased firing of the effected nerve [5, 11, 12, 14, 35, 63, 76, 89]. Areas of neuronal demyelination are also potential sites for the formation of ephaptic connections that are thought to be involved in the formation of repetitive stimulation loops within the area of injury [11, 13, 51, 62]. The indirect modulation

of sodium channels has been proposed as one of the possible mechanisms of action for gabapentin [79] and may be the source of gabapentin's effect in the CCI model. Carbamazepine is known to function through the reduction of central [42] and peripheral [28] posttetanic potentiation as well as through voltage-dependent sodium channel blockade [83]. Although gabapentin has no direct effect on voltage-dependent sodium channel blockade [71], a similar increase in the pain threshold if produced by carbamazepine and gabapentin in the CCI model, although only suggestive, would be consistent with different mechanisms acting through a common site. Indeed, sodium channel blockade has been proposed as the primary, if not the only, mechanism through which neuropathic analgesia is mediated [31].

Gabapentin may produce its effect similarly in phase II of the formalin test. Following the initial local irritation and release of inflammatory mediators, formalin produces significant local tissue destruction altering the morphology of surrounding tissue and all neural elements within and closely adjacent to the site of injury [9]. Acutely, formalin acts by cross-linking protein molecules and altering membrane permeability in adjacent viable membrane. As fixation proceeds during phase II of the formalin test, high frequency neuronal firing is initiated as a result of injury potentials related to the destruction of the terminal elements of all afferent neurons and demyelination of the distal segments of the A-β and A-δ fibers. The effect of gabapentin on the phase II response of the formalin test would appear to be mediated through the stabilization of hyperactive membranes in injured neuronal tissue perhaps in part through the modulation of altered sodium channel activity. During tissue repair,

regenerating, hypersensitive neuromas and viable demyelinated terminal neuronal segments with high sodium, potassium, and possibly calcium channel density extend into healing tissue and are more exquisitely sensitive to mechanical and thermal stimulation and to the influence of inflammatory mediators released at the site of tissue injury and tissue repair [7, 10, 11, 33, 43, 45, 61, 75, 77, 78, 86, 91]. In light of the effect of gabapentin on pain behaviors in the CCI and Chung models and in phase II of the formalin test, the hypersensitive membranes found in injured and healing neural tissue predictably may be responsive to treatment with gabapentin through the modulation of one or more of these altered channels [15].

Since the increased firing of central pathways acutely is likely to be similar in each experimental model, it would seem that gabapentin's primary influence on reducing pain of neuropathic quality is most likely mediated peripherally, however, it is possible that gabapentin mediates its effect centrally. CCI is known to alter GABAergic modulation of spinal dorsal horn neurons that produces heat-hyperalgesia [23, 39, 50, 68]. Although the heat-hyperalgesia is exacerbated by bicucullin, a $GABA_A$-receptor antagonist, is reduced by muscimol, a $GABA_A$-receptor agonist [92, 93], and is relieved by baclofen, a $GABA_B$-receptor agonist [66, 92], gabapentin does not act directly through either $GABA_A$ or $GABA_B$ receptors [1, 32, 57, 69]. If acting through GABAergic mechanisms, gabapentin is more likely to have an indirect effect on this central mechanism [88], perhaps through the enhancement of GABA-mediated inhibition by augmenting GABA currents [38, 58], enhancing GABA release [20, 80], or by increasing glutamic acid decarboxylase (GAD) activity and the rate of gamma-aminobutyric acid (GABA)

synthesis [72, 73].

Gabapentin also binds to neurons in areas with high concentrations of glutamate synapses, such as layers I and II of neocortex, the dendritic layers of the hippocampus (CA1, CA2, and CA3 subfields and the dentate gyrus), and the molecular layers of the cerebellum [27, 69]. It is probable that neuronal activity in these areas is reduced since each of the proposed mechanisms for gabapentin's effect have been to enhance glutamate degradation by increasing glutamate dehydrogenase (GDH) activity and by reducing glutamate synthesis through inhibiting branched-chain amino acid aminotransferase (BCAT) activity [19, 29, 30, 38, 41, 54, 72, 73, 80]. In the absence of altering the paw withdrawal threshold in the injected paws (present study), it is possible that gabapentin's effect through these central supraspinal sites may reduce the cognitive and emotional contribution to nociception. Our observation that rats were able to sleep during phase II of the formalin test, is suggestive of some alteration in perhaps the more subtle affective component of pain. Furthermore, Singh et al. [65] have recently shown that gabapentin demonstrates antinociceptive and anxiolytic effects that are reversed by the intracerebroventricular administration of D-serine that is mediated through supraspinal mechanisms [32]. Additionally, the dorsal horn of the spinal cord and the trigeminal nuclei, also have high concentrations of glutamate terminals and could well be a site for gabapentin's indirect modulation of glutamate receptors at the glycine binding site of the NMDA receptor [2, 65]. The similar augmentation of the afferent signal in each of the acute pain models under consideration, however, argues against these regions as a unique site of action. Subsequent changes in the dorsal

horn due to sprouting and/or loss of afferent modulating neurons associated with repetitive stimulation that are thought to contribute to the development of hyperalgesia and allodynia in neuropathic pain, could also explain how stimulation of even a few intact peripheral neurons could result in a suprathreshold influence over a larger population of neurons [39, 84, 85], but it is unlikely that these mechanisms play a significant role at such early stages following experimental manipulation.

In conclusion, gabapentin has been shown to have no effect on pain initiated by CFA-induced inflammation. It is likely that gabapentin's effect in the treatment of neuropathic pain is mediated through modulation of peripheral mechanisms related to the altered function of ion channels in damaged neurons. Such a mechanism suggests that the improved nociceptive pain in clinical reports may have an underlying neuropathic component that is reduced by gabapentin administration.

ACKNOWLEDGMENTS

Gabapentin provided through the courtesy of Parke-Davis. We thank Dr. Anthony Vaccarino for assistance in performing the formalin test.

LITERATURE CITED

1. Bartoszk, G.D.; Reimann, W. Preclinical characterization of the anticonvulsant gabapentin. In: 16th Epilepsy International Congress. Ciba-Geigy, Basel; 1985; 1.

2. Bennett, G.J. Animal models of neuropathic pain. In: Proceedings of the 7th World Congress of Pain. In: Progress in Pain Research and Management, v.2, G.F. Gebhart, D.L. Hammond, and T.S. Jensen, eds., IASP Press, Seattle, WA; 1994; 495-510.

3. Bennett, G.J.; Xie, Y.-K. A peripheral mononeuropathy in rat that produces disorders of pain sensation like those seen in man. Pain, 33:87-107; 1988.

4. Beydoun, A.; Uthman, B.M.; Sackellares, J.C. Gabapentin: Pharmacokinetics, efficacy, and safety. Clin. Neuropharmacol., 18:471-481; 1995.

5. Calvin, W.H.; Devor, M.; Howe, J.F. Can neuralgias arise from minor demyelination? Spontaneous firing, mechosensitivity and afterdischarge from conducting axons. Exp. Neurol., 75:755-763; 1982.

6. Campbell, J.N.; Mayer, R.A.; Davis, K.D.; Raja, S.N. Sympathetically maintained pain: A unifying hypothesis. In: Hyperalgesia and Allodynia. W.D. Willis, Jr., ed., Raven Press, Ltd., New York; 1992; 141-149.

7. Clatworthy, A.L.; Illich, P.A.; Castro, G.A.; Walters, E.T. Role of peri-axonal inflammation in the development of thermal hyperalgesia and guarding behavior in a rat model of neuropathic pain. Neurosci. Letters, 184:5-8; 1995.

8. Davis, K.D.; Treede, R.D.; Raja, S.N.; Meyer, R.A.; Campbell, J.N. Topical application of clonidine relieves hyperalgesia in patients with sympathetically maintained pain. Pain, 47:309-317; 1991.

9. Dennis, S.G.; Melzack, R. Comparison of phasic and tonic pain in animals. In: Advances in Pain Research and Therapy, Vol. 3; J.J. Bonica, ed. Raven Press, New York; 1979; 747-760.

10. Devor, M. Potassium channels moderate ectopic excitability of nerve-end neuromas in rats. Neurosci. Lett., 40:181-186; 1983.

11. Devor, M. The pathophysiology of damaged peripheral nerves. In: Textbook of Pain. Wall P.D. and R. Melzack, eds., 3rd Ed. Edinburgh:Churchill Livingstone; 1994; 79-100.

12. Devor, M.; Govrin, L.R.; Angelides, K. Na^+ channel immunolocalization in peripheral mammalian axons and changes following nerve injury and neuroma formation. J. Neurosci., 13:1976-1992; 1993.

13. Devor, M.; Wall, P.D. Cross-excitation in dorsal root ganglia of nerve-injured and intact rats. J. Neurophysiol., 64:1733-1746; 1990.

14. England, J.D.; Gamboni, F.; Ferguson, M.A.; Levinson, S.R. Sodium channels accumulate at the tips of injured axons. Muscle & Nerve 17:593-598; 1994.

15. England, J.D.; Happel, L.T.; Kline, D.G.; Gamboni, F.; Thouron, C.L.; Liu, Z.P.; Levinson, S.R. Sodium channel accumulation in humans with painful neuromas. Neurology, 47:272-276; 1996a.

16. England, J.D.; Levinson, R.S.; Shrager, P. Immunocytochemical investigations of sodium channels along nodal and internodal portions of demyelinated axons. Micro. Res. Tech., 34:445-451; 1996b.

17. Galer, B.S. Neuropathic pain of peripheral origin: Advances in pharmacologic treatment. Neurology, 45 (suppl 9):S17-S25.

18. Gallego, R.; Ivorra, I.; Morales, A. Effects of central or peripheral axotomy on membrane properties of sensory neurones in the petrosal ganglion of the cat. J. Physiol. (Lond.), 391:39-56; 1987.

19. Goldlust, A.; Su, T.-Z.; Welty, D.F.; Taylor, C.P.; Oxender, D.L. Effects of the anticonvulsant drug gabapentin on the enzymes in metabolic pathways of glutamate and GABA. Epilepsy Res., 22:1-11; 1995.

20. Gotz, E.; Feuerstein, T.J.; Lais, A.; Meyer, D.K. Effects of gabapentin on release of gamma-aminobutyric acid from slices of rat neostriatum. Arzneimittel-Forschung, 43:636-638; 1993.

21. Gould, T.N.; Paul, D.J.; Gould, H.J., III. Analgesic effects of gabapentin on inflammatory pain in rat. J. Invest. Med., 45:6A; 1997.

22. Haley, J.E.; Sullivan, A.F.; Dickenson, A.H. Evidence for spinal *N*-methyl-D-aspartate receptor involvement in prolonged chemical nociception in the rat. Brain Res., 518:218-226; 1990.

23. Hama, A.T.; Sagen, J.; Pappas, G.D. Morphological characterization of dorsal horn spinal neurons in rats with unilateral constriction nerve injury. Neurol. Res., 16:297-304; 1994.

24. Han, H.C.; Na, H.S.; Yoon, Y.W.; Chung, J.M. Ectopic discharges from injured afferent fibers in a rat model of neuropathic pain. Soc. Neurosci. Abstr., 20:760; 1994.

25. Handwerker, H.O.; Reeh, P.W. Nociceptors: Chemosensitivity and sensitization by chemical agents. In: Hyperalgesia and Allodynia. W.D. Willis, Jr., ed., Raven Press, Ltd., New York, pp. 1992; 107-115.

26. Hargreaves, K.; Dubner, R.; Brown, R.; Flores, C.; Joris, J. A new and sensitive method for measuring thermal nociception in cutaneous hyperalgesia. Pain, 32:77-88; 1988.

27. Hill, D.R.; Suman-Chauhan, N.; Woodruff, G.N. Localization of [^{3}H]-gabapentin to a novel site in rat brain: autoradiographic studies. Eur. J. Pharmacol. Mol. Pharmacol., 244:303-309; 1993.

28. Honda, H.; Allen, M.B. The effect of an iminostilbine derivative (G 32883) on peripheral nerves. J. Med. Assoc. Ga., 62:38-42; 1973.

29. Honmou, O.; Kocsis, J.D.; Richerson, G.B. Gabapentin potentiates the conductance increase induced by nipecotic acid in CA1 pyramidal neurons in vitro. Epilepsy Res., 20:193-202; 1995a.

30. Honmou, O.; Oyelese, A.A.; Kocsis, J.D. The anticonvulsant gabapentin enhances promoted release of GABA in hippocampus: A field potential analysis. Brain Res., 712:273-277; 1995b.

31. Hunter, J.C. Antidepressants as analgesics: New ideas on mechanisms and efficacy. 8th World Congress on Pain, 1996; 423.

32. Hwang, J.-H.; Yaksh, T.L. The effect of intrathecal gabapentin on tactile-evoked allodynia in a surgically-induced neuropathic pain model in the rat. In press; 1997.

33. Jassar, B.S.; Pennefather, P.S.; Smith, P.A. Changes in sodium and calcium channel activity following axotomy of B-cells in bullfrog sympathetic ganglion. J. Physiol. (Lond.) 472:203-231; 1993.

34. Kajander, K.C.; Bennett, G.J. Onset of a painful peripheral neuropathy in rat: A partial and differential deafferentation and spontaneous discharge in A beta and A delta primary afferent neurons. J. Neurophysiol., 68:734-744; 1992.

35. Kajander, K.C.; Wakisaka, S.; Bennett, G.J. Spontaneous discharge originates in the dorsal root ganglion at the onset of a painful peripheral neuropathy in the rat. Neurosci. Lett., 138:225-228; 1992.

36. Kim, S.H.; Chung, J.M. An experimental model of peripheral neuropathy produced by segmental spinal nerve ligation. Pain, 50:355-363; 1992.

37. Kim, S.H.; Na, H.S.; Sheen, K.; Chung, J.M. Effects of sympathectomy on a rat model of peripheral neuropathy. Pain, 55:85-92; 1993.

38. Kocsis, J.D.; Honmou, O. Gabapentin increases GABA-induced depolarization in rat neonatal optic nerve. Neurosci. Lett., 171:181-184; 1994.

39. Laird, J.M.; Bennett, G.J. An electrophysiological study of dorsal horn neurons in the spinal cord of rats with an experimental peripheral neuropathy. J. Neurophysiol., 71:2072-2085; 1993.

40. Levine, J.D.; Taiwo, Y.O.; Heller, P.H. Hyperalgesic pain: Inflammatory and neuropathic. In: Hyperalgesia and Allodynia. W.D. Willis, Jr., ed., Raven Press, Ltd., New York, 1992; 117-123.

41. Löscher, W.; Hönack, D.; Taylor, C.P. Gabapentin increases aminooxyacetic acid-induced GABA accumulation in several regions of rat brain. Neurosci. Lett., 128:150-154; 1991.

42. Maciewicz, R.; Bouckoms, A.; Martin, J.B. Drug therapy of neuropathic pain. Clin. J. Pain, 1:39-49; 1985.

43. Matzner, O.; Devor, M. Hyperexcitability at sites of nerve injury depends on voltage-sensitive Na+ channels. J. Neurophysiol., 72:349-359; 1994.

44. McLachlan, E.M.; Jänig, W.; Devor, M.; Michaelis, M. Peripheral nerve injury triggers noradrenergic sprouting within the dorsal root ganglia. Nature, 363:543-546; 1993.

45. McMahon, S.B. Mechanisms of sympathetic pain. Brit. Med. Bull., 47:584-600; 1991.

46. McQuay, H.; Carroll, D.; Jadad, A.R.; Wiffen, P.; Moore, A. Anticonvulsant drugs for management of pain: A systematic review. Brit. Med. J., 311:1047-1052.

47. Mellick, G.A.; Mellick, L.B. Reflex sympathetic dystrophy (RSD) treated with gabapentin (Neurontin). Arch. Phys. Med. Rehab., 78:98-105; 1996.

48. Mellick, G.A.; Seng, M.L. The use of gabapentin in the treatment of reflex sympathetic dystrophy and a phobic disorder. AJPM, 5:7-9; 1995.

49. Morris, G.L., III. efficacy and tolerability of gabapentin in clinical practice. Clin. Ther., 17:891-900; 1995.

50. Nachemson, A.; Bennett, G.J. Does pain damage spinal neurons?: Transsynaptic degeneration on rat following a surgical incision. Neurosci. Lett., 162:78-80; 1993.

51. Ochoa, J. Pain in local nerve lesions. In: Abnormal nerves and muscles as impulse generators. Culp, W.J. and J. Ochoa, eds. Cambridge:Oxford University Press, 1983; 568-587.

52. Ochoa, J. Thermal hyperalgesia as a clinical symptom. In: Hyperalgesia and Allodynia. W.D. Willis, Jr., ed., Raven Press, Ltd., New York, 1992; 151-163.

53. Perl, E.R. Alterations in the responsiveness by nerve injury. In: Hyperalgesia and Allodynia. W.D. Willis, Jr., ed., Raven Press, Ltd., New York, 1992; 59-79.

54. Petroff, O.A.C.; , Rothman, D.L.; Behar, K.L.; Lamorueux, D.; Mattson, R.H. The effect of gabapentin on brain GABA levels in patients with epilepsy. Ann. Neurol., 39:95-99; 1996.

55. Rang, H.P.; Bevan, S.; Dray, A. Chemical activation of nociceptive peripheral neurones. Brit. Med. Bull., 47:534-548; 1991.

56. Ramsay, R.E. Clinical efficacy and safety of gabapentin. Neurology, 44(suppl 5):S23-S30; 1994.

57. Reiman, W. Inhibition by GABA, baclofen and gabapentin of dopamine release from rabbit caudate nucleus: Are there common or different sites of action? Eur. J. Pharmacol., 94:341-344; 1983.

58. Rock, D.M.; Kelly, K.M.; MacDonald, R.L. Gabapentin actions on ligand- and voltage-gated responses in cultured rodent neurons. Epilepsy Res., 16:89-98; 1993.

59. Rosner, H.; Rubin, L.; Kestenbaum, A. Gabapentin adjuvant therapy in neuropathic pain states. Clin. J. Pain, 12:56-58; 1996.

60. Sato, J.; Perl, E.R. Adrenergic excitation of cutaneous pain receptors induced by peripheral nerve injury. Science, 251:1608-1610; 1991.

61. Scadding, J.W. development of ongoing activity, mechanosensitivity, and adrenaline sensitivity in severed peripheral nerve axons. Exp. Neurol., 73:345-364; 1981.

62. Seltzer, Z.; Devor, M. Ectopic transmission in chronically damaged peripheral nerves. Neurol., 29:1061-1064; 1979.

63. Sernagor, E.; Yarom, Y.; Werman, R. Sodium-dependent regenerative responses in dendrites of axotomized motoneurons in the cat. Proc. Natl. Acad. Sci. (USA), 83:7966-7968; 1986.

64. Shir, Y.; Seltzer, Z. Effects of sympathectomy in a model of causalgiform pain produced by partial sciatic nerve injury in rats. Pain, 45:309-320; 1991.

65. Singh, I.; Field, M.J.; Ferris, P.; Hunter, J.C.; Oles, R.J.; R.G. Williams, R.G.; Woodruff, G.N. The antiepileptic agent gabapentin (Neurontin) possesses anxiolytic-like and antinociceptive actions that are reversed by D-Serine. Psychopharmacology, 127:1-9; 1996.

66. Smith, G.D.; Harrison, S.M.; Birch, P.J.; Elliott, P.J.; Malcangio, M.; Bowery, N.G. Increased sensitivity to the antinociceptive activity of (+/-)-baclofen in an animal model of chronic neuropathic, but *not* chronic inflammatory hyperalgesia. Neuropharmacol., 33:1103-1108; 1994.

67. Study, R.E.; Kral, M.G. Spontaneous action potential activity in isolated dorsal root ganglion neurons from rats with a painful neuropathy. Pain, 65:235-242 1996.

68. Sugimoto, T.; Bennett, G.J.; Kajander, K.C. Transsynaptic degeneration in the superficial dorsal horn after sciatic nerve injury: Effects of a chronic constriction injury, transection, and strychnine. Pain, 42:205-213; 1990.

69. Suman-Chauhan, N.; Webdale, L.; Hill, D.R.; and Woodruff, G.N. Characterization of [^{3}H] gabapentin binding to a novel site in rat brain: Homogenate binding studies. Eur. J. Pharmacol., 244:293-301; 1993.

70. Swerdlow, M. Anticonvulsant drugs and chronic pain. Clinical Neurophysiol., 7:51-82; 1984.

71. Taylor, C.P. The anticonvulsant lamotrigine blocks sodium currents from cloned alpha-subunits of rat brain Na^+ channels in a voltage-dependent manner but gabapentin does not. Soc. Neurosci. Abstr., 19:1631; 1993.

72. Taylor, C.P. Emerging perspectives on the mechanism of action of gabapentin. Neurology, 44 (suppl 5) S10-S16; 1994.

73. Taylor, C.P. Gabapentin: Mechanisms of action. In: Antiepileptic Drugs, eds. R.H. Levy, R.H. Mattson, and B.S. Meldrum, 4th ed., Raven Press, New York, NY, 1995; 829-841.

74. Titmus, M.J.; Faber, D.S. Axotomy-induced alterations in the electrophysiological characteristics of neurons. Prog. Neurobiol., 35:1-51; 1990.

75. Tracey, D.J.; Walker, J.S. Pain due to nerve damage: Are inflammatory mediators involved: Inflamm. Res., 44:407-411; 1995.

76. Wall, P.D.; Devor, M. Sensory afferent impulses originate from dorsal root ganglia as well as from the periphery in normal and nerve injured rats. Pain, 17:321-339; 1983.

77. Wall, P.D.; Devor, M.; Inbal, R.; Scadding, J.W.; Schonfeld, D.; Seltzer, Z.; Tomkiewicz, M.M. Autotomy following peripheral nerve lesions: Experimental anaesthesia dolorosa. Pain, 7:103-111; 1979.

78. Wall, P.D.; Gutnick, M. Properties of afferent nerve impulses originating from a neuroma. Nature, 248:740-741; 1974.

79. Wamil, A.W.; McLean, M.J. Limitation by gabapentin of high frequency action potential firing by mouse central neurons in cell culture. Epilepsy Res., 17:1-11; 1994.

80. Welty, D.F.; Schielke, G.P.; Vartanian, M.G.; Taylor, C.P. Gabapentin anticonvulsant action in rats: Disequilibrium with peak drug concentrations in plasma and brain microdialysate. Epilepsy Res., 16:175-181; 1993.

81. Wheeler-Aceto, H.; Cowan, A. Standardiztion of the rat paw formalin test for the evaluation of analgesics. Psychopharmacology, 104:35-44; 1991.

82. Willis, W.D., Jr. Hyperalgesia and allodynia: Summary and overview. In: Hyperalgesia and Allodynia. W.D. Willis, Jr., ed., Raven Press, Ltd., New York, 1992; 1-11.

83. Willow, M.; Gonoi, T.; Catterall, W.A. Voltage clamp analysis of the inhibitory actions of diphenylhydantoin and carbamazepine on voltage-sensitive sodium channels in neuroblastoma cells. Mol. Pharmacol., 27:549-558; 1985.

84. Woolf, C.J. evidence for a central component of postinjury pain hypersensitivity. Nature, 306:686-688; 1983.

85. Woolf, C.J. Excitability changes in central neurons following peripheral damage: Role of central sensitization in the pathogenesis of pain. In: Hyperalgesia and Allodynia. Willis, W.D., Jr., ed. Raven Press, New York, 1992; 221-243.

86. Xiao, W.-H.; Bennett, G.J. Magnesium suppresses neuropathic pain sensations in rats via a spinal site of action. Brain Res., 666:168-172; 1994.

87. Xiao, W.-H.; Bennett, G.J. Gabapentin relieves abnormal pains in a rat model of painful peripheral neuropathy. Soc. Neurosci. Abstr., 21:356.17; 1995.

88. Xiao, W.-H.; Bennett, G.J. Gabapentin relieves abnormal pain sensations via a spinal site of action in a rat model of painful peripheral neuropathy. In press; 1997.

89. Xie, Y.; Zhang, J.; Petersen, M.; LaMotte, R.H. Functional changes in dorsal root ganglion cells after chronic nerve constriction in the rat. J. Neurophysiol., 73:1811-1820; 1995.

90. Xie, Y.-K.; Xiao, W.-H. Electrophysiological evidence for hyperalgesia in the peripheral neuropathy. Sci. China (B), 33:663-672; 1990.

91. Xie, Y.K.; Xiao, W.H.; Li, H.Q. the relationship between new ion channels and extopic discharges from a region of nerve injury. Science in China Ser B, 36:68-74; 1993.

92. Yamamoto, T.; Yaksh, T.L. Spinal pharmacology of thermal hyperesthesia induced by incomplete ligation of sciatic nerve: I. Opioid and nonopioid receptors. Anesthesiol., 75:817-826; 1991.

93. Yamamoto, T.; Yaksh, T.L. effects of intrathecal strychnine and bicuculline on nerve compression induced thermal hyperesthesia and selective antagonism by MK-801. Pain, 54:79-84; 1993.

FIGURE LEGENDS

Figure 1. The consistent relationship between baseline forepaw (circles) and hindpaw (squares) withdrawal latencies. Paw withdrawal latencies were determined for rats (n=126) as described in METHODS.

Figure 2. Control values for paw withdrawal before and after CFA injection. Rats (n=15) were tested for paw withdrawal latency before CFA injection. After CFA injection, normal saline was administered subcutaneously 1 hour prior to testing. A dramatic reduction in the withdrawal latency is noted in the injected paw that improves with time but latencies do not return to pre-injection values. Little effect is noted in non-injected paws.

Figure 3. Effect of gabapentin on paw withdrawal latencies. Groups of rats received gabapentin (40 mg/kg) (n=29) or normal saline (n=15) subcutaneously 1 hour prior to testing. The responses obtained following gabapentin administration are virtually identical to those obtained following normal saline administration.

Figure 4. Dose-response curves for gabapentin. Four groups of rats (n=12) were given gabapentin subcutaneously on 3 consecutive days, 6 days after the injection of CFA in doses ranging from 20-160 mg/kg 1 hour prior to testing. Responses are similar to those of saline injected controls. No clear dose-response relationship was observed. The response to ibuprofen (100 mg/kg) (n=12) was identical to that following gabapentin administration.

Figure 5. Effect of gabapentin, carbamazepine, and saline on paw withdrawal thresholds in CFA injected paws. Three groups of rats received a subcutaneous

injection of gabapentin (40 mg/kg) (n=18), carbamazepine (40 mg/kg) (n=18), or normal saline (n=15). Neither gabapentin nor carbamazepine produced a significant analgesic effect.

Figure 6. Effects of morphine, gabapentin, and ibuprofen on mean tail-flick latency. Morphine (10 mg/kg), gabapentin (40 mg/kg), or ibuprofen (40 mg/kg) was administered to rats (n=12) and then tested for tail-flick latency at the intervals indicated in METHODS. The greater than expected response to morphine is thought to be related to the paired housing of rats. Gabapentin and ibuprofen did not alter tail-flick response.

Figure 7. Effects of morphine, gabapentin, and ibuprofen on mean hotplate latency. The same rats used to determine tail-flick latencies depicted in Figure 6 were also tested for hotplate analgesic response 45 minutes after administration of drug. Latency to hotplate stimulation was prolonged 3-fold following morphine administration when compared to baseline. Responses following gabapentin and ibuprofen administration were not significantly different than baseline.

Figure 8. Effect of gabapentin on mean response in the formalin test. Two groups to 11 rats received subcutaneous injections of either gabapentin (160 mg/kg) or normal saline, 30 minutes prior to a subcutaneous injection of 5% formalin into the plantar surface of 1 hindpaw. Gabapentin reduced the time that the injected paw was elevated above the floor of the observation box during phase II (10-90) minutes) but not phase I (0-10 minutes) of the formalin test.

Figure 9. The effect of gabapentin on phase II of the formalin test was most

profound between 40 and 80 minutes after the formalin injection. A repeated measures, mixed design ANOVA resulted in a significant main effect for treatment ($p < 0.05$). Periods of statistically significant differences in aversive behavior between gabapentin-treated and saline-treated groups ($p = 0.05$) are indicated by an asterisk.

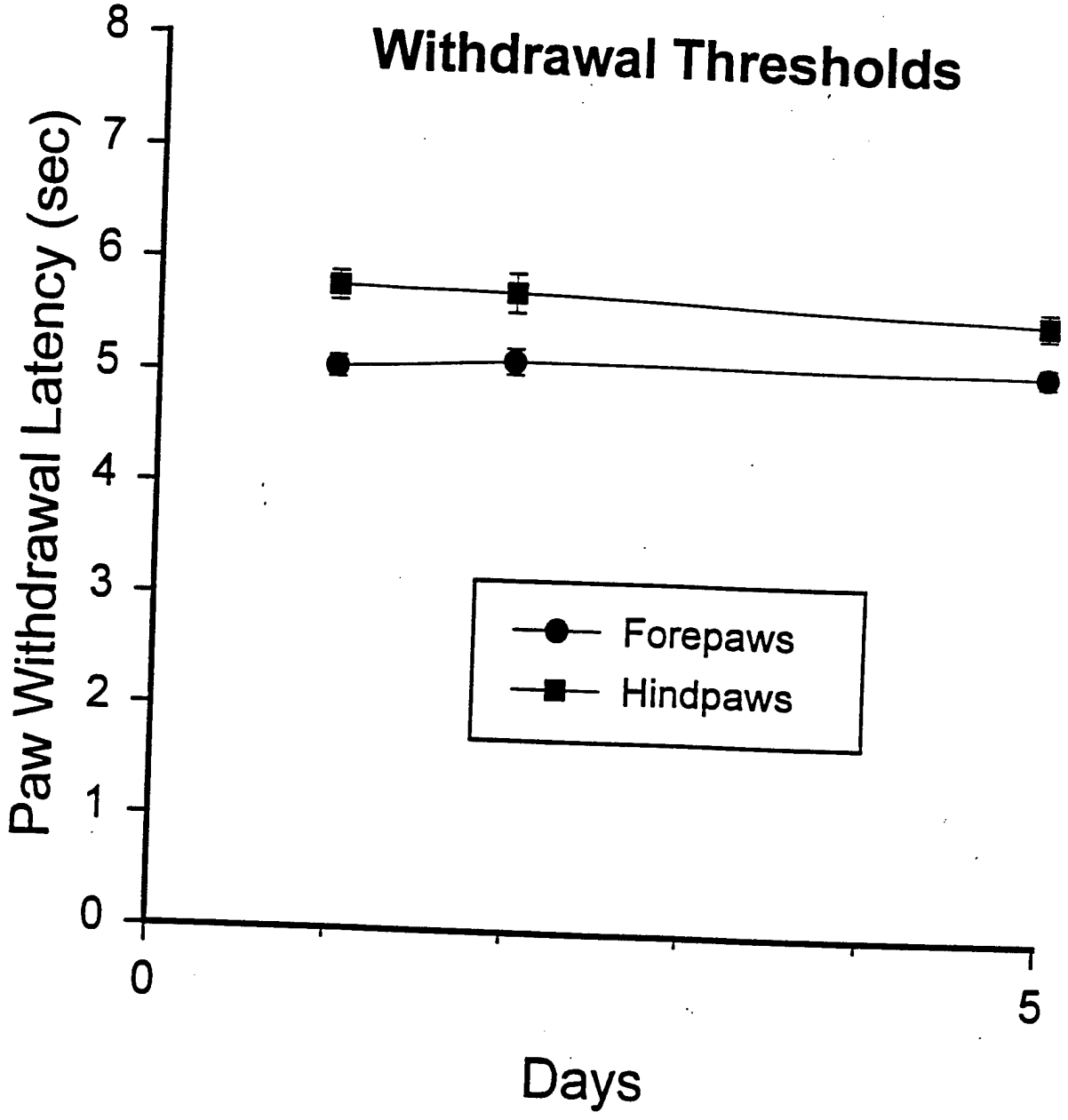
Withdrawal Thresholds
Paw Withdrawal Latency (sec)
8
7
6
5
4
3
2
1
0
0
5
Days
Forepaws
Hindpaws

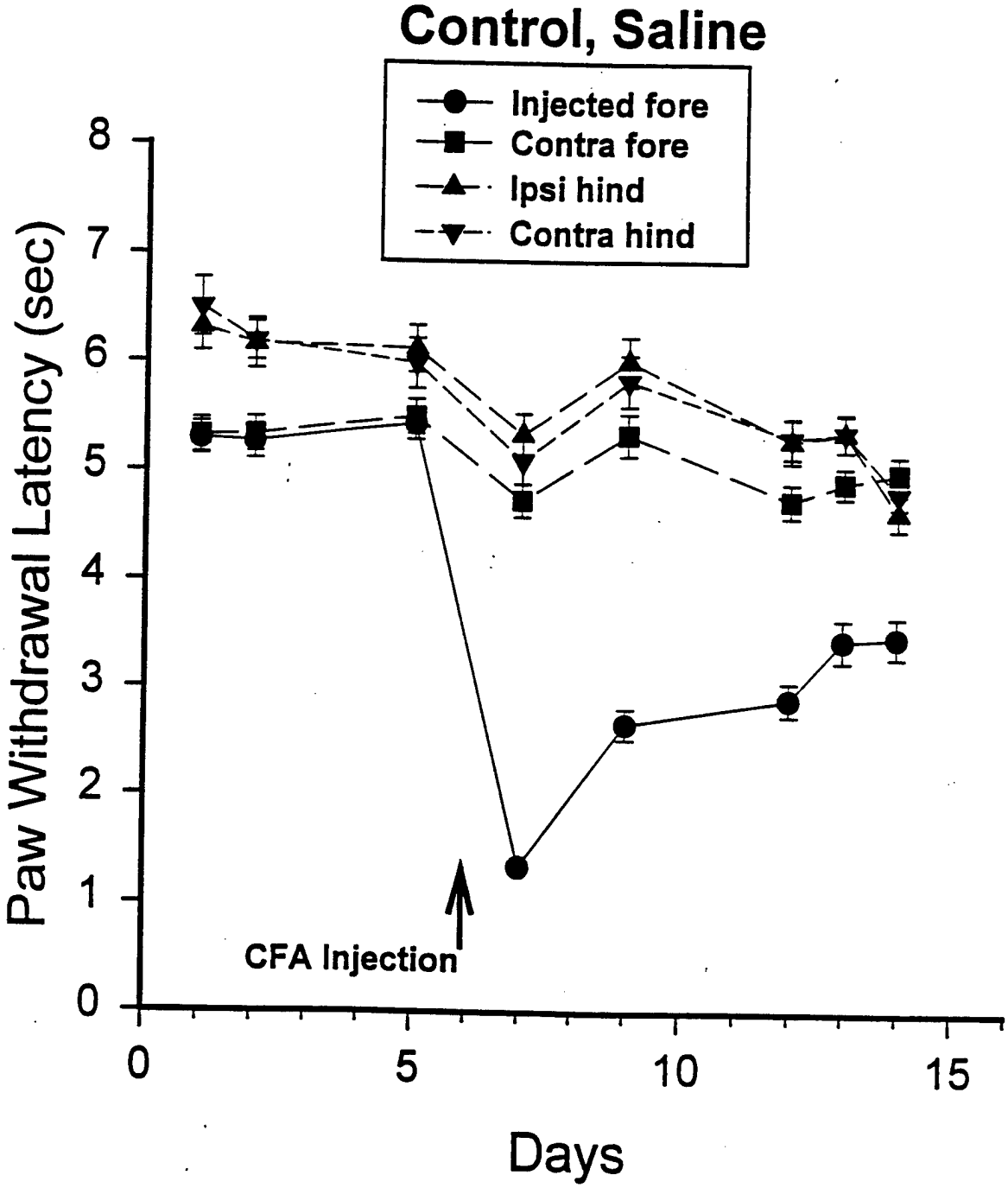
Control, Saline
Injected fore
Contra fore
Ipsi hind
Contra hind
Paw Withdrawal Latency (sec)
0
1
2
3
4
5
6
7
8
CFA Injection
0
5
10
15
Days

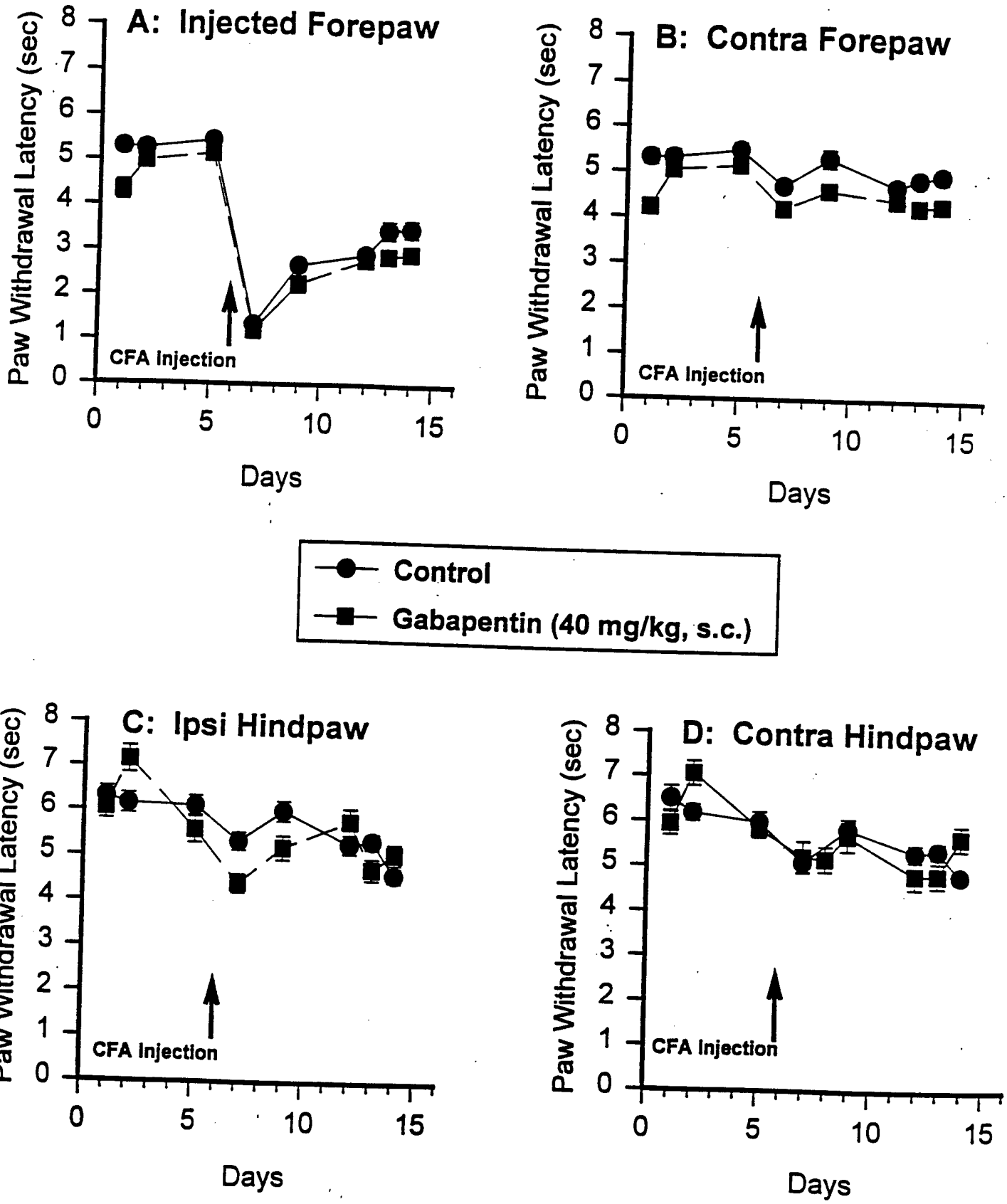
A: Injected Forepaw
B: Contra Forepaw
C: Ipsi Hindpaw
D: Contra Hindpaw
Paw Withdrawal Latency (sec)
Days
CFA Injection
0
1
2
3
4
5
6
7
8
0
5
10
15
Control
Gabapentin (40 mg/kg, s.c.)

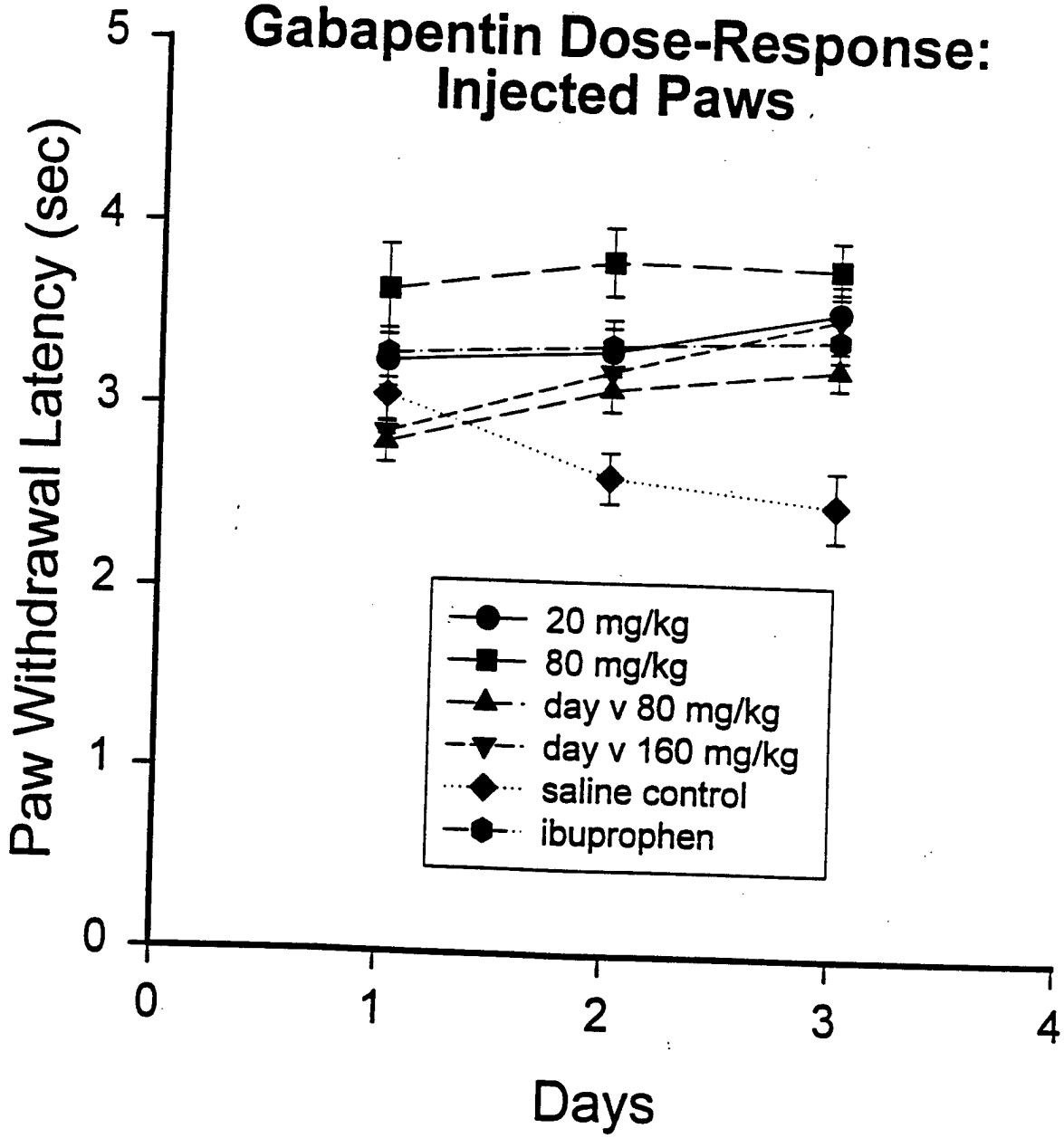
Gabapentin Dose-Response:
Injected Paws
Paw Withdrawal Latency (sec)
5
4
3
2
1
0
0
1
2
3
4
Days
20 mg/kg
80 mg/kg
day v 80 mg/kg
day v 160 mg/kg
saline control
ibuprophen

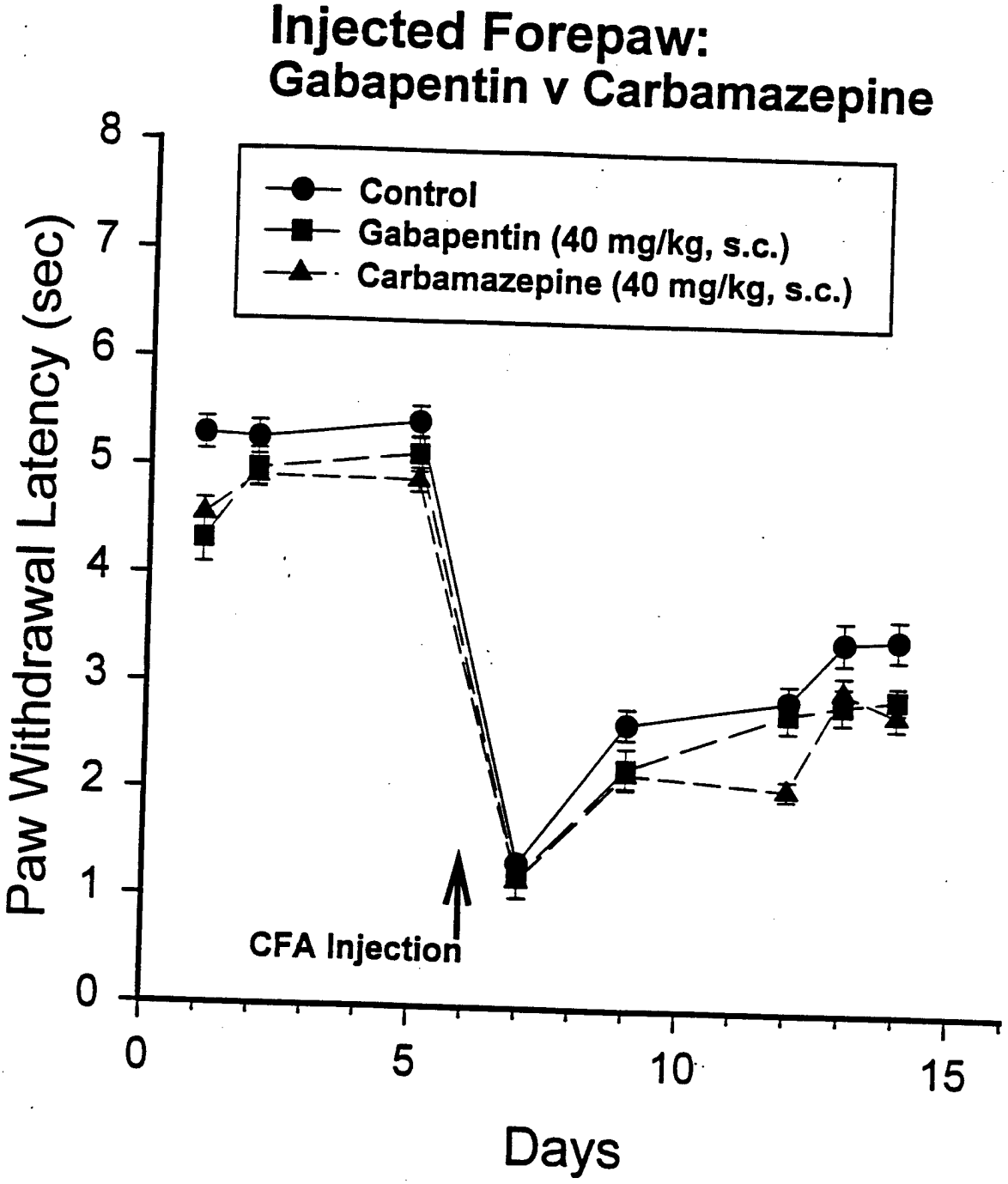
Injected Forepaw:
Gabapentin v Carbamazepine
Control
Gabapentin (40 mg/kg, s.c.)
Carbamazepine (40 mg/kg, s.c.)
Paw Withdrawal Latency (sec)
0
1
2
3
4
5
6
7
8
CFA Injection
0
5
10
15
Days

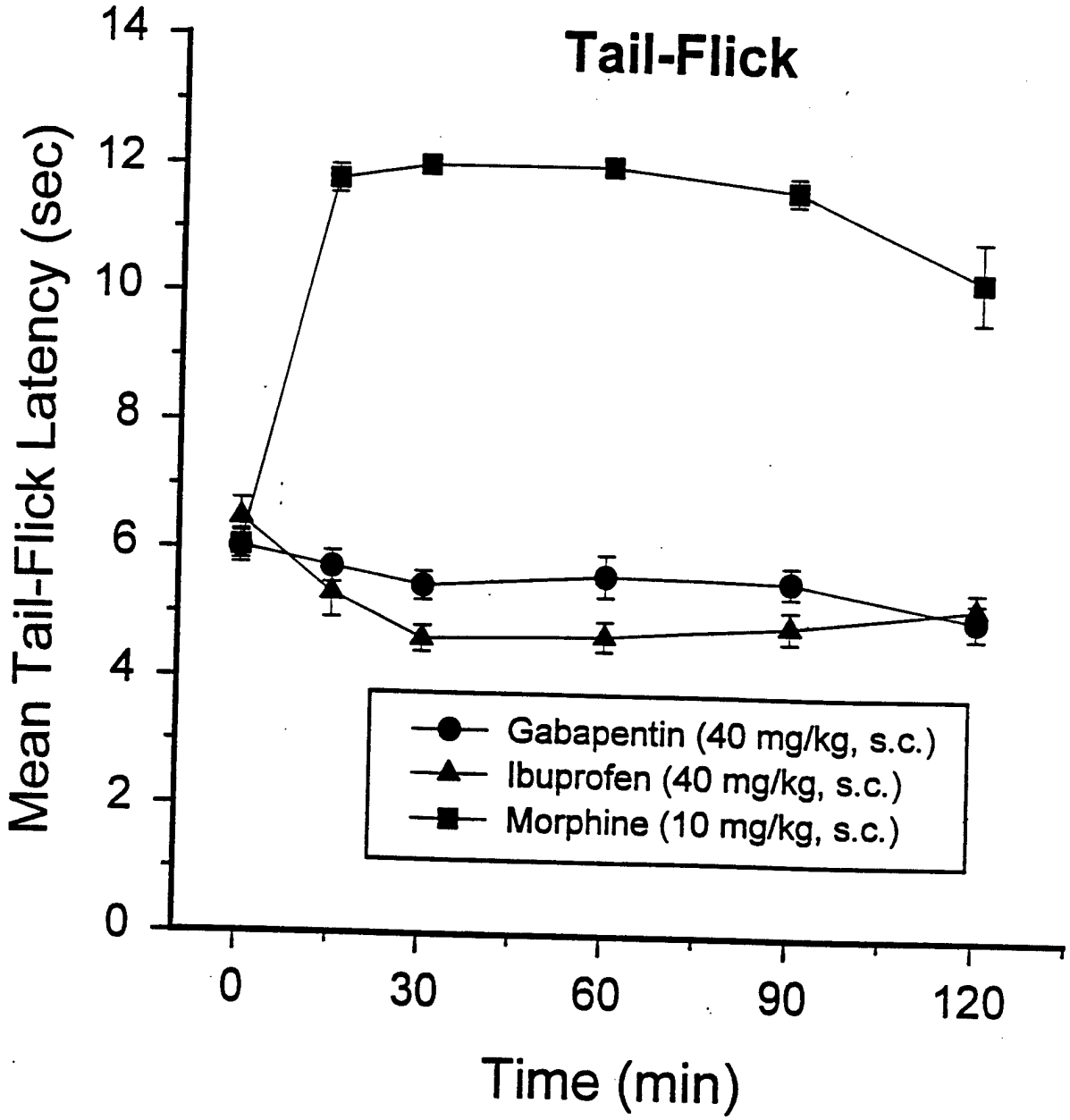
Tail-Flick
Mean Tail-Flick Latency (sec)
14
12
10
8
6
4
2
0
0
30
60
90
120
Time (min)
Gabapentin (40 mg/kg, s.c.)
Ibuprofen (40 mg/kg, s.c.)
Morphine (10 mg/kg, s.c.)

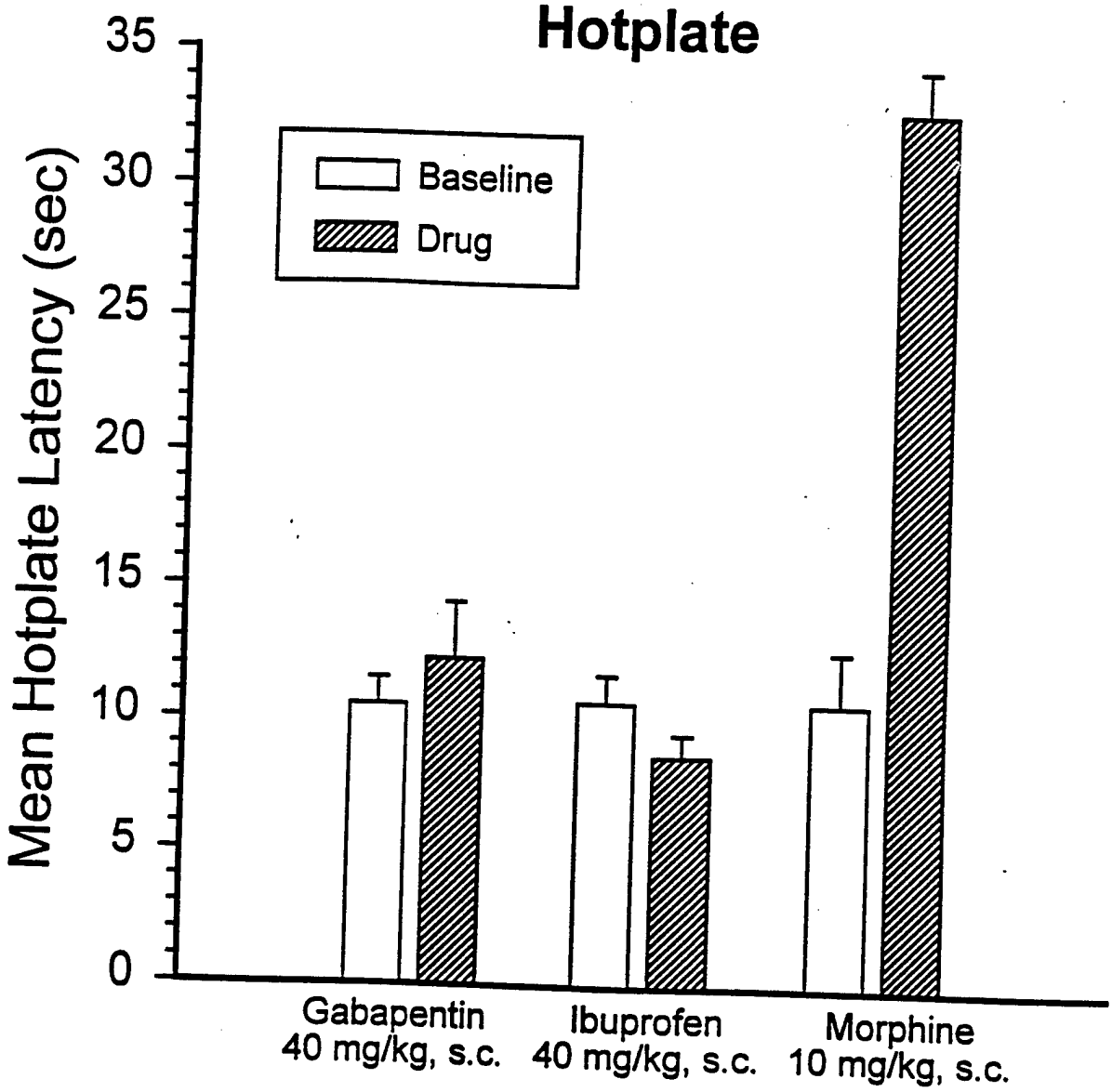
Hotplate
Mean Hotplate Latency (sec)
35
30
25
20
15
10
5
0
Baseline
Drug
Gabapentin
40 mg/kg, s.c.
Ibuprofen
40 mg/kg, s.c.
Morphine
10 mg/kg, s.c.

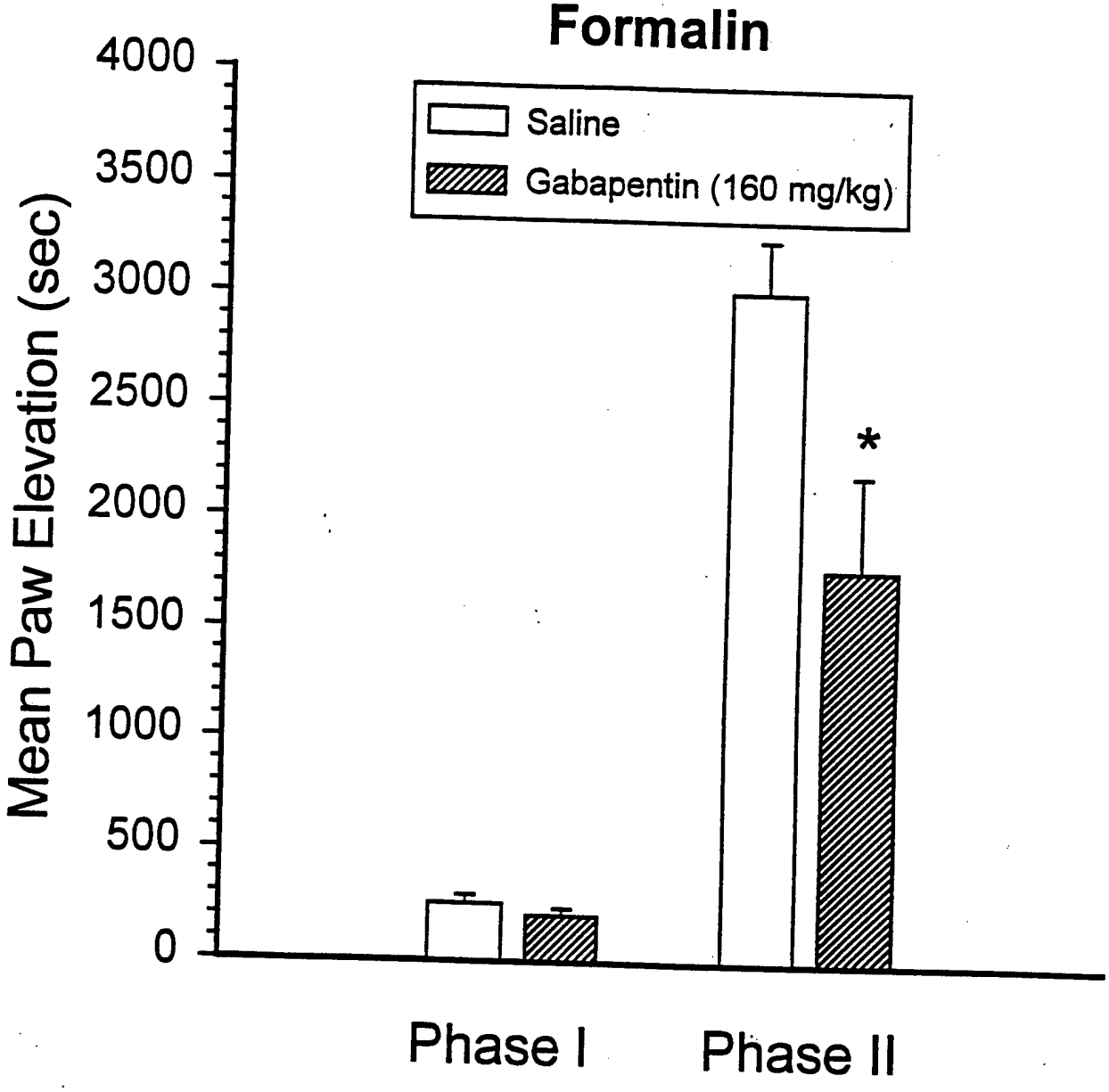
Formalin
Saline
Gabapentin (160 mg/kg)
Mean Paw Elevation (sec)
4000
3500
3000
2500
2000
1500
1000
500
0
*
Phase I
Phase II

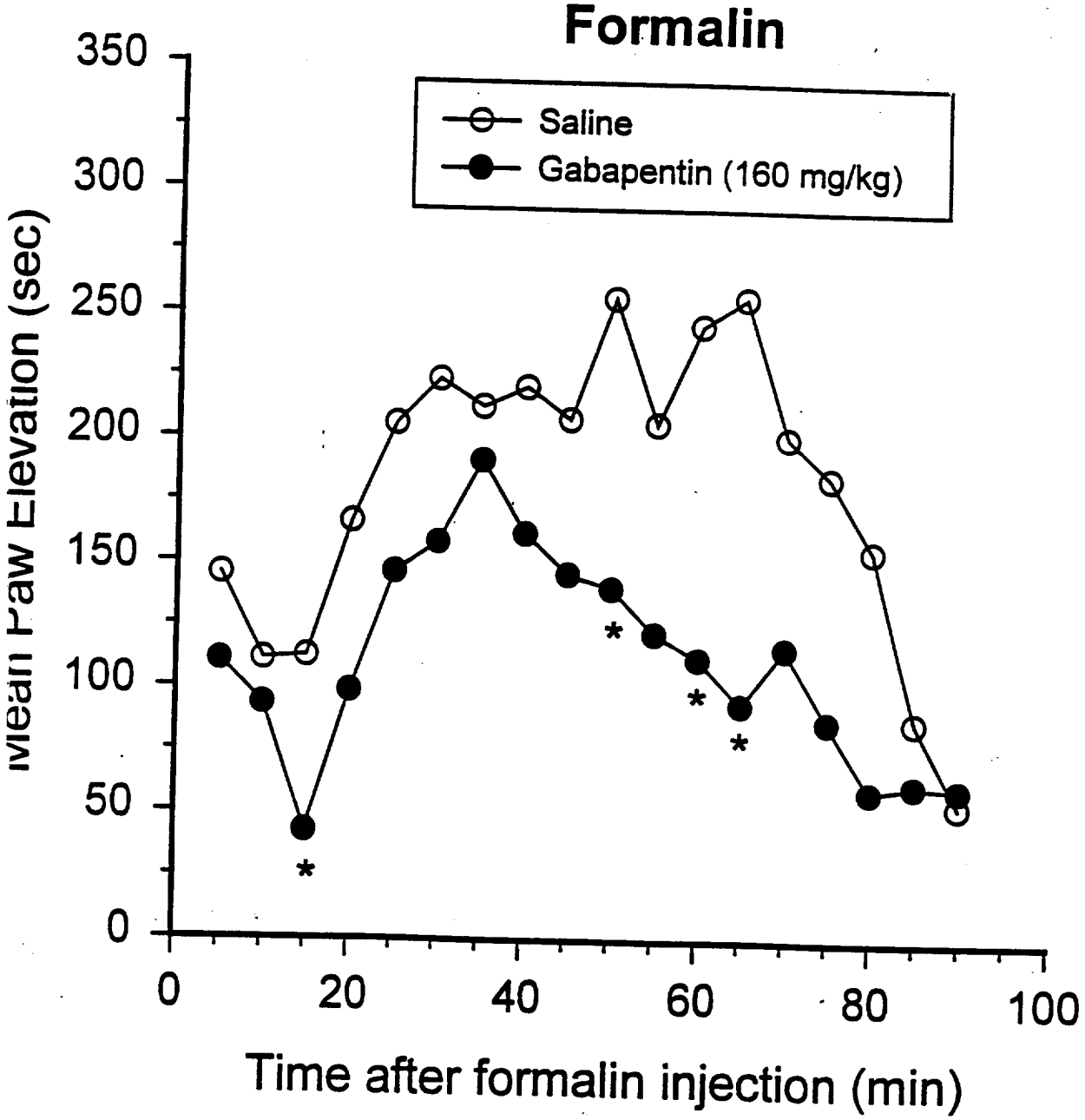
Formalin
Saline
Gabapentin (160 mg/kg)
Mean Paw Elevation (sec)
350
300
250
200
150
100
50
0
0
20
40
60
80
100
Time after formalin injection (min)
*
*
*
*